2001

Investigation of the peroxovanadate sol-gel process and characterization of the gels

Craig Joseph Fontenot
Iowa State University

INFORMATION TO USERS

This manuscript has been reproduced from the microfilm master. UMI films the text directly from the original or copy submitted. Thus, some thesis and dissertation copies are in typewriter face, while others may be from any type of computer printer.

The quality of this reproduction is dependent upon the quality of the copy submitted. Broken or indistinct print, colored or poor quality illustrations and photographs, print bleedthrough, substandard margins, and improper alignment can adversely affect reproduction.

In the unlikely event that the author did not send UMI a complete manuscript and there are missing pages, these will be noted. Also, if unauthorized copyright material had to be removed, a note will indicate the deletion.

Oversize materials (e.g., maps, drawings, charts) are reproduced by sectioning the original, beginning at the upper left-hand corner and continuing from left to right in equal sections with small overlaps.

Photographs included in the original manuscript have been reproduced xerographically in this copy. Higher quality 6" x 9" black and white photographic prints are available for any photographs or illustrations appearing in this copy for an additional charge. Contact UMI directly to order.

ProQuest Information and Learning
300 North Zeeb Road, Ann Arbor, MI 48106-1346 USA
800-521-0600

Investigation of the peroxovanadate sol-gel process and characterization of the gels

by

Craig Joseph Fontenot

A dissertation submitted to the graduate faculty

in partial fulfillment of the requirements for the degree of

DOCTOR OF PHILOSOPHY

Major: Chemical Engineering

Program of Study Committee:
G. L. Schrader, Major Professor
L.K. Doraiswamy
S.K. Mallapragada
Pat Thiel
Scott Chumbley

Iowa State University

Ames, Iowa

2001

Graduate College
Iowa State University

This is to certify the doctoral dissertation of

Craig Joseph Fontenot

has met the dissertation requirement of Iowa State University

Signature was redacted for privacy.

Major Professor

Signature was redacted for privacy.

For the Major Program

DEDICATION

This work is dedicated to my parents, Wildon Joseph Fontenot and JoLynn Marie Fontenot. It was they whom encouraged my natural curiosity, which led to where I am today. I would thank my mother for her unconditional nurturing love and for always understanding; and my father for caring enough to impart the hard lessons and for teaching me to persevere, even when the outlook is bleak.

TABLE OF CONTENTS

CHAPTER 1

GENERAL INTRODUCTION

1.1 Introduction

Vanadium oxide, either pure, mixed with other transition metals, or promoted, is an important catalyst in the selective oxidation of many hydrocarbons. Crystalline V_2O_5 has been reported to selectively oxidize paraffins (propane), diolefins (1,3-butadiene), alcohols and aromatics like benzene. Other binary oxide phases containing vanadium have also been studied using the similar feedstocks. For example, binary compounds containing vanadium and molybdenum[1], niobium [2], antimony[3] have all been evaluated for catalytic activity.

The selective oxidation of 1,3-butadiene over VMoO catalysts is of recent interest and the incorporation of additional components, such as rhenium or niobium, may be desirable. The VMoO system has shown promise, having shown selectivity to the two notable, industrially important products: maleic anhydride and furan.[4] Other interesting intermediates include 3,4-epoxy-1-butene and the unstable intermediate, 2-butene-1,4-dial. In recent studies, it was reported that selectivity to furan decreased while a concomitant increase in selectivity to maleic anhydride was observed as the % MoO_3 was increased in the solid solution α–phase.[4] This study also indicated that the addition of water to the feedstock substantially increased both the activity of the catalyst and the selectivity to earlier oxidation products.

In the crystalline state, and at concentrations of $MoO_3 < 14$ mole %, a single solid solution (α) phase is observed. At higher loading of MoO_3 a new phase (β) is observed to form. We are interested in studying the nature of the solid solution phase. The solid state synthesis route is limited to solid solutions of 14 mole % MoO_3 or less, so that preparation of a

single solid-solution phase at Mo concentrations greater than this can not be attained via this synthesis technique.

Prior to this sol-gel work, the VMoO catalysts were previously prepared via solid state synthesis, in which the two oxides were ground, intimately mixed and melted together in a quartz tube. This high temperature synthesis route resulted in compounds which had very low surface areas (~1 m^2/g). In addition, these synthesis conditions typically produce the most stable phase(s) corresponding to the lowest Gibbs free energy. In this work, new synthesis techniques have been explored which would allow: control of the phases present, alteration of the oxidation states of the metal constituents, and higher surface areas. This approach could potentially allow the synthesis of gels, supersaturated solid solutions and even meso-structured compounds. Current research efforts in this area almost exclusively involve metal alkoxides as the reactive precursor in synthesizing these metastable phases. Although the reactivity of alkoxides can be controlled by changing pH, water concentration and/or the alcohol solvent they are expensive and extremely sensitive to air and water (they must be handled in a inert environment).

Peroxovanadates are very attractive in that they are inexpensive, easy to work with, and form gels. Like alkoxides, the reactivity can be controlled by varying the pH (although in the case of peroxovanadates a different species is formed when the pH is varied). Also, peroxo complexes of molybdenum[5] and niobium[6] have been reported in the literature, and we have been able to synthesize a peroxorhenate in laboratory, so the incorporation of other metals should be possible.

1.2 Research Objectives

This research focused on the entire gelation process, including both the sol-gel solution chemistry, the structural connectivity of the gels along and the sites of water adsorption. The goal of this catalyst synthesis research was to gain a better understanding of the structure or connectivity of the gel along with determining the sites of water coordination. Understanding both the nature of the active sites involved in the selective oxidation reaction and the chemistry of the catalyst synthesis are the first steps to being able engineer the next generation of catalysts.

The research objectives for the sol-gel solution chemistry (Chapter 3) were to characterize and elucidate the chemical pathway to gel formation (i.e. chemical intermediates, precursor to gel formation, role of pH). This understanding might then lead to the ability to: (1) synthesize super-saturated solid state compounds which exceed the expected equilibrium concentrations (2) control of the oxidation state of one or more of the metal components in the catalyst (4) synthesize novel metal oxides, including meso-structured phases and new gels, to screen for catalytic ability, (5) synthesize metal oxide catalysts having a surface area of between 10 –20 m^2/g and (6) adapt this synthesis procedure to include binary and even ternary systems.

The objectives of the solid state gel studies (Chapters 4-6) were to: (1) characterize the materials synthesized and determine the connectivity, and (2) determine the role or sites of water chemisorption so that the oxidation catalysis could be better understood.

1.3 Explanation of Dissertation Format

The dissertation consists of seven chapters and one appendix. Figures and references are located at the end of each chapter. Chapter 1 gives a brief overview of the sol-gel process as

applied to catalyst synthesis. Chapter 2 is an in-depth literature review, which focuses on the gelation process, including characterization of both the solution and of the solid-state gels. Chapters 3, 4, 5 and 6 are articles published (or submitted) by the author in refereed journals. In Appendix A, the results of the Partial Charge Model as applied to the peroxovanadate system are reported. Finally, Chapter 7 draws general conclusions and offers suggestions for the direction of future research. The research presented herewith represents original work conducted by the author.

1.4 References

[1] Watson, Rick B.; Ozkan, Umit S. **K/Mo Catalysts Supported over Sol-Gel Silica-Titania Mixed Oxides in the Oxidative Dehydrogenation of Propane.** J. Catal. (2000), 191(1), 12-29. CODEN: JCTLA5 ISSN:0021-9517. AN 2000:188020 CAPLUS

[2] Jackson, P.; Fisher, K. J.; Willett, G. D. **Some reactions and thermochemistry of NbO3-: oxidation and reduction, hydrogen bond strength, and catalytic activation of primary alcohols.** Int. J. Mass Spectrom. (2000), 197 95-103. CODEN: IMSPF8 ISSN:1387-3806. CAN 132:213290 AN 2000:185358 CAPLUS

[3] Satsuma, Atsushi; Phiyanalinmat, Satit; Yashiro, Miki; Hattori, Tadashi. **Number of surface redox sites of V-Sb-O catalysts.** Res. Chem. Intermed. (2000), 26(2), 113-119. CODEN: RCINEE ISSN:0922-6168. CAN 132:142584 AN 2000:130681 CAPLUS

[4] Schroeder, W.D., Fontenot, C.J., Schrader, G.L., J. Cat.(2001), accepted

[5] Reynolds, M., Butler, A., **Oxygen-17 NMR, Electronic and Vibrational Spectroscopy of Transition Metal Peroxo Complexes: Correlation with Reactivity.** Inorg. Chem. (1996), 35(8), 2378-83

[6] Passoni, L. C.; Siddiqui, M. R. H.; Steiner, A.; Kozhevnikov, I. V. **Niobium peroxo compounds as catalysts for liquid-phase oxidation with hydrogen peroxide.** J. Mol. Catal. A: Chem. (2000), 153(1-2), 103-108. CODEN: JMCCF2 ISSN:1381-1169. AN 2000:168938 CAPLUS

CHAPTER 2

LITERATURE REVIEW

2.1 Vanadates in Solution

Even in the absence of peroxides, a large variety of vanadate species can exist at equilibrium in solution. In fact, usually equilibrium exists between two or more species. The predominant species present is mainly a function of pH and vanadium concentration (Figure 1).[1] In highly alkaline (pH >14) solutions $V^{(V)}$ is found as the orthovanadate ion, $[VO_4]^{3-}$. Each of the four oxygen atoms in this oxoanion are equivalent. In dilute solutions ($C_v < 10^{-4}$ M), as the pH is decreased protonation occurs, giving such species as $[H_nVO_4]^{3-n}$. The overall charge of the species decreases with pH to the point of zero charge (ZPC), which is pH = 2 for vanadium. Below this pH the monomeric dioxovanadate cation $[VO_2]^+$, is observed.

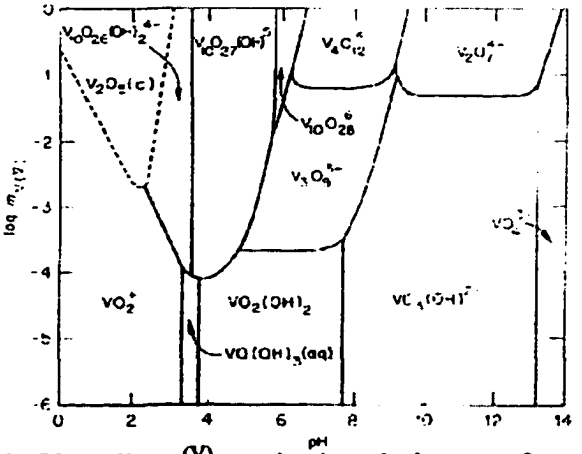

Figure 1. Vanadium $^{(V)}$ species in solution as a function of concentration and pH.[1]

Above this pH, the coordination of vanadium is observed to increase to six and the decavanadate ion $[V_{10}O_{28}]^{6-}$ is formed. This large ion can be observed in several protonated forms, $[H_nV_{10}O_{28}]^{(6-n)-}$, n = 1 or 2, depending on the pH.

Neither the decavanadate ion, nor any of its protonated forms are thought to be a precursor for further condensed species. At pH < 5, the diprotonated decavanadate ion is further protonated and forms the dioxovanadium cation according to:

$$V_{10}O_{28}^{6-} + H^+ \rightarrow HV_{10}O_{28}^{5-}$$
$$HV_{10}O_{28}^{5-} + H^+ \rightarrow H_2V_{10}O_{28}^{4-}$$
$$H_2V_{10}O_{28}^{4-} + 14H^+ \rightarrow 10VO_2^+ + 8H_2O$$

In acidic solutions (pH < 3), the VO_2^+ ion is predominant. The pH/concentration dependence of these species can be seen in Figure 1. In 1969, Griffith et al[2] report Raman band assignments for many of the vanadates found in solution. The ones of interest for our studies are the dioxovanadium cation and the decavanadate anion, which can be seen in Figure 2. Another useful characterization tool is solution NMR. In 1979, Howarth et al.[3] reported ^{51}V NMR shifts for many of the vanadates found in solution, including the ones of interest in our studies. These include: VO_2^+ at –545 ppm, decavanadate –420 to –530 ppm, $V_4O_{14}^{4-}$ at –577.6 ppm and $V_5O_{15}^{5-}$ at –570 ppm. ^{17}O NMR shifts were reported[9] for these same species. In general, there were three main categories of ^{17}O shifts: (1) 0-100 ppm, which corresponds to a coordinated water, (2) 550-650 ppm, which corresponds to tetrahedrally coordinating O^{2-} or OH^-, and (3) 1000-1200 ppm, which corresponds to octahedrally coordinating O^{2-} or OH^-. ^{17}O NMR spectra for the VO_2^+ moiety have not ever been reported, presumably because of

fast proton exchange with the solvent.[4] Some authors have interpreted this as an indication that the VO_2^+ cation has a symmetrical chemical environment.[23]

2.2 Peroxovanadates

Vanadium peroxo complexes resulting from the reaction of a metavanadate salt and hydrogen peroxide in aqueous solution have been extensively characterized via Raman spectroscopy,[5 6 7] ^{51}V NMR,[8 9] ^{17}O NMR,[8 9] and UV visible spectroscopy.[10 11] Most of the recent literature is in general agreement, although there are still discrepancies regarding the nature of the peroxo ligand and the structure of the complexes.

The recent discovery that these complexes are biomimetic[12] make this chemistry attractive from a research standpoint. However, at this time, our interest is in the use of these peroxovanadates as a reactive precursor in catalyst synthesis. While this is not a novel idea, the literature reports only one other group to attempt a similar approach,[11] which described what was thought to be a redox reaction between a peroxovanadate and Sb_2O_3 to form a xerogel, although the chemical mechanism and characterization of the complexes was not reported. This work resulted in U.S. Patent 4784979 .[13]

The peroxovanadate to gel reaction, in which the peroxovanadates were derived not from the metavanadate, but from the reaction of V_2O_5 and hydrogen peroxide in aqueous solution is not well understood. Peroxovanadates derived from the former have been characterized and it may have been assumed that the V_2O_5/H_2O_2 system will behave in a similar manner to the aqueous metavanadate/ H_2O_2 system, even though the latter has a counter ion present in solution. In any case, the aqueous V_2O_5/hydrogen peroxide system is

preferred for our synthesis in that the lack of counter ion simplifies both the solution and solid-state characterization.

The following review consists entirely of work done on the metavanadate/ H_2O_2 system, except for the UV visible spectra presented by Bradzil et al..[11] The species present in solution are a function of pH, $n(H_2O_2)/n(V)$, and total concentration of vanadium. At concentrations of vanadium of 0.01mol/dm^3 or less, and $n(H_2O_2)/n(V) = 2$ and pH < 7 the reaction of hydrogen peroxide with $V^{(5+)}$ results in a either a one or two bidentate O_2^{2-} ligands depending on the pH of the solution. These species interconvert as the pH changes. Conte et al. reported that the monoperoxovanadate cation is the predominant species at pH < 2.3, while at pH > 2.3 the diperoxovanadate anion is predominant. A neutral diperoxovanadate species was reportedly detected[16] with ^{51}V NMR. This species had a maxima in concentration at pH = 2.3. Both the mono-and diperoxovanadate species have been reported to be stable in their respective pH domains although the monoperoxovanadate cation has been reported to be the better oxidant[16].

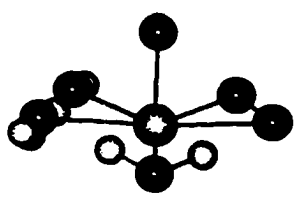

Monoperoxovanadate Cation

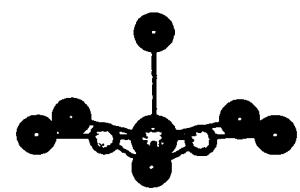

Diperoxovanadate Anion

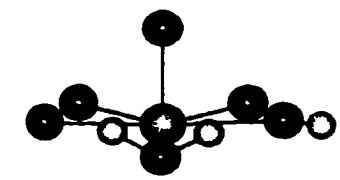

Protonated
Diperoxovanadate

These complexes can be characterized using uv-spectroscopy. The monoperoxovanadate cation has λ_{max}= 460 nm, while the diperoxovanadate anion has λ_{max}=

330 nm. However, the monoperoxo cation is has been reported to photolytically decompose[10] when exposed to exciting light of wavelengths of 313, 365 and 436 nm so that this technique is not useful for *in situ* characterization of the reaction. [13]

Laser Raman Spectroscopy (LRS) can be used *in situ* for solutions of low vanadium concentration. For these peroxovanadate species, some laser-induced decomposition has been reported. The Raman spectra of the monoperoxo and diperoxo both have a sharp peak at about 992 cm^{-1} which corresponds to the stretching mode of the V=O. The bidentate peroxide ligand creates local C_{2v} symmetry which has three IR and Raman active modes: a sharp peak at about 890 cm^{-1} which corresponds to the O_p-O_p stretch, the symmetric $\nu^1(V\text{-}O_p)$ stretch at about 630 cm^{-1} and the asymmetric $\nu^3(V\text{-}O_p)$ stretch at about 540 cm^{-1}. In the monoperoxo complex, the peroxide is symmetrically coordinated while in the diperoxo complex, the presence of the extra bidentate peroxo ligand increases the bond length of the $V\text{-}O_{cis}$ relative to the $V\text{-}O_{trans}$. This can be seen in Figure 2. Although the O_p– O_p bond in the diperoxo complex is longer than in the monoperoxo complex, there is no distinguishable difference in the observed band.

With monoperoxo complexes, the symmetric and asymmetric modes overlap at approximately 560 cm^{-1}. Oxodiperoxo complexes can be either pentagonal pyramidal or pentagonal bipyramidal depending on the coordination number of the vanadium.[7] These different orientations result in recognizable differences in the observed Raman bands for the symmetric and asymmetric stretches.

Fortunately, these vibrational modes are structure sensitive, so we can distinguish between monoperoxo, pentagonal pyramidal and pentagonal bipyprimidal complexes. With monoperoxo complexes, the bands corresponding to the symmetric and asymmetric metal-

peroxo vibrations overlap at approximately 560 cm^{-1}. A monodentate ligand on a diperoxo complex will result in a splitting of the two bands of approximately 100 cm^{-1}, with maxima at about 630 and 520 cm^{-1}, while an additional bidentate ligand will cause a splitting of only 40 cm^{-1} [7]. In general, as the coordination number of the diperoxovanadate increases from six to seven, the complex coverts from a pentagonal pyramidal to a pentagonal bipyramidal structure. Complexes with a long axial bond in the *trans* position to the V=O bond are considered pseudo-pentagonal bipyramidal. The differences in coordination result in an increase in the difference of $\nu^1(V\text{-}O_p)$- $\nu^2(V\text{-}O_p)$, and a shift $\nu^3(V\text{-}O_p)$ shifts to a lower wavenumber. The diperoxo complex, $VO(O_2)_2H_2O^-$ is six-fold coordinated and has a pentagonal pyramidal structure.

Finally, the band resulting from the $\nu(V\text{-}OH_2)$ is very weak and has been assigned to a band at 460 cm^{-1}. [5] It should also be noted that in the case of an unidentate end-on bound hydroperoxide, only one $V\text{-}O_p$ stretch would be observed and an -OOH deformation should be observed above 1100 cm^{-1}. [14]

Another characterization technique applicable to this system is ^{51}V and ^{17}O NMR, although the chemical shifts are not well understood. Generally, but not without exception the ^{51}V shifts increase upon protonation and also upon substitution of OO^{2-}. [3] Most recently, Conte *et al.* reported[16] ^{51}V chemical shifts (δ), relative to $VOCl_3$, of –540 ppm for the monoperoxo complex, -692 ppm for the diperoxo complex and –702 for the neutral protonated diperoxo complex. This was the first report in the literature of this neutral species. Also reported in this paper were *ab initio* calculations, which confirmed the most probable site of protonation. This site is thought to be one of the four peroxo oxygen's (O_p). These

calculations also indicated that the preferred orientation of peroxovanadium complexes in water are octahedral. This conflicts with the pentagonal pyramidal or pentagonal bipyramidal structures proposed by Schwendt[15].

Howarth et al[3] reported ^{51}V shifts for some of the peroxovanadates of interest. They reported a ^{51}V chemical shift of -549 ppm for the monoperoxo complex, and -700 for the diperoxo complex. Also reported was a dimer with a shift of about –672 ppm. In 1997, Conte et al reported[16] observing a protonated diperoxovanadate species, $[VO(O_2)2(OH_2)\ H]$ at –702 ppm, which is neutral in charge. It is worth noting that Howarth reported that the mono and diperoxo monomeric species below pH 14 are octahedral while those at high pH or more than two peroxides per vanadium are tetrahedral. They reported that all peroxide ligands are formally taken to be unidentate.

Howarth[3] also reported that ^{17}O shifts fell into three distinct regions: 0-100, 550-650, and 1000-1250 ppm. They proposed that these regions correspond to coordinated H_2O, tetrahedrally coordinated O^{2-} or OH^-, and octahedrally coordinating O^{2-} or OH^-.

2.3 Partial Charge Model

Sol-gel precursors may undergo a variety of transformations in solution. The Partial Charge Model (PCM), first introduced by Sanderson and modified by Henry and Livage, gives us a simple way to predict which species may be present. At equilibrium, the chemical potential of every species in solution will be equal. Analogously, the electrons of a molecule transfer from atom to atom until they all reach the same chemical potential. Each atom will

then have an electronic charge (δ_e). The chemical potential of these electrons may be written as:

$$\mu_e = \mu_e^a - \eta^a \delta_e$$

where μ_e^a denotes the chemical potential of the electron on the isolated atom, η^a is the hardness of atom a, and δ_e is the electronic charge of the atom.

Since the electronegativity of an atom (χ_x) is the negative of the chemical potential (μ_e) of the electrons, the electronegativity can be described in terms of the partial charges (δ) of either atoms or molecules. Using these relationships, the electronegativity (χ_x) of an atom X can be written as a function of the atom's hardness (η_x) and its partial charge (δ_x):

$$\chi_x = \chi_x^o + \eta_x \delta_x \qquad (1)$$

where η_x is the Pearson hardness of atom X. Softness (σ_x), which provides some measure of electron polarizability, is related to the Pearson hardness as:

$$\sigma_x = 1/\eta_x \qquad (2)$$

Softness (σ_x), or polarizability, increases as the size of the electron cloud increases with the radius (r) of atom X). It follows that hardness varies as 1/r. Electronegativity is proportional to Z_{eff}/ r^2 using the Allred-Rochow scale. Combining the two previous relationships, we arrive at:

$$\eta = k(\chi^o)^{0.5} \tag{3}$$

where k is a constant which depends on the electronegativity scale. This constant k = 1.36 when Pauling electronegativities are converted to the Allred-Rochow scale.

The over-all charge, z, of a chemical species is equal to the sum of the partial charges of all individual atoms. This sum can be written as:

$$z = \sum_i \delta_i \tag{4}$$

Substituting equations 1 and 3 into 4, and using the knowledge that at equilibrium all atoms in complex C will have the same electronegativities, $\chi_i = \chi(C)$, we find that:

$$\chi_C = \frac{\sum_i \sqrt{\chi_i^o} + 1.36z}{\sum_i 1/\sqrt{\chi_i^o}} \tag{5}$$

If this complex C is in aqueous solution then we must consider the partial charge of water. Once this is related to the pH of the solution, we have a way to predict which species is likely to be present. At a pH of 7, theoretical calculations made by linear combination of the 2s and 2p atomic orbitals of oxygen and the 1s orbital of hydrogen predict values[17] of $\delta(O) = -0.4$ and $\delta(H) = 0.2$. Since $z = 0$ at pH = 7, $\chi(H_2O)$ is calculated to be 2.491. The Nernst equation relates the chemical potential of a proton to pH:

$$\mu(H^+) = \mu^o(H^+) - \beta pH \qquad \text{where } \beta = 2.3RT \tag{6}$$

Knowing that $\mu(H^+)$ is related to $\chi(H^+)$ through equation 1, and that $\chi(H^+) = 2.491$ (at pH = 7 and 25° C) and (assuming that the $[H_7O_3]^+$ and the $[H_9O_4]^+$ ions are present) $\chi(H^+) = 2.631$ at pH =0 we can write:

$$\chi(H^+) = \chi(H_2O) = \chi(C) = 2.631 - 0.02\ pH \qquad (7)$$

If we assume the $[H_5O_2]^+$ ion is dominant at pH =0, $\chi(H^+) = 2.732$, equation 7 changes to:

$$\chi(H^+) = \chi(H_2O) = \chi(C) = 2.732 - 0.035\ pH \qquad (8)$$

H 2.10 307																	He 3.20 411
Li 0.97 747	Be 1.57 587											B 2.02 517	C 2.50 465	N 3.07 420	O 3.50 393	F 4.10 363	Ne 5.10 326
Na 1.01 732	Mg 1.29 647											Al 1.47 606	Si 1.74 557	P 2.11 506	S 2.48 467	Cl 2.83 437	Ar 3.50 393
K 0.91 771	Ca 1.04 721	Sc 1.23 663	Ti 1.32 640	V 1.56 589	Cr 1.59 583	Mn 1.63 576	Fe 1.72 561	Co 1.75 556	Ni 1.80 548	Cu 1.75 556	Zn 1.66 571	Ga 1.82 545	Ge 2.00 520	As 2.20 496	Se 2.50 465	Br 2.69 448	Kr 3.10 418
Rb 0.89 779	Sr 0.99 739	Y 1.19 674	Zr 1.29 647	Nb 1.45 611	Mo 1.56 589	Tc 1.67 569	Ru 1.78 551	Rh 1.84 542	Pd 1.85 541	Ag 1.68 567	Cd 1.60 581	In 1.49 602	Sn 1.89 535	Sb 1.98 523	Te 2.15 501	I 2.33 482	Xe 2.60 456
Cs 0.87 788	Ba 0.97 747		Hf 1.36 631	Ta 1.50 600	W 1.59 583	Re 1.88 536	Os 1.99 521	Ir 2.05 514	Pt 2.00 520	Au 2.02 517	Hg 1.80 548	Tl 1.60 581	Pb 1.92 531	Bi 2.03 516	Po 2.12 505	At 2.28 487	Rn 2.30 485
Fr 0.86 793	Ra 0.95 754																

Figure 8. Allred-Rochow Electronegativities (χ_i) and Softness (σ_i) of Atoms X_i [18]

Jolivet and Livage worked out that for a complex $C = [M(OH)_h(OH_2)_{N-h}]^{(z-h)+}$, the electronegativity of the complex C can be written:

$$\chi_c = \frac{\sqrt{\chi_M^o} + N\sqrt{\chi_O^o} + (2N - h)\sqrt{\chi_H^o} + 1.36z}{\frac{1}{\sqrt{\chi_M^o}} + \frac{N}{\sqrt{\chi_O^o}} + \frac{2N - h}{\sqrt{\chi_H^o}}} \qquad (9)$$

If the electronegativity of this complex is the same as the water molecules with which it is in solution (Equation 7), we can solve for the number of hydroxo ligands (h) and the charge of the hydrolyzed species $(z\text{-}h)^+$ we might expect to find.

$$h = [z - \delta(M(OH_2)_N]/[1-h] \qquad (10)$$

$$z - h = \delta_M + N\delta_O + (2N-\eta)\delta_H \qquad (11)$$

Vanadium and molybdenum are small high valent cations possessing empty $d\pi$ orbitals which tend to coordinate with the $p\pi$ orbitals of oxygen. This favors the formation of metal-oxygen double bonds, which decreases the partial charge of the metal cation. Spontaneous internal proton transfer is thought to occur at low pH, so that oxo-aqueous species (i.e. VO_2^+) are observed rather than hydroxo-aqueous species (i.e. $V(OH)_4(OH_2)_2^+$).[19]

2.4 Vanadium Sols and Gels

Vanadium sols were first reported in the literature by Ditte,[20] in 1885. Since then over 100 papers have been written on the subject. However, very few are related to catalyst preparation. Sol-gel chemistry allows the control needed to engineer mono-dispersed powders, homogeneous glasses, thin films and even fibers, and does not require the high temperatures of other synthesis techniques. At these lower temperatures, non-equilibrium metastable phases, such as the ones previously mentioned and others such as super saturated

solid solutions and even meso-structured compounds are being synthesized. Seeing the enormous potential, recent research has intensified in this area.

V_2O_5 sols have been obtained by various ways. Ditte heated ammonium vanadate in a platinum crucible, reacted this with hot nitric acid and poured the mixture into water. Müller[21] poured molten vanadium pentoxide into water and Ostermann[22] reacted hydrogen peroxide with V_2O_5 forming a red-gelatinous product. Vanadium oxytricloride has been used in the alkoxide route, while more recently, McCormick,[23] starting with sodium metavanadate, used an ion exchange column to remove the sodium while acidifying the solution. The resulting solution was observed to form a gel.

Vanadium gels have been reported to form fibers and even layered structures.[24] Intercalation of various ions and molecules, including water, occurs readily in these gels, although crystalline V_2O_5 does not dissolve in water. Hydration occurs in the layered, fibrous and amorphous states.

The most widely accepted mechanism of gelation from an aqueous vanadate solution was hypothesized by Livage[25] in 1988. It was proposed that the reactive precusor is the neutral species $[VO(OH)_3]^\circ$. Experimental evidence for this intermediate has never been reported. The vanadium atoms in this neutral precursor would have a large positive partial charge (δ_V=+0.62) so that coordination expansion most likely would occur through the addition of a nucleophilic species. Between pH 2 and 6, these neutral intermediates are thought to react and lead to the formation of decavanadic acid:

$$10[VO(OH)_3]^\circ \rightarrow [H_6V_{10}O_{28}]^\circ \rightarrow [H_2V_{10}O_{28}]^{4-} + 4H^+ + 12H_2O$$

Since these neutral decavandate species are strong acids, spontaneous deprotonation leads to solutions of decavanadic acid $[H_2V_{10}O_{28}]^{4-}$ and possibly $[H_3V_{10}O_{28}]^{3-}$. These polyanions cannot be precursors for further condensed species. Since OH groups in water are more negatively charged (δ_{OH}=-0.2) than the OH groups in $[VO(OH)_3]^\circ$ (δ_{OH}=-0.09)[26], the former is a better nucleophile than the latter. Hence, coordination increases through water addition as:

$$[VO(OH)_3]^\circ + 2H_2O \rightarrow [VO(OH)_3(OH_2)_2]^\circ$$

The neutral vanadium is now six-fold coordinated with one water coordinated trans to the V=O bond (in the z direction), and the other water opposite an OH group on the equatorial plane. The V-O bonds of the equatorial plane are inequivalent in the x and y direction (Figure 3a). The y direction contains two OH groups, while the x direction contains an OH group and a coordinated H_2O water molecule. Condensation occurs much faster along the x direction via olation, as a good nucleophile (OH) and a good leaving group (H_2O) are present. Also, olation is a faster process since a proton transfer is not required for this mechanism to proceed. Oxolation, which does require a proton transfer, proceeds at a slower rate along the y direction. A cartoon of this gelation process can be seen in Figure 3b.

The dispersion of V^{4+} species in the predominantly V^{5+} is responsible for the mixed-valence properties of the gel[27], and the color of V_2O_5 gels seems to be determined by the percentage of V^{4+} species present.. Although the V^{4+} percentage is usually about 1%, it can be as large as 10% when the synthesis is preformed in an organic solvent.[28] When the V^{4+}

percentage reaches 20%, the gel turns green and flocculates.[29] It has been proposed by several groups [30, 23] that the V^{4+} species is the initiator for condensation. This may be because the V^{4+} ion is larger, and larger ions favor coordination expansion, or because V^{4+}-OH are weaker acids than V^{5+}-OH. The former has been reported to be one of the major factors influencing the formation of condensed species from tetrahedrally coordinated inorganic or metal-organic species.[31] Catalytic effects of V^{4+} in the predominantly V^{5+} material are, as of yet, unstudied.

The fibrous nature of hydrated vanadium gels ($V_2O_5 \cdot nH_2O$) has been studied using electron microscopy[35]. These ribbon-like fibers are about 10 nm wide and greater than 1μm in length. Smaller sections, about 100 nm long and 2 nm wide form first. They subsequently self assemble, edge-to-edge, forming a wider, ribbon-like structure (Figure 4).[32] The ansiotropy of these segments allows the formation of further ordered colloids, called tactoids (Figure 5). Tactoids are thought to form when solid-solid interactions become strong enough (i.e. concentrated sol) to keep the colloids mutually aligned.[33]

Electron diffraction has been utilized[34] to determine the molecular dimensions of the repeating structure. This structure is similar to orthorhombic V_2O_5 in that the *b* parameter is nearly identical. The *a* parameter is much larger, having increased from 11.51 Å to 27 Å. This may be due to the presence of hydroxyl groups that are stable at temperatures less than 300 ° C.

Hydrated gels, $V_2O_5 \cdot nH_2O$, are obtained via condensation and hydrolysis of vanadium alkoxides or vanadate solutions. When dried ambiently the gels contain roughly 1.8

moles H_2O per mole V_2O_5. The removal of water can be achieved through thermal treatment and this process can be described as[35]:

$$V_2O_5 \cdot 1.8\ H_2O \rightarrow V_2O_5 \cdot 0.5\ H_2O \rightarrow V_2O_5\ (\text{amorphous}) \rightarrow V_2O_5\ (\text{crystalline})$$

Amorphous V_2O_5 was observed above 250 °C, and crystallization into orthorhombic V_2O_5 was observed as temperatures began to exceed 350 °C.[35] Water desorption has been reported to be reversible at water contents above $V_2O_5 \cdot 0.5\ H_2O$, and is dependent on the partial pressure of water above the gel. The desorption isotherm is Brunauer type II, suggesting multi-layer adsorption.[36] In this model the first layer of molecules are chemisorbed to the substrate, while subsequent layers are physisorbed. Since the structure of these gels is often layered, the water molecules are thought to be intercalated.[35] As the water is incorporated between planar sheets of the oxide, the gel swells, and the basal distance increases by increments of 2.8 Å, which is the van der Waals diameter of H_2O.

In 1993, McCormick et al. examined the vanadia oxide gel formed from the acidification of 0.1, 0.2 and 0.4 M sodium metavandate solutions using ^{51}V NMR. Immediately after ion exchange, the solution contained the di- and triprotonated decavanadate ion and the dioxovandatate cation. Some polymerization occurred immediately. This coincided with the disappearance of the triprotonated decavanadate ion. After a period of induction, polymerization began again. Since they observed the initial presence of V^{4+} (initially at a concentration of only 0.001 M.) they proposed that polymerization was initiated by a dimer that was formed between the reaction of the V^{4+} species and the VO_2^+ cation. Although, this explains the induction period, it does not explain the immediate formation of the colloidal solid that they reported observing.

The polymerization began again after about 50 hours, and was nearly complete by 120 hours. The red viscous sol that formed was examined using ^{51}V MAS NMR. They found that the sol exhibited a single resonance at –547 ppm, which is nearly identical to the shift observed for the VO_2^+ cation in solution. They proposed that the vanadium chemical environment in the gel was very similar to that of the VO_2^+ cation, which has a symmetrical environment[37,4]. The VO_2^+ cation is though to have a symmetrical environment since the oxygen is unobservable with ^{17}O NMR, due to what is thought to be rapid oxygen exchange with the solvent. Although they spun their samples at 10 kHz, spinning side bands were not observed. They concluded that the vanadium chemical environment in the polymer was probably symmetrical, and very similar to that found in the VO_2^+ cation. ^{17}O MAS NMR results were also reported for the same gels. Oxygen resonances were reported at 1430, 1407, 1396, 1380, 1150, 688 and 223 ppm. The peaks between 1500-1300 ppm were assigned to V=O groups, the peak at 688 ppm to a V_2O group and the peak at 223 ppm to coordinated water.

In 1999, Livage[38] reported concentration profiles as determined using ^{51}V NMR for the reaction of V_2O_5 with H_2O_2. They demonstrated that dissolution of the oxide led to the formation of unstable diperoxo $[VO(O_2)_2]^{2-}$ species which decomposed to form monoperoxo species $[VO(O_2)]^+$. Vanadate and decavanadic acid entities were observed before polymerization occurred and $V_2O_5 \cdot nH_2O$ was formed.

2.5 List of Figures

2.6 References

[1] Baes, C., Mesmer, R., **The Hydrolysis of Cations.** (1976). John Wiley & Sons: New York. P 210

[2] Griffith, William P.; Lesniak, P. J. B. **Raman studies on species in aqueous solutions. III. Vanadates, molybdates, and tungstates.** J. Chem. Soc. A (1969), (7), 1066-71. CODEN: JCSIAP CAN 70:109648 AN 1969:109648 CAPLUS

[7] Howarth, Oliver W.; Hunt, John R. **Peroxo complexes of vanadium(V); a vanadium-51 nuclear magnetic resonance study.** J. Chem. Soc., Dalton Trans. (1979), (9), 1388-91. CODEN: JCDTBI ISSN:0300-9246. CAN 92:51133 AN 1980:51133 CAPLUS

[4] Hibbert, R., Logan, N., **Contrast in the hydrolysis of $VOCl_3$ and $VO(NO_3)_3$: A multinuclear magnetic resonance study.** J. Chem. Soc Dalton Trans (1986) 369-372

[5] Schwendt, P.; Pisarcik, M. **Vibrational spectra of vanadium(V) compounds. VI. Raman spectra of vanadium(V) oxodiperoxo complexes.** Chem. Pap. (1988), 42(3), 305-10. CODEN: CHPAEG CAN 109:239552 AN 1988:639552 CAPLUS

[6] Schwendt, P.; Pisarcik, M. **Raman spectral study on the structure of vanadium(V) oxodiperoxo complexes in aqueous solution.** Spectrochim. Acta, Part A (1990), 46A(3), 397-9. CODEN: SAMCAS ISSN:0584-8539. CAN 113:14011 AN 1990:414011 CAPLUS

[7] Schwendt, Peter. **Vibrational spectra of vanadium(V) compounds. V. Stretching vibrations of the V(O2) group and structure of vanadium(V) peroxy complexes.** Collect. Czech. Chem. Commun. (1983), 48(1), 248-536. CODEN: CCCCAK ISSN:0366-547X. CAN 98:151982 AN 1983:151982 CAPLUS

[8] Howarth, Oliver W.; Hunt, John R. **Peroxo complexes of vanadium(V); a vanadium-51 nuclear magnetic resonance study.** J. Chem. Soc., Dalton Trans. (1979), (9), 1388-91. CODEN: JCDTBI ISSN:0300-9246. CAN 92:51133 AN 1980:51133 CAPLUS

[9] Harrison, Aidan T.; Howarth, Oliver W.. **High-field vanadium-51 and oxygen-17 nuclear magnetic resonance study of peroxovanadates(V).** J. Chem. Soc., Dalton Trans. (1985), (6), 1173-7. CODEN: JCDTBI ISSN:0300-9246. CAN 103:133849 AN 1985:533849 CAPLUS

[10] Shinohara, Nobuyoshi; Nakamura, Yayoi. **Photochemical reactions of the oxoperoxovanadium(V) complex in an acidic aqueous solution.** Bull. Chem. Soc. Jpn. (1989), 62(3), 734-7. CODEN: BCSJA8 ISSN:0009-2673. CAN 110:240029 AN 1989:240029 CAPLUS

[11] Brazdil, James F.; Toft, Mark A.; Bartek, Joseph P.; Teller, Raymond G.; Cyngier, Roseann M. **Sol-Gel Method for Preparing Vanadium-Antimony Oxide Catalysts.** Chem. Mater. (1998), 10(12), 4100-4103. CODEN: CMATEX ISSN:0897-4756. CAN 130:17634 AN 1998:678102 CAPLUS

[12] Vilter, H., Phytochemistry (1984), 23, 1387-1390.

[13] Toft, Mark A.; Brazdil, James F., Jr.; Glaeser, Linda C. **Catalyst and catalyst precursor containing vanadium oxide and antimony oxide.** U.S. (1988), 6 pp. CODEN: USXXAM US 4784979 A 19881115 CAN 110:83015 AN 1989:83015 CAPLUS

[14] Butler, Alison; Clague, Melissa J.; Meister, Gretchen E. **Vanadium Peroxide Complexes.** Chem. Rev. (Washington, D. C.) (1994), 94(3), 625-38. CODEN: CHREAY ISSN:0009-2665. CAN 120:288314 AN 1994:288314 CAPLUS

[15] Schwendt, P.; Pisarcik, M. **Raman spectral study on the structure of vanadium(V) oxodiperoxo complexes in aqueous solution.** Spectrochim. Acta, Part A (1990), 46A(3), 397-9. CODEN: SAMCAS ISSN:0584-8539. CAN 113:14011 AN 1990:414011 CAPLUS

[16] Conte, Valeria; Di Furia, Fulvio; Moro, Stefano. **The chemistry of peroxovanadium species in aqueous solutions. Structure and reactivity of a neutral diperoxovanadium complex as provided by 51V-NMR data, ab initio calculations and kinetic results.** J. Mol. Catal. A: Chem. (1997), 120(1-3), 93-99. CODEN: JMCCF2 ISSN:1381-1169. CAN 127:100328 AN 1997:343826 CAPLUS

[17] Pierre, Alain C., **Introduction to Sol-Gel Processing**, Kluwer Academic Publishing (1998), p. 13

[18] Jolivet J.P., Henry M., Livage J., **"De la solution a l'oxyde"**, InterEditions/CNRS Editions, Paris (1994)

[19] Livage, J., **Sol-gel synthesis of heterogeneous catalysts from aqueous solutions.** Cat. Today(1998) 41, 3-19

[20] Ditte A. C.R. Acad. Sci. Paris (1885) 101 698

[21] Muller, E., Z. Chem. Inde Kolloide (1911) 8 302

[22] Ostermann, W., Wiss. Ind. Hamburg (1922) 1 17

[23] Pozarnsky, G. A.; McCormick, A. V.. **51V NMR and EPR study of reaction kinetics and mechanisms in V2O5 gelation by ion exchange of sodium metavanadate solutions.** Report (1993), (Rept. No. TR-7; Order No. AD-A266956), 27 pp. CAN 123:153661 AN 1995:757102 CAPLUS

[24] Aldebert, P., Haesslin H., Baffier N., Livage J., **Vanadium pentoxide gels III. X-ray and neutron diffraction study of highly concentrated systems: one dimensional swelling.** J. Colloid Inter. Sci (1984) 98(2) 478

[25] Livage, J.; Henry, M.; Sanchez, C.. **Sol-gel chemistry of transition metal oxides.** Prog. Solid State Chem. (1988), 18(4), 259-341. CODEN: PSSTAW ISSN:0079-6786. CAN 111:141135 AN 1989:541135 CAPLUS

[26] Henry, M., Jolivet J., Livate J., **Aqueous Chemistry of Metal Cations: Hydrolysis, Condensation and Complexation.** J Struct. Bond. (1992) 77 154

[27] Gharbi, N., Sanchez C, Livage J, Lemerle J., Nejem L, Lefebrvre J., **Mixed valence polyvanadic acid gels.** Inorg. Chem., (1982) 21 2758-2765

[28] Hioki, S., Ohishi, T., Takahashi, K., Nakazawa, T., J. Ceram. Soc. Jpn., Int. Ed., (1989), 97, 617

[29] Babonneau, F., Barboux, P., Josien, F, Livage J, J. Chim. Phys (1985) 82 761

[30] Livage, J.. **Vanadium pentoxide gels.** Chem. Mater. (1991), 3(4), 578-93. CODEN: CMATEX ISSN:0897-4756. CAN 115:57777 AN 1991:457777 CAPLUS

[31] Livage, J.; Henry, M.; Sanchez, C.. **Sol-gel chemistry of transition metal oxides.** Prog. Solid State Chem. (1988), 18(4), 259-341. CODEN: PSSTAW ISSN:0079-6786. CAN 111:141135 AN 1989:541135 CAPLUS

[32] Bailey, J.K., Nagase, T., Pozarnsky, G.A., McCartney, M.L., **Better Ceramics through Chemistry IV.** Mat. Res. Soc. Proc. (1990) 180 759

[33] Heller, W., **In Polymer Colloids II.**, Ed. Fitch E.,; Plenum Ress: New York, 1980; p. 153

[34] Legendre, J., Livage, J., J. Colloid Inter. Sci. (1983) 94, 75

[35] Aldebert, P., Baffier, N., Gharbi, N., Livage J., J. Mater. Res. Bull. (1981) 16, 669

[36] Barboux, P., Morineau, R., Livage J., Solid State Ionics (1988), 27, 221

[37] Harris, R.K. **Nuclear Magnetic Resonance Spectroscopy**; Wiley & Sons: New York, 1986: p 144

[38] Alonso, B.; Livage, J. *J. Sol. State Chem.* **1999**, 148, 16.

a)

940 cm^{-1}
917 cm^{-1}

b)

1006-1001 cm^{-1}
980 cm^{-1}
935 cm^{-1}
840 cm^{-1}
595 cm^{-1}
550 cm^{-1}
450 cm^{-1}
320 cm^{-1}

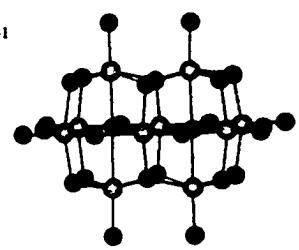

Figure 2. Laser Raman bands and structure of a) dioxovanadium cation, and b) decavanadate anion.

a)

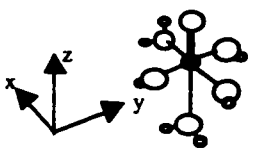

b)

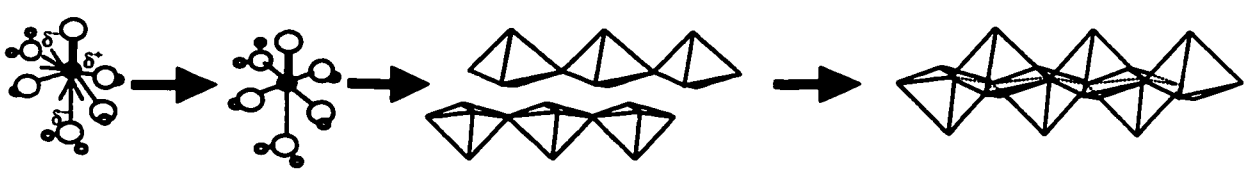

coordination expansion olation (fast) oxolation (slow)

Figure 3. a) Inequivalent directions in the proposed intermediate and b) neutral $[VO(OH)_3]^o$ coordination expansion,chain and double chain formation.[19]

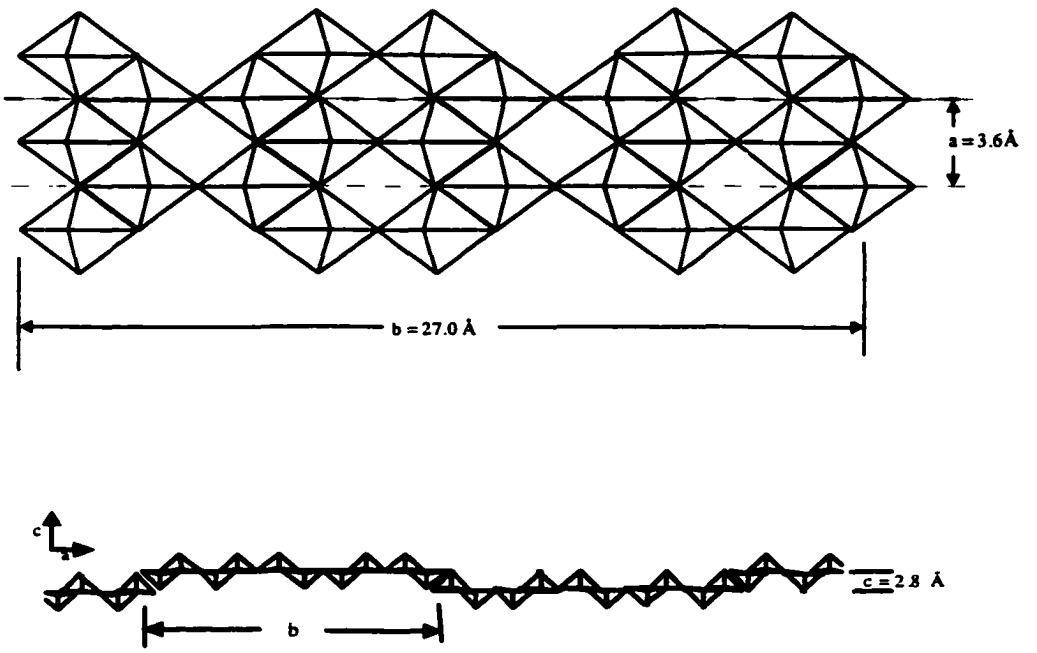

Figure 4. V_2O_5 ribbon structure.[34]

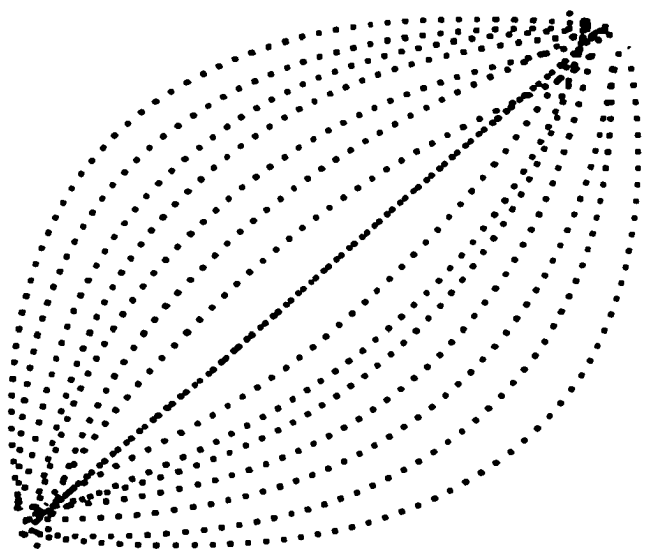

Figure 5. Tactoid Schematic

CHAPTER 3

Vanadia Gel Synthesis via Peroxovanadate Precursors. Part I: In Situ Laser Raman and ^{51}V NMR Characterization of the Gelation Process

A Manuscript Published in the Journal of Physical Chemistry B (2000), 104, 16622

Craig J. Fontenot*+, Jerzy W. Wiench+, M. Pruski+, and G. L. Schrader*+#

Department of Chemical Engineering and*
Ames Laboratory – USDOE+
Iowa State University
Ames, IA 50011

Abstract

Vanadium oxide gels derived from aqueous solution of V_2O_5 and H_2O_2 have been investigated using in situ ^{51}V NMR and laser Raman spectroscopic techniques. On the basis of this characterization, a pathway for peroxovanadate decomposition has been proposed, including the presence of two peroxovanadate dimers. New Raman bands and assignments for these species are reported. Gelation was observed to begin both before and after the peroxovanadate decomposition, depending on the initial molar ratios of H_2O_2/V and the total concentration of vanadium. Experimental ^{51}V NMR evidence suggested that the VO_2^+ species was directly involved in the formation of the gel.

key words: V_2O_5 gels, peroxo vanadate characterization, in situ laser Raman spectroscopy, in situ ^{51}V NMR spectroscopy

---

 # author to whom correspondence should be addressed

3.1 Introduction

Transition metal oxides such as MoO_3, WO_3, TiO_2, and V_2O_5 can be prepared by the dissolution of metals, metal oxides, or metal salts into aqueous solutions of H_2O_2. [1, 2, 3] V_2O_5 materials prepared by this chemistry have important electronic and ionic properties utilized in antistatic coatings, battery cathodes, and electrical components. Extensive work has been performed on the convenient synthesis of V_2O_5 gels from H_2O_2 and $NaVO_3$, including a process involving ion exchange.[4, 5] More recently, the preparation of materials ($V_2O_5 \cdot nH_2O$) by a sol-gel procedure utilizing V_2O_5 has also been reported.[6] Peroxovanadates derived from V_2O_5 are attractive precursors to vanadia gels in that they are inexpensive and fairly easy to handle. Gel formation occurs quite readily, but as for alkoxide sol-gel preparation routes, the reactivity of the precursor solutions depends on pH, temperature, and reactant concentrations.

Our interest in peroxovanadates is based on their use for catalyst synthesis via sol-gel chemistry.[7, 8] Using this route, we have been able to prepare a wide range of mixed metal oxide catalysts that are active for reactions such as the conversion of 1,3-butadiene to valuable selective oxidation products. Preparation of binary and ternary materials having wide ranges of composition and solid solution behavior has been possible. Bradzil et al. have described the preparation of vanadium-antimony oxide catalysts for the selective oxidation or ammoxidation of several hydrocarbons.[9,10] The advantages of these materials were increased catalytic activity, milder preparation conditions, homogeneous distribution of the metal constituents, increased surface area and porosity, and resistance to attrition[11]. These improvements were attributed to the microcrystalline nature of the catalyst resulting from thermal treatment of the sol-gel material. The driving force for

the preparation of these catalysts was thought to be a redox reaction between the V^{5+} peroxo complex and Sb^{3+} (Sb_2O_5) which formed a vanadium antimonate xerogel comprised of V^{4+} and Sb^{5+}. These researchers also suggested that additional characterization of the sol-gel chemistry and the reaction mechanisms would be desirable, especially using *in situ* spectroscopic techniques.

Characterization of reacting species during formation of a gel is challenging, and only a few techniques are likely to be applicable and informative under *in situ* conditions. Both laser Raman and NMR spectroscopies have been previously used by our research group for *in situ* characterization of catalysts. Prior research has indicated that formation of several vanadium peroxo complexes species is likely and that interconversion may be relatively easy. The reaction of metavanadate salts and H_2O_2 in aqueous solutions has been characterized by Raman,[12, 13, 14, 15] ^{51}V NMR,[16, 17, 18, 19] ^{17}O NMR,[18] and UV visible spectroscopy, [9, 20] Although most of the recent literature is in general agreement regarding the identification of these species, discrepancies still exist regarding the structure of the complexes and the spectral assignments. Some researchers have been able to directly relate characterization of the precursor species to V_2O_5 gel formation. The condensation of vanadates from a metavanadate precursor was studied by McCormick et. al..[4, 5] An ion-exchange column was used to obtain an acidic solution containing the dioxovanadate cation and protonated forms of the decavanadate anion. Using ^{51}V and ^{17}O NMR to follow the reaction, these researchers reported that the dioxovanadate cation was the initiator for condensation. The V_2O_5-H_2O_2 preparation route may be expected to behave similarly to the $NaVO_3$-H_2O_2 method, and further characterization utilizing ^{51}V NMR spectroscopy has been performed by Livage et al..[6]

These researchers demonstrated that dissolution of the oxide led to the formation of unstable diperoxo $[VO(O_2)_2]^{2-}$ species which decomposed to form monoperoxo species $[VO(O_2)]^{+}$. Vanadate and decavanadic acid entities were then produced before polymerization formed $V_2O_5 \cdot nH_2O$.

The research reported here has focused on the combined used of laser Raman and ^{51}V NMR to elucidate the sol-gel chemistry relevant to the preparation of active, selective, and stable selective oxidation catalysts involving V_2O_5 and other components. In order to provide a clearer basis for identification of the vanadate species present in aqueous H_2O_2 solutions, we will first summarize the assignment of spectral features observable by laser Raman and NMR spectroscopies. We will then discuss the *in situ* characterization of four representative samples, emphasizing procedures relevant to V_2O_5-based catalysts. More extensive characterization of the final solid state material and the catalytic activity will be reported in other publications .[7, 8]

3.2 Experimental

3.2.1 Sample Preparation. Preparation conditions for the V_2O_5 gels are summarized in Table 1 (samples A, B, C, and D). 0.1 M peroxovanadate solutions were prepared by addition of 30% H_2O_2 (Fisher Chemicals) to slurries of de-ionized water and V_2O_5 (Alpha Aesar). 0.5 M peroxovanadate solutions were prepared by addition of V_2O_5 to H_2O_2. Temperatures were controlled using a Brinkmann Instruments circulating liquid bath. Samples A, B, and C were maintained at 25 °C. Preparations at high concentrations of V_2O_5 or H_2O_2 at 25 °C were completed within a minute; thus for sample D, the temperature was reduced to 5 (±1) °C in order to perform the *in situ* characterization studies.

3.2.2 Characterization

3.2.2.1 Laser Raman Spectroscopy. Laser Raman spectra were obtained using Coherent 532-50 diode-pumped laser (532 nm, 50 mW at the source) and were collected at 180° using a Kaiser probe head coupled via fiber optics to a Kaiser Holospec f/1.8 spectrometer. For Raman characterization, the temperature was controlled using a water-jacketed *in situ* flow cell. For high concentrations of vanadium (> 0.5 M), laser-induced decomposition was observed at room temperature, as reported by other researchers. To avoid sample decomposition, a Bruker RFS-200 FT Raman Spectrometer (1024 nm, 50 mW at the source), was used to confirm spectral assignments. Liquid samples were also spun to reduce sample heating and decomposition.

3.2.2.2 ^{51}V Nuclear Magnetic Resonance. ^{51}V NMR spectroscopy was performed at 9.4 T using a Chemagnetics™ Infinity spectrometer operated at 105.17 MHz. Liquid samples were placed in glass tubes for use with a standard Chemagnetics 5-mm probe. Measurements were performed at temperatures between 5°C and 25°C (± 0.5°C). Typically, 30-120 spectra were obtained during the sol-gel processes which required up to 140 h. Due to fast longitudinal relaxation, a delay of only 50 ms between scans was needed to record fully equilibrated magnetization. Approximately 720 scans were collected to produce an intense ^{51}V signal. Liquid spectra exhibited narrow resonances that could be assigned to various reaction products and intermediates. The concentrations of various species were determined using deconvolution and integration software available from Spinsight™. The liquid state spectra reported in this work do not include the V^{4+} species, which are paramagnetic. In addition, the solid products of our synthesis

'drop out of sight' as they condense at the bottom of the NMR tube, outside of the coil. Even if they remained in the coil, however, they would not be observable in the static NMR experiments due to the chemical shift anisotropy and quadrupolar broadening. A detailed solid state NMR analysis of the solid products of our synthesis is described elsewhere.[21] All spectra are reported with reference to vanadium oxy-trichloride ($VOCl_3$), using the δ scale with negative values being upfield.

3.2.2.3 pH Measurements. All pH measurements were taken using an Orion Model 410A meter and an Orion Ross Sure-Flow glass body electrode

3.2.2.4 UV-Visible Spectroscopy. Spectra were obtained using a Shimadzu UV 3101PC instrument with a 0.01 cm pathlength. Application of this technique was difficult since some vanadium species exhibit photochemical sensitivity: for example, the monoperoxo cation has been reported to decompose at wavelengths of 313, 365 and 436 nm.[20] Evolution of O_2 during the reaction was also problematic since bubbles tended to collect on the cuvette walls.

3.3 Results

A large number of vanadate complexes were observed in solution during the gelation procedures employed in these studies. Therefore, a summary will be provided of the results obtained with laser Raman and NMR spectroscopies, the primary techniques used in this study. Subsequently, utilization of these techniques to examine gelation phenomena under *in situ* conditions will be discussed. Although the LRS and ^{51}V NMR spectra correlate quite well, some subtle differences may be apparent: the time noted in the LRS spectra may be

slightly different than the time noted in the NMR spectra., although the difference likely is not greater than 1 minute. Other techniques were also employed in this research, and the results will be described as appropriate.

3.3.1 Characterization of Species Observed in Peroxovanadate Solutions

The peroxovanadate species observed in our experiments and their corresponding Raman and ^{51}V NMR assignments are summarized in Table 2. The species present in solution were a function of total concentration of vanadium, H_2O_2/V molar ratio, and pH. To facilitate the discussion, these species are identified in boldface numerics.

At concentrations of vanadium of 0.01 mol/dm^3 or less, concentration ratios of $H_2O_2/V = 2$, and pH < 7, the reaction of H_2O_2 with V_2O_5 resulted in coordination of either one or two bidentate O_2^{2-} ligands. These peroxo species interconverted as pH was altered. Both the mono- (**1**) and diperoxo (**2**) complexes have been reported to be fairly stable within specific pH domains, although the monoperoxo cation has been observed to be a better oxidant than the diperoxo anion.[22] Laser Raman spectra of **1** and **2** have been previously reported.[12, 23, 24] For our studies the V=O stretches for these species were observed at about 977 and 985 cm^{-1} respectively; the δ(V=O) deformations were observed at about 314 cm^{-1}, consistent with other studies.[23, 24] The bidentate peroxide ligand has local C_{2v} symmetry resulting in three IR and Raman active modes: the O_p-O_p stretch, the symmetric ν^1(V-O_p) stetch, and the asymmetric ν^3(V-O_p) stretch. For **1**, the coordination is symmetric, and the symmetric and asymmetric stretches [ν^s(V-O_p) and ν^{as}(V-O_p)] overlap around 540 cm^{-1}. Diperoxo complexes can have pentagonal

pyramidal or pentagonal bipyramidal coordination (**2, 3, 4**).[24] For **2**, the presence of the additional bidentate peroxo ligand (in addition to the coordinated water molecule) increases the bond length of V-O_{cis} relative to V-O_{trans} (Figure 1), where O_{cis} and O_{trans} denote the oxygen atoms adjacent to, or across from, the coordinated water ligand. This asymmetry results in a splitting of the symmetric and asymmetric V-O_p bands,[15] so that the symmetric ν^1(V-O_p) band was observed at about 633 cm^{-1} and the asymmetric ν^3(V-O_p) band was observed at about 542 cm^{-1}. Although the O_p– O_p bond in **2** is longer than in **1**, there was no distinguishable difference in the position of the observed band.[15] It should also be noted that in the case of an unidentate, end-on coordinated hydroperoxide, only one V-O_p stretch would be observed, and an OOH deformation should be observed above 1100 cm^{-1}.[25]

The ^{51}V NMR peak for **1** was observed at -541 ppm. Conte et. al.[17] reported a shift of -540 ppm. For **2**, a peak was present at -695 ppm, which Conte et.al reported at -692 ppm. The peak at -705 ppm was assigned to **3**. This species reported was observed in one other study to have a shift of -702 ppm.[17] Species **4**, observed at –749 ppm, was previously reported[16] to have a ^{51}V NMR peak at -746 ppm.

In our studies we also detected Raman bands for a symmetric diperoxovanadate dimer (**5**) and an asymmetric peroxo-dimer (**6**). Bands at 960, 910 and 598 cm^{-1} were assigned to **5**, which probably corresponded to V-O_b-V, O_p-O_p and the V-O_p vibrations, respectively. Since the V-O-V stretch was observed near the V=O stretch (~ 995 cm^{-1}), a linear μ_2-bridging oxygen ligand (O_b) having some π character was likely present. The absence of splitting of the symmetric and asymmetric V-O_p stretches was consistent with the lack of H_2O coordination in the same plane as the η^2-peroxo ligands. Therefore, the

local structure of each vanadium was octahedral, not pentagonal bipyramidal. Bands at 955, 910, 599, and in the 400 and 500 cm^{-1} region were assigned to the asymmetric dimer, **6**. The bands at 955, 910 as well as 599 cm^{-1} were analogous to the symmetrical dimer, while the bands between 400 and 500 cm^{-1} were assigned to V-OH stretches.

The ^{51}V NMR shift at -670 ppm was assigned to **5**, which is in agreement with a previous report.[16] The shifts at -669 and -674 ppm were assigned to **6**, previously reported to occur at -670.6 and -674 ppm.[18]

^{51}V NMR shifts for the decavanadate anion (**7**) were observed at -425, -502 and -518 ppm. Shifts for this species have been reported[26] to occur at -420, -495 and -510 ppm. ^{51}V NMR shifts for the diprotonated decavanadate (**8**) were observed at -428, -513 and -533 ppm. These were previously reported[4] at -426, -512, and -531 ppm. Raman bands for this species were observed at 1007, 980, 935, 836, 547, and 314 cm^{-1}.

Raman bands for VO_2^+ (**9**) were observed at 940 cm^{-1}. Raman bands for this species have been previously reported[14] at 940, 912 and 348 cm^{-1}. The ^{51}V NMR shifts for **9**, **10**, **11**, **12**, **13**, and **14** were observed at –545, -574, -577, -584, -561, and –754 ppm, respectively. These shifts were previously reported at –545.9 [16], –573.6[27], -577.6[28], -586[28], -562[16] and -760[16] ppm, respectively. Species **15**, **16**, and **17**, previously unreported, were observed at -613, -641 and -720 ppm.

Raman band assignments for the pyrovanadates (**10**) and the cyclic metavanadates $(VO_3)_n^{n-}$ (species **11** and **12**) have been previously reported[28] to occur at 945, 905, 630, 490, and 360 cm^{-1}. For **11**, we observed Raman bands at 948, 900, 635, 490 and 360 cm^{-1}.

3.3.2 Characterization of the Vanadia Gel Formation

SAMPLE A. ^{51}V NMR at 20 min (after peroxide addition) revealed that **2** was predominant [Figure 2(a)]. Also present (in order of decreasing signal intensity) were **5**, **1**, and **3**. Raman data [Figure 3(a)] acquired at this time revealed a very strong band at 537 cm^{-1}, which was assigned to **1** and **2**. The strong band at 598 cm^{-1} was assigned to **5**, while the sharp band at 876 cm^{-1} was assigned to the $\nu(O_p\text{-}O_p)$ stretch of H_2O_2. A broad band between 1023 cm^{-1} and 930 cm^{-1} was assigned to the superposition of the V=O stretch for **2** (990 cm^{-1}), **1** (977 cm^{-1}), and **3** (present in a low concentration). Sharp bands at 893 cm^{-1} and 314 cm^{-1} were assigned to **1** and **2**. The UV-visible spectra of sample 1 showed a shoulder at 330 nm (due to the diperoxovanadate anion) which was observed at 45 min had weakened by 65 min. For 160 min, a broad absorbance was seen at lower wavelengths.

At 40 min, Raman bands emerged at 960 and 911 cm^{-1} [Figure 3(b)]; these features persisted until 68 min. The Raman bands were the most intense from 40 to 60 min [Figure 4(a) and 4(b)]. ^{51}V NMR revealed that **1**, **2**, and **5** [Figure 2(b)] were present at this time, the latter at its maximum concentration. As explained in section 3.1, some Raman bands were assigned to **1** and **2** based on previous work[12]. The Raman bands at 911 and 596 cm^{-1} could not be assigned to either of these species and therefore were assigned to **5**. As time

progressed, the band corresponding to the O_p-O_p stretch (876 cm^{-1}) from excess H_2O_2 decreased in intensity, until its intensity was very low at 68 min. A decrease in the concentration of **2** coincided with the loss of H_2O_2.

At 158 min, ^{51}V NMR characterization revealed the presence of **8**, while **5** had nearly disappeared [Figure 2(c)]. Raman acquired at this time [Figure 3(c)] showed bands characteristic of **8**. The band at 936 cm^{-1} could also be assigned to **9**, but another band at 910 cm^{-1} would also be expected[14]. By 1240 min [Figure 3(d)], bands corresponding to **8** had become more distinct, but little change was observed in the Raman characterization after this time.

At $t > 200$ min, only **1**, **8**, and **9** were present in solution, as clearly revealed by ^{51}V NMR spectroscopy. The concentration of **8** and **9** increased as **1** disappeared (this transformation was nearly complete at about 1400 minutes). At this point, the peaks due to **8** and **9** began to decrease in intensity, coinciding with the initial sol-gel formation. **8** was not detected after about 1800 min, leaving only **9** in solution [Figure 2(d)].

SAMPLE B. At 7 min (pH =1.42), the solution was clear and red. ^{51}V NMR revealed that **2** was the predominant species. Also observed [in order of decreasing signal intensity, see Figure 5(a)] were **5**, **1**, and **9**. The Raman spectrum [Figure 6(a)] at this time showed a sharp band at 876 cm^{-1} for H_2O_2. Another strong band observed at 538 cm^{-1} corresponded to **2**. The broad band observed between 1000 cm^{-1} and about 960 cm^{-1} involved an overlap of bands for **2** and **5**. A sharp band began to become distinguishable at 890 cm^{-1} and was assigned to **1** and **2**. The band at 597 cm^{-1} was assigned to **5**, while the band at ~315 cm^{-1} was due to **1** and **2** (although **1** was again present in low concentration). A broad shoulder was also observed at

631 cm^{-1} and was assigned to **2**. The UV-visible spectrum of sample 2, taken at 45 min revealed the presence of **2** (330 nm). By 65 min, this maximum had disappeared, but a strong absorbance was observed at $\lambda < 360$ nm.

The ^{51}V NMR spectra obtained between 55 to 80 min revealed interesting transformations: peaks assigned to **2** decreased in intensity, while those for **5** increased to a maximum at ~68 min [Figure 5(b)] then decreased. Meanwhile, **8** appeared at 60 min and increased in concentration. The pH changed substantially in this time domain from ~1.5 at 55 min to ~2.2 at 80 min. The Raman spectra taken at 55 min [Figure 6(b)] and 60 min [Figure 6(c)] showed **5** was at its maximum. As the reaction proceeded, there was a further decrease in intensity of the peroxide band at 876 cm^{-1}, compared to bands for **1** and **2**. At about 70 min the Raman band at 876 cm^{-1} had nearly disappeared, indicating that H_2O_2 was eliminated [Figure 6(d)]. As for Sample A, there was a concomitant decrease in the concentration of **2**. The pH of the solution at this time was 1.45, and without excess peroxide, **1** rather than **2** would be expected to be the dominant species[17, 18]

At 268 min, the solution was a clear and dark red for pH = 2.45. The Raman spectrum showed bands corresponding to **8**. The ^{51}V NMR spectrum showed that in addition to **8** species **1** and **9** were also present [Figure 5(c)]. The Raman spectra did not change significantly at later times.

After 1000 min, the ^{51}V NMR spectrum [Figure 5(d)] showed peaks corresponding to **8** and **9**. At 1600 min, the total vanadium concentration in solution began to decrease, corresponding to the formation of a solid.

SAMPLE C. ^{51}V revealed that up until about 500 minutes, only **2** was found in solution [Figure 7(a)]. Raman confirmed this result [Figure 8(a)]. However, several new species were detected in the ^{51}V spectrum at 562 minutes [Figure 7(b)]. The shifts were, in order of decreasing signal integral: species **2, 4, 13, 12, 8, 10,** and **9**. Except for a decrease in the H_2O_2 band at 875 cm^{-1} and an increase in the shoulder band at 500 cm^{-1}, the Raman spectra [Figure 8(b)] were unchanged at this time. For sample C at 45 minutes, the UV-visible spectra showed a maximum at 330 nm revealing the presence of **2**. However, unlike samples A and B, this maximum persisted throughout the experiment until 160 min. A decrease in the absorbance at 330 nm over time was observed revealing the decomposition of **2**.

By 1770 minutes, **11** and an unknown species (associated with the ^{51}V NMR peak at -613 ppm) had appeared [Figure 7(c)]. The species previously observed were still present although relative concentrations had changed. Raman at this time [Figure 8(c)] revealed a very broad band between 1100 and 910 cm^{-1}, which results from the overlap of several resonances, corresponding to the species **2, 4,** and **10**. Other bands were unchanged.

By 3350 minutes, the ^{51}V NMR peak assigned to **10** was predominant [Figure 7(d)]. At this time the pH was measured to be 6.9, and this species was expected to be present at equilibrium conditions.[27] In fact, except for **2**, the peroxovanadates were no longer present. The Raman spectrum [Figure 8(d)] showed bands at 948 cm^{-1} and 635 cm^{-1} which were assigned to **10**.

SAMPLE D. At 5 minutes, ^{51}V NMR shifts were observed (in order of decreasing signal integral) for **2, 14,** and an unknown species at -640 ppm [Figure 9(a)]. The Raman spectrum at this time [Figure 10(a)] showed a very strong band at 878 cm^{-1}. This band involved both

H_2O_2 (878 cm^{-1}) and **2** (890 cm^{-1}) and also possibly involved overlap with a shoulder at 910 cm^{-1}, perhaps due to **14**. Excess peroxide produced such a large Raman band intensity that the other bands in this region were not discernable. A very broad band observed in the range 1015 to 930 cm^{-1} and a maximum at 994 cm^{-1} resulted from a superposition of several bands involving **2** (990 cm^{-1}) and probably the V-O_b-V stretch of **14** (~955 cm^{-1}). The band at 599 cm^{-1} was assigned to **14** [probably ν(V-O_p)]. The sharp band at 535 cm^{-1} corresponded to **2**.

By 174 min, the Raman shoulder bands at both 955 and 910 cm^{-1} appeared more pronounced [Figure 10(b)]. This observation correlated with the ^{51}V NMR results, which show that the signals due to **14** had increased [Figure 9(b)]. Also, a broad Raman band was observed between 478 and 423 cm^{-1}, that was assigned to V-OH stretches for **14**. Raman spectra at $t > 174$ minutes were difficult to obtain due to the extremely dark color of the solution.

By 341 minutes, the band at 955 cm^{-1} was more pronounced. The bands at 989, 896 and 910 cm^{-1} were also more prominent. All other bands noted at the previous times were still observed [Figure 10(c)]. The corresponding ^{51}V NMR data [Figure 9(c)] showed further increase in the signal due to **14**, along with the unassigned peaks at -640 and -726. Since there were two unidentified species present, the Raman band at 955 cm^{-1} could not be unambiguously assigned.

At 393 minutes, ^{51}V NMR signals for all the species except **2** had increased [Figure 9(d). The signals for **14** were at their maximum. Raman spectra were difficult to obtain due to the darkening of the solution. At that time, Raman bands corresponded to **14** (955, 910,

599, 490-410 cm^{-1}) and **2** (989, 893, 535 cm^{-1}). The band at 878 cm^{-1} was absent indicating that H_2O_2 was no longer present [Figure 10(d)].

At 415 minutes, ^{51}V NMR signals for all previously mentioned species had decreased in intensity. New signals corresponding to **3** and **6** had appeared [Figure 9(e)], with **6** being the prevalent species in solution. At this point, the solution had turned dark red and was sufficiently viscous to effectively trap small O_2 bubbles evolved from the solution. Although Raman data became even more difficult to obtain due to the increasingly dark color of the sample, bands could be observed at 1026, 706, 497, and 268 cm^{-1} [Figure 11(a)]. The band at 1026 cm^{-1} may be the V=O stretch for a short segment of the polymeric chain.

At 485 minutes, ^{51}V NMR showed that the bands due to **3** had increased sharply in intensity, while the concentration of **6** apparently was unchanged [Figure 9(f)]. All other species had decreased in concentration. Again, the solution was very dark and viscous. Raman bands were observed [Figure 11(b)] at 1026, 706, 516, and 268 cm^{-1}. The increased viscosity leads us to believe that the band at 1026 cm^{-1} was the V=O stretch of a short polymer segment.

At 614 min, ^{51}V NMR showed that the concentration of **3** had increased at the expense of **6** [Figure 9(g)]. The total amount of vanadium in solution began to decrease indicating that formation of a solid had begun. By 1011 min, a gel was visible and only **3** and **6** were found in solution [Figure 9(h)]. By 1523 min, the reaction was nearly complete, and a solid had formed. The Raman spectrum of this wet gel showed strong bands at 703, 516 and 271 cm^{-1}. The weak band at 1026 cm^{-1}, previously observed at 485 min, had re-appeared [Figure 11(c)].

3.4 Discussion

3.4.1 Solution Chemistry

Preparation conditions for samples A and B (C_V =0.1 M, peroxide:vanadium = 7.9) were similar, except for the pH: for sample A, the pH was lowered using HCl, while the pH of sample B was unadjusted. The same vanadium species were identifiable for these synthesis conditions, although the time of observation and the relative concentrations of the complexes differed (Figures 12-15). The only exception was the protonated diperoxovanadate species, observed only for sample A. A plausible conversion pathway is given below:

$$V_2O_5 + 2H^+ + 2H_2O_2 + 3H_2O \rightarrow 2VO(O_2)(OH_2)_3^+ \quad (1)$$

$$VO(O_2)(OH_2)_3^+ + H_2O_2 \Leftrightarrow VO(O_2)_2(OH_2)^- + 2H^+ + 2H_2O \quad (2)$$

$$2VO(O_2)_2(OH_2)^- + 2H^+ \rightarrow [V(O_2)_2(OH_2)]_2O^\circ + H_2O \quad (3)$$

$$[V(O_2)_2(OH_2)]_2O^\circ + 3H_2O + 2H^+ \rightarrow 2VO(O_2)(OH_2)_3^+ + O_2 \quad (4)$$

$$2VO(O_2)(OH_2)_3^+ \rightarrow 2VO_2^+ + O_2 + 6H_2O \quad (5)$$

$$10VO_2^+ + 8H_2O \Leftrightarrow H_2V_{10}O_{28}^{4-} + 14H^+ \quad (6)$$

$$VO_2^+ + H_2O_2 + 2H_2O \rightarrow VO(O_2)(OH_2)_3^+ \quad (7)$$

$$VO_2^+ \rightarrow \text{solid} \quad (8)$$

The diperoxovanadate anion was the predominant peroxo species in solution initially. However, the decomposition of the peroxo complexes was thought to occur primarily through reactions (4) and (5) involving the monoperoxo and dimer species. This is in partial agreement with a previous study[19], which reported that the most likely pathway of the η^2– peroxo ligand species was by decomposition of the monoperoxovandate cation. The role of the dimer has not been clearly established previously, and in our studies this major intermediate appears to introduce a new pathway for peroxo decomposition. In another recent study[6] (molar ratio of $H_2O_2/V = 29.4$), an increase in peroxide concentration was observed to have the following effects: (1) the monoperoxovanadate cation was a predominant species in solution; (2) the diperoxovandate anion was stable for a longer time; (3) the dimer was only observed in trace amounts; and (4) the gel formed rapidly. An increase in the H_2O_2/V ratio would initially favor the formation of more monomer than dimer species. A higher concentration of peroxide would also result in a lower pH through reaction (2), and therefore the monoperoxo species would be expected to dominate.

The consistency of the proposed chemistry and the trends in pH are most easily analyzed for sample A since the species evolved in a sequential manner. The Raman spectra showed that H_2O_2 was present until about 40 minutes, so reaction (2) continued until this time. The cycle, monoperoxo→diperoxo→dimer→monoperoxo [reactions (2), (3) and (4)] continued as long as excess peroxide was available. The pH remained constant during this cycle, which indicated that in the absence of other reactions the rate of reaction (2) equaled the sum of the rates of reactions (3) and (4). Once the excess peroxide had been consumed, reaction (2) ceased (H^+ was no longer produced), and reaction (5) proceeded. Reactions (3)

and (4) still occurred, although now without reaction (2) occurring the pH was observed to increase.

Eventually, all of the peroxo complexes decomposed, and at long times (> 150 minutes), only the diprotonated decavanadate anion, the dioxovanadium cation, and the monoperoxovanadate cation were detected. The relative concentrations of the first two species mentioned remained relatively constant until the monoperoxovanadate cation had disappeared. The protonated diperoxovanadate complex was existed only in the presence of excess H_2O_2 and in highly acidic solutions (pH < 1). As the monoperoxovanadate cation disappeared, the over-all vanadium concentration in solution as detected by ^{51}V NMR began to decrease, indicating that the polymerization process had begun. For sample A, polymerization began at about 1700 minutes, and proceeded rapidly until the decavanadate ion was depleted (Figure 13). In sample B, the same trends were observed although the decavavanadate ion was not depleted (Figure 15). In both samples A and B, the decavanadate ion acted as the source of vanadium in solution [reaction (6) reverse].

3.4.2 Gelation

Gelation occurred only in the presence of the VO_2^+ cation (i.e. samples A, B, and D) and was believed to proceeed via a similar mechanism as reported by other authors,[4, 29] with the VO_2^+ cation being directly involved. Gelation was not observed in samples that did not contain the VO_2^+ cation (i.e. sample C where the diperoxovanadate decomposed slowly to form the expected equilibrium species [Figure 16]).

Samples A, B and D yielded solids of very similar composition, as will be detailed in the second part of this study.[21] The condensation/gelation processes that

occurred in samples A and B were believed to occur as the VO_2^+ cation or a reactive intermediate[4,29] reacted through oxolation to form chains. The exact precursor for polymerization is still unclear, but involvement of the VO_2^+ species is strongly indicated. Livage[29] has stated that the neutral $VO(OH_3)$ species is the reactive precursor. $VO(OH)_3$ has been reported[30] to be formed via the hydroloysis of VO_2^+ as:

$$VO_2^+ + 2H_2O \leftrightarrow H^+ + VO(OH)_3^\circ{}_{(aq)}$$

This neutral species has only been observed at total vanadium concentrations of 0.0001 M or less.[30] Coordination then increases through water addition as:

$$[VO(OH)_3]^\circ + 2H_2O \rightarrow [VO(OH)_3(OH_2)_2]^\circ$$

The neutral vanadium is proposed to be six-fold coordinated with one water coordinated trans to the V=O bond (in the axial or z-direction) and the other water opposite an OH group on the equatorial plane. The V-O bonds of the equatorial plane are non-equivalent in the x and y direction. There are two OH groups in the x direction, while in the y direction there is an OH group and H_2O (Figure 17). Condensation proceeds much faster along the direction containing the OH group and the H_2O. This occurs via olation since a good nucleophile (OH) and a good leaving group (H_2O) are present. Olation does not require a proton transfer and proceeds quickly, forming a chain-like polymer. Oxolation, which does require an internal proton transfer, proceeds at a slower rate along the direction containing the two OH groups and connects the chains to form ribbon structures (Figure 17).

For both samples A and B, the resulting gel was initially brown, but within hours the color turned dark red. Work done by McCormick, et al.[4, 5] on the condensation of an acidified metavanadate solution discussed several possible routes of $[V^{5+}O_2]^+ \rightarrow$ polymer. Using ESR, they reported detecting small amounts of $[V^{4+}O]^{2+}$. Although present at very low concentrations (~ 0.001 M), they proposed that the dimerization of the $[V^{(5+)}O_2]^+$ and $[V^{4+}O]^{2+}$ to form a mixed valence species might initiate polymerization[31]. However, their experiments utilized an ion exchange column, which according to their report,[4] was the source of the V^{4+} needed to initiate this dimerization. In the current work, an ion exchange column was not utilized, but a similar polymerization process likely occurred. Since V^{4+} cannot be observed using the NMR techniques used in this work and since the total concentration of vanadium in solution remained constant until polymerization began, the amount of V^{4+} present, if any, is very small. If V^{4+} existed during our preparations, the source might be attributed to: (1) the reduction of the dioxovanadate cation (observed in acidic media[32]):

$$[V^{(5+)}O_2]^+ + 2H^+ + e^- \rightarrow H_2O + [V^{(4+)}O]^{2+}$$

and/or (2) the reduction of V^{5+} to V^{4+} with O_2^- to form a V^{4+}-OO moiety. This reaction has also been reported in the literature[33]. McCormick et al.[4] concluded that the most likely route was as follows:

$$H_2V_{10}O_{28}^{4-} + 14\,H^+ \rightarrow 10\,[V^{5+}O_2]^+ + 8\,H_2O$$

$$[V^{5+}O_2]^+ + [V^{4+}O]^{2+} \rightarrow V_p^{\bullet} + 8\,H_2O$$

$$V_p^{\bullet} + [V^{5+}O_2]^+ \rightarrow V_p + V_p^{\bullet}$$

$$V_p \rightarrow V_h + H^+$$

where V_p is the vanadium site in the polymer, V_p^* is the reactive site on polymer, and V_h is the hydrolyzed polymer.

We did not observe any polymerization in samples A and B until all of the peroxovanadates had decomposed. For sample A, this occured at about 1400 minutes and in sample B at about 1600 minutes. Since H_2O_2 has been reported[33] to oxidize V^{4+} to V^{5+}, it is conceivable that the monoperoxovanadate cation oxidizes the available V^{4+}, effectively scavenging the proposed initiator and stopping polymerization. Polymerization began either at exactly the same time, or immediately after the monoperoxovandate cation had entirely disappeared. Other authors have reported that V^{4+} can be considered a polymerization initiator.[33], [34] In sample D, gelation began much sooner, at about 600 minutes (Figure 19), even though the temperature was much lower. Gelation began and proceeded in the presence of several peroxovanadates, some of which are still unknown. It is not clear whether these were involved in gel formation or were simply trapped within the gel matrix. By 1000 minutes the entire liquid volume and the remaining species in solution were trapped within the solid matrix. The resulting material was initially green, but within hours it had turned dark brown. The initial green color might be attributed to the shorter chain lengths of the polymer, or it may indicate that the gel had more than 20% of the vanadium present as V^{4+}. [35]

As the polymerization proceeded, broadening of the VO_2^+ peak was observed in some of the samples. At the same time, the FWHM of the dioxovanadate ^{51}V NMR peak in sample A remained relatively constant. Sample B behaved quite differently, as the FWHM of this same peak increased from a value of 493 Hz at t = 31.5 hours to a value of 1333 Hz at t = 87

hours (Figure 20). The broadening of this peak in sample D was even greater as it was observed to increase from 620 Hz at 600 minutes to 1200 Hz at 1800 minutes. McCormick[4] et al observed some broadening of this peak, although to a much lesser extent. Most likely, this broadening is associated with the reduced mobility of ^{51}V nuclei in increasingly longer polymeric chains. The interaction of observable V^{5+} with paramagnetic V^{4+} may cause additional broadening.

During polymerization of samples A and B, the pH was constant. McCormick et al. [4,5] reported similar observations in the polymerization of an ion-exchanged $NaVO_3$ solution. Since the main source of vanadium in solution was the decavanadate ion, a large number of H^+ were required [reverse of reaction 6] to convert the vanadium (in the form of $H_2V_{10}O_{28}^{4-}$) back to VO_2^+. They concluded that the source of H^+ must not be from the solution. Proposed sources for H^+ were: i) hydrolysis of the dioxovanadium cation according to the reaction:

$$VO_2(H_2O)_4^+ \rightarrow H^+ + VO_2(OH)(OH_2)_3$$

and/or ii) hydrolyis of the polymer by the reaction:

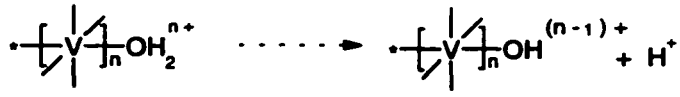

The pH was not observed to change significantly in our experiments as the solid was forming (Figures 13 and 15), so either hypotheses are consistent with our data.

3.5 Conclusions

Our experiments indicate that several peroxovanadate dimers were involved in the η^2-peroxo ligand decomposition. These dimers were present only in excess H_2O_2 and were fairly unstable. Despite this, they were present in appreciable amounts. Raman bands for previously uncharacterized peroxovanadates were observed in several samples. The bands at 960 cm^{-1}, 910 $cm^{-1}$and 600 cm^{-1} were assigned to a symmetrical neutral dimer, $[V(O_2)_2]_2O(OH_2)_2$. This species was only present for lower pH's (samples A and B) and when the diperoxovanadate anion (and excess H_2O_2) was present. A similar dimer was observed in sample D. Raman bands for this asymmetrical dimer ($H_4[(OO)_2OVOVO_2(OO)]$), were observed at 955, 910, 599, and between 500-400 cm^{-1}. Both of these dimers were major intermediates in the reactions we observed.

Solutions having lower peroxide/vanadium ratios and lower total vanadium concentrations formed compounds having similar morphologies. The peroxovanadates present in these samples eventually decomposed before gelation began, leaving a solution containing the diprotonated decavanadate ion and the dioxovanadate cation. Gelation proceeded via the same precursors as previously reported by other authors.[4, 5, 29] The addition of HCl increased the rate of solid formation, while the addition of NH_4OH resulted in the expected equilibrium species(further condensation was not observed). At higher peroxide:vanadium ratios and higher vanadium concentrations, the process differed, and seemed to result in a different material. Even at much lower temperatures, gelation began more quickly and in the presence of several peroxovanadates. When gelation was complete, the aqueous solution initially present was entirely contained within the final solid gel. The morphology of this gel was

different than previously reported.[21] This may be due the shorter polymer segments which were present in this sample.

It has been recently reported[6] that the addition of excess hydrogen peroxide these peroxovanadate solutions only slows the condensation process, but will not lead to a new form vanadium oxide gel. Our results indicate that the addition of excess peroxide increases the duration of the diperoxovanadate stability. But once the excess peroxide has been consumed, condensation begins much sooner. In addition, at higher vanadium concentrations and peroxide:vanadium ratios, different peroxo species were observed. Condensation began while these species were still present and shorter polymer segments were formed.

Acknowledgement: The authors would especially like to thank Dr. R. E. McCarley of the Department of Chemistry and the Ames Laboratory-USDOE for helpful discussions. This work was conducted with support from the Ames Laboratory – USDOE under grant No. W-7405-Eng-82.

3.6 List of Figures

Figure 1. Pentagonal pyramidal structure of diperoxovanadate anion, where X is H_2O.

Figure 2. ^{51}VSolution NMR of sample A at: (a) 20 min (b) 40 min (c) 158 min and (d) 1800 min

Figure 3. Laser Raman Spectra of Sample A at (a.) 20 min (b) 40 min (c.) 60 min (d) 158 min (e) 1240 min

Figure 4. Laser Raman Spectra of Sample A (when dimer was at a maximum) at (a.) 40 min and (b) 60 min.

3.7 List of Tables

3.8 References

[1] Kudo, T.; Okamoto, H.; Matsumotot, K.; Sasaki, Y. *Inorg. Chim. Acta* **1986**, 111, L27.

[2] Aakoi, A.; Nogami, G. *J. Electrochem Soc.* **1996**, 143, L191.

[3] Hinokuma, K.; Ogasawara, K.; Kishimoto, A.; Kudo, T. *Solid State Ionics* **1992**, 507, 53.

[4] Pozarnsky, G. A.; McCormick, A. V. *Chem. Mater.* **1994**, 6, 380.

[5] Pozarnsky, G. A.; McCormick, A. V. *J. Mater. Chem.* **1994**, 4(11), 1749.

[6] Alonso, B.; Livage, J. *J. Sol. State Chem.* **1999**, 148, 16.

[7] Schroeder, W.D.; Fontenot, C.J.; Schrader, G.L., submitted

[8] Schroeder, W.D.; Fontenot, C.J.; Schrader, G.L., in preparation

[9] Brazdil, James F.; Toft, Mark A.; Bartek, Joseph P.; Teller, Raymond G.; Cyngier, Roseann M. *Chem. Mater.* **1998**, 10(12), 4100.

[10] Brazdil, J.F. *CHEMTECH* **1999**, 29, 1, 23.

[11] Toft, Mark A; Brazdil, James F., Jr.; Glaeser, Linda C. U.S. Patent 4784979, **1988**.

[12] Schwendt, P.; Pisarcik, M. *Spectrochim. Acta A* **1990**, 46A(3), 397.

[13] Campbell, Nicholas J.; Dengel, Andrew C.; Griffith, William P. *Polyhedron* **1989**, 8(11), 1379.

[14] Griffith, William P.; Lesniak, P. J. *J. Chem. Soc. A* **1969**, (7), 1066.

[15] Schwendt, P.; Volka, K.; Suchanek, M. *Spectrochim. Acta A* **1988**, 44A(8), 839.

[16] Howarth, Oliver W.; Hunt, John R. *J. Chem. Soc., Dalton Trans.* **1979**, (9), 1388.

[17] Conte, Valeria; Di Furia, Fulvio; Moro, Stefano. *J. Mol. Catal. A: Chem.* **1997**, 120(1-3), 93.

[18] Harrison, Aidan T.; Howarth, Oliver W *J. Chem. Soc., Dalton Trans.* **1985**, (6), 1173.

[19] Jaswal, J.S.; Tracey, A.L. *Inorg. Chem.* **1991**, 30, 3718.

[20] Shinohara, Nobuyoshi; Nakamura, Yayoi *Bull. Chem. Soc. Jpn.* **1989**, 62(3), 734.

[21] Fontenot, C.J.; Wiench, J.W., Pruski, M;, Schrader, G.L. to be submitted (2000)

[22] Conte, V.; Furia, F.; Moro, S. *J. Mol. Cat. A* **1997**, 117, 139.

[23] Schwendt, P.; Pisarcik, M. *Chem. Pap.* **1988**, 42(3), 305.

[24] Schwendt, Peter. *Collect. Czech. Chem. Commun.* **1983**, 48(1), 248.

[25] Butler, Alison; Clague, Melissa J.; Meister, Gretchen, E. *Chem. Rev.* (Washington, D. C.) *1994*, 94(3), 625.

[26] Howarth, O.W.; Richards, R.E. *J. Chem. Soc. A* **1965**, 864

[27] Heath, Elizabeth; Howarth, Oliver W. *J. Chem. Soc., Dalton Trans.* **1981**, (5), 1105.

[28] Griffith, W.P.; Wickins, T.D. *J. Chem. Soc. (A)* **1966**, 1087.

[29] Livage, J.; Henry, M.; Sanchez, C. *Prog. Solid State Chem.* **1988**, 18(4), 259.

[30] Baes, C., Mesmer, R., *The Hydrolysis of Cations*, John Wiley and Sons. New York. 1976; Chapter 10.

[31] Rodriguez, R. *Principles of Polymeric Systems*; John Wiley and Sons. New York, 1988

[32] Latimer, W.M. *Oxidation Potentials*, 2nd Ed., Prentice-Hall, New York. 1952

[33] Liochev, S.; Fridovich, I. *Arch. Biochem. Biophy.* **1991**, 291, 2, 379.

[34] Gharbi, N.; Sanchez, C.; Livage, J.; Lemerle, J.; Nejem, L.; Lefebvre, J. *J. Inorg. Chem.* **1982**, 21, 2758.

[35] Sanchez, C., Navavi, M., Tauelle, F. *Mater. Res. Soc. Symp. Proc.* **1988**, 121, 93

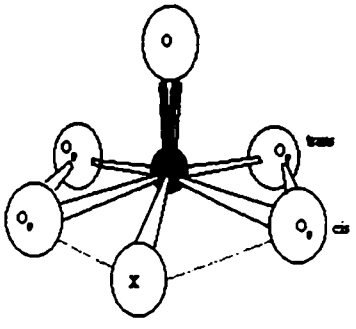

Figure 1. Pentagonal pyramidal structure of diperoxovanadate anion, where X is H_2O.

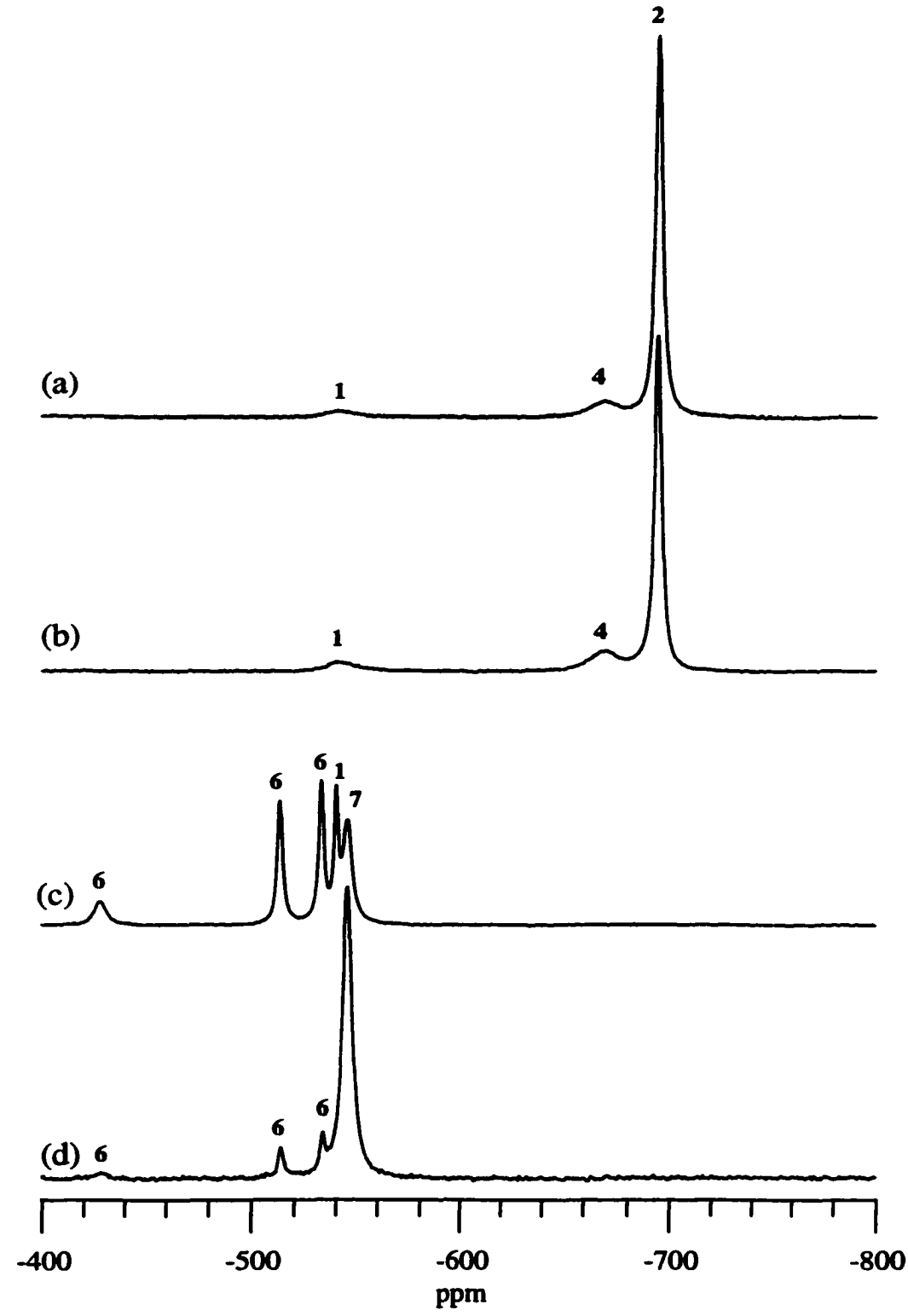

Figure 2. ^{51}VSolution NMR of sample A at: (a) 20 min (b) 40 min (c) 158 min and (d) 1800 min

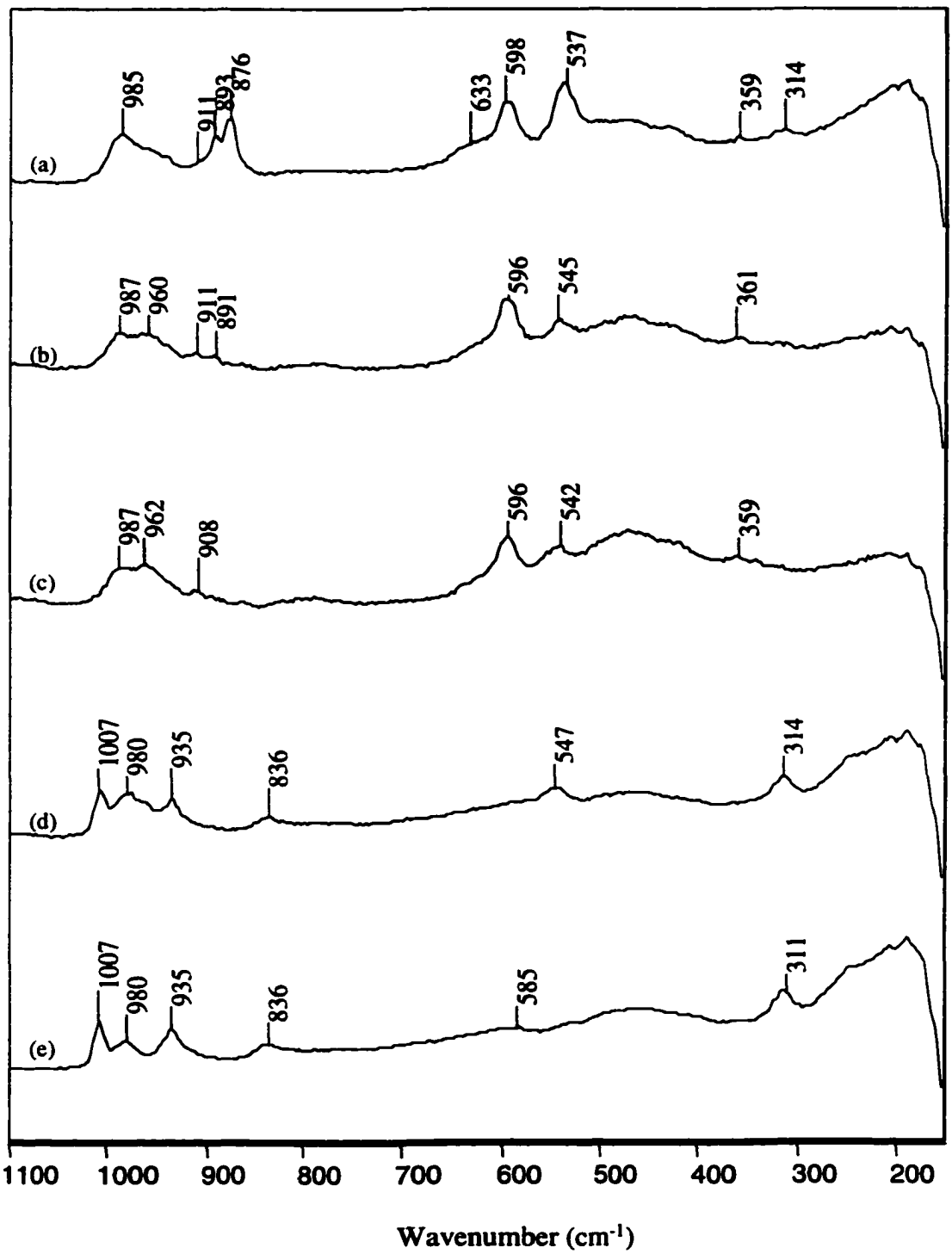

Figure 3. Laser Raman Spectra of Sample A at (a.) 20 min (b) 40 min (c.) 60 min (d) 158 min (e) 1240 min

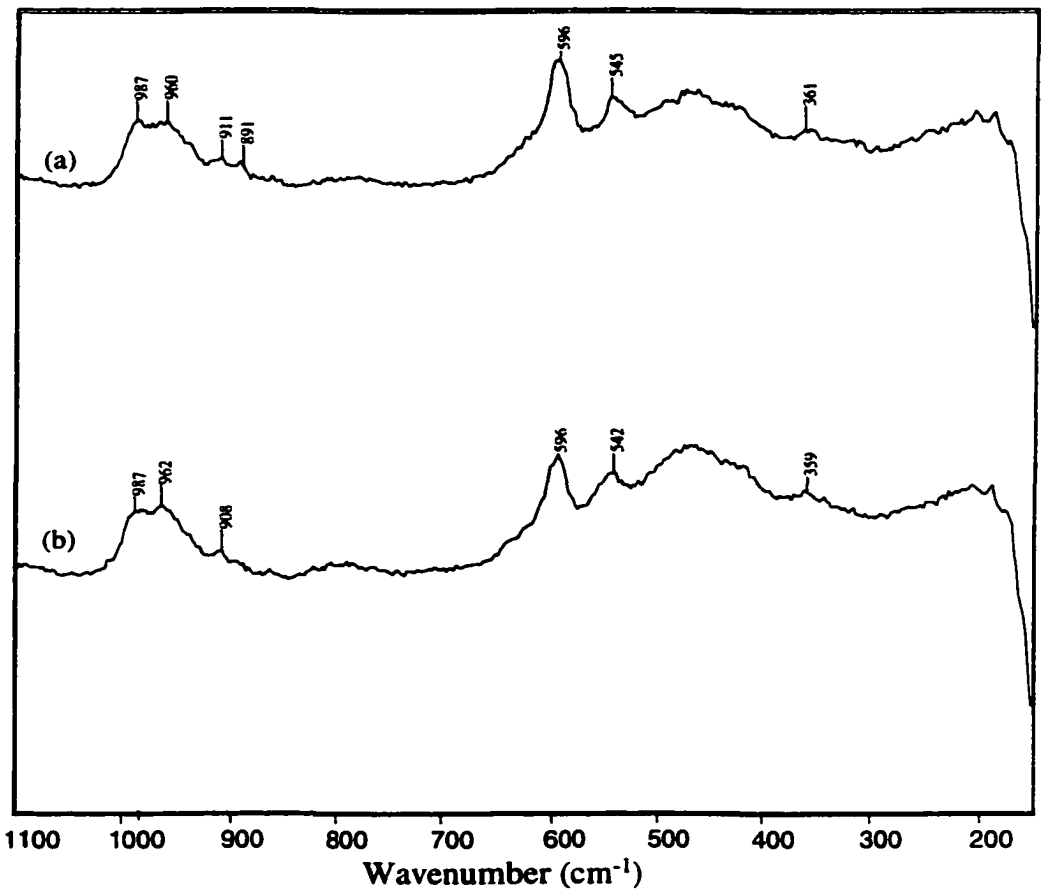

Figure 4. Laser Raman Spectra of Sample A (when dimer was at a maximum) at (a.) 40 min and (b) 60 min

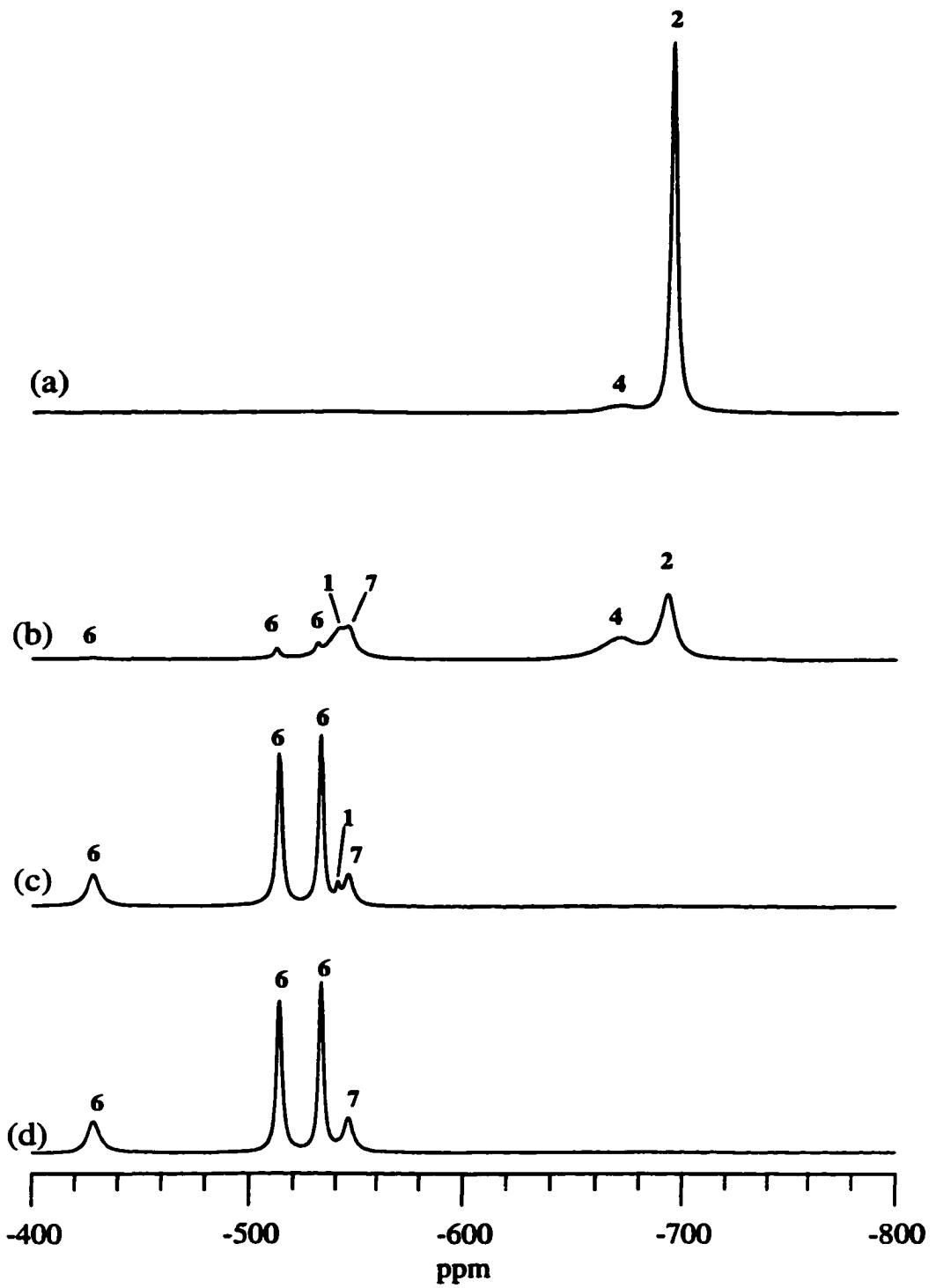

Figure 5. ^{51}V Solution NMR of sample B at: (a) 7 min (b) 68 min (c) 268 min and (d) 1000 min

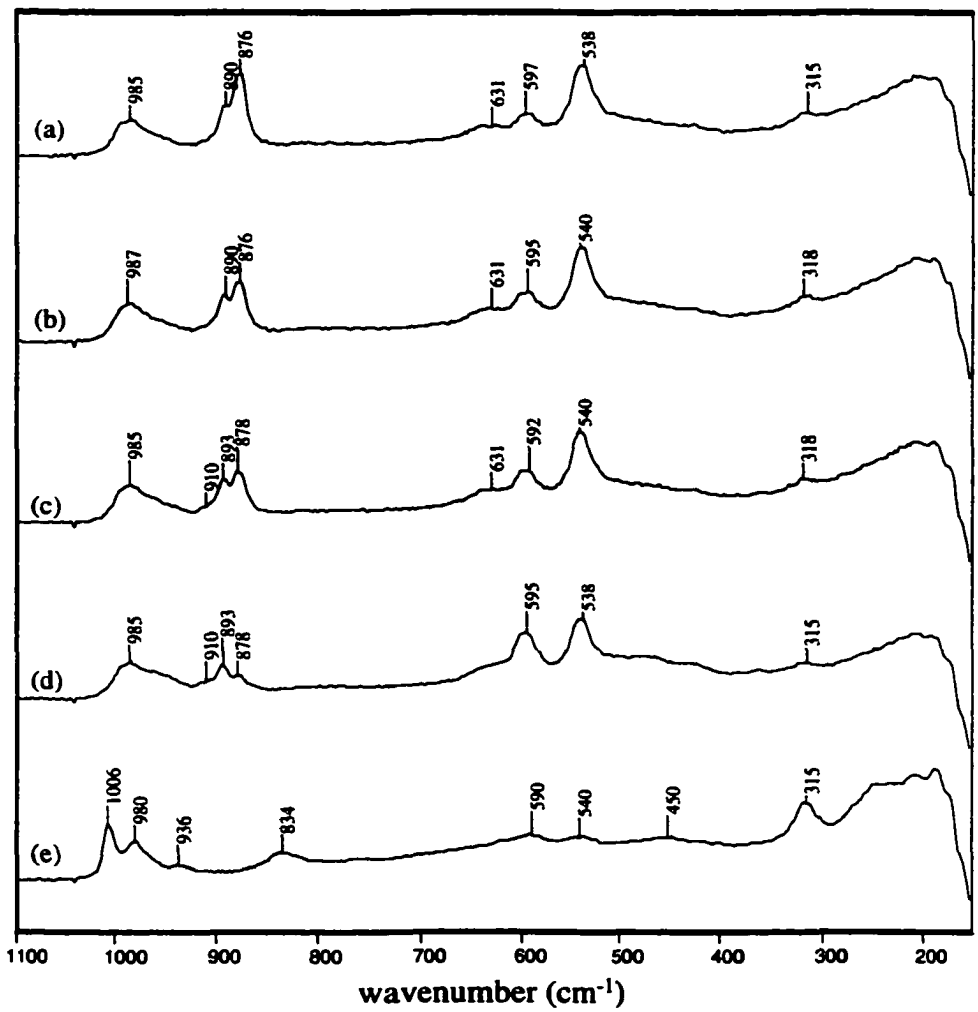

Figure 6. Laser Raman Spectra of Sample B at (a.) 7 min (b) 55 min (c.) 60 min (d) 70 min (e) 268 min

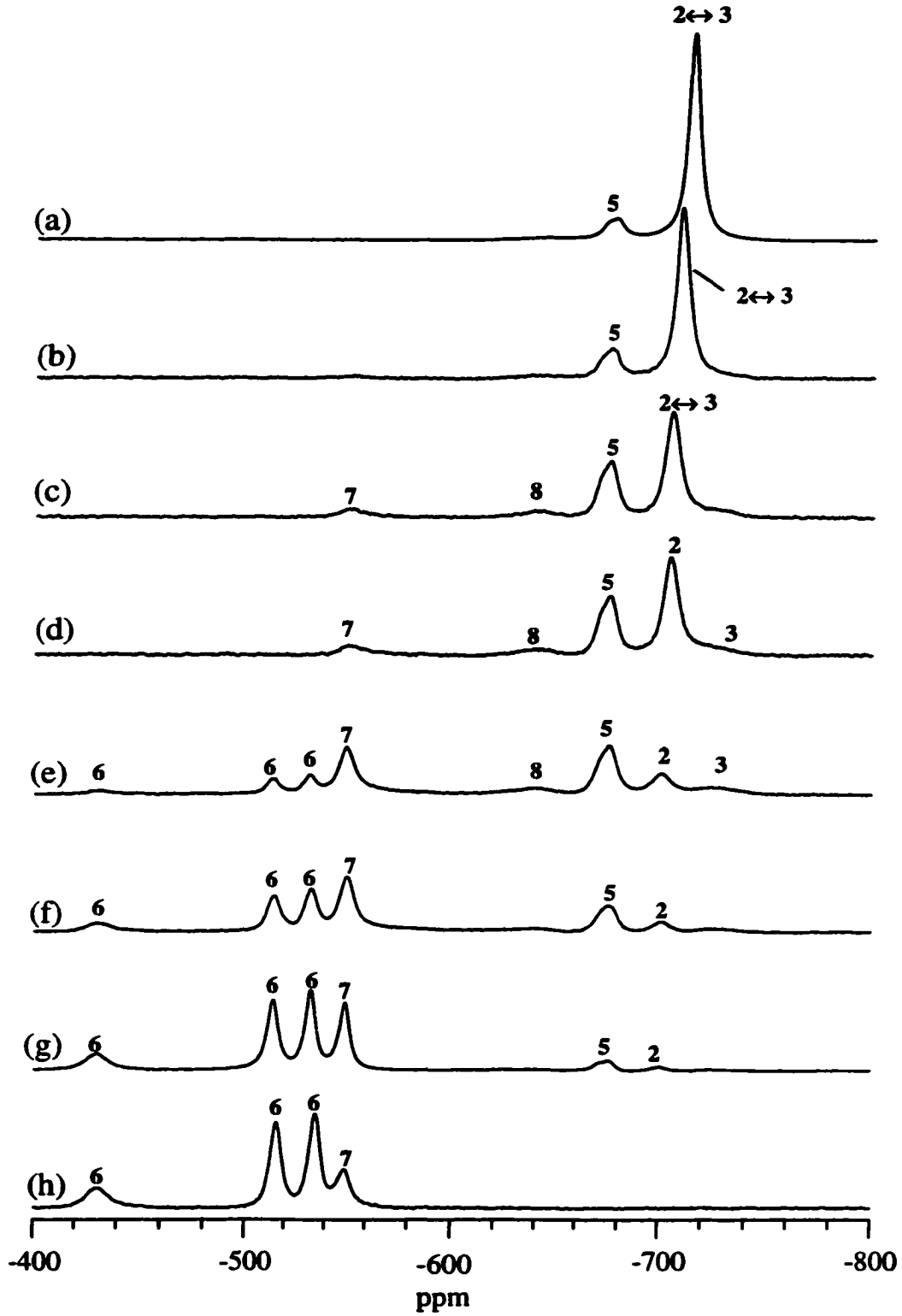

Figure 7. ^{51}V Solution NMR of sample C at: (a) 5 min (b) 174 min (c) 341 min (d) 393 min (e) 415 min (f) 485 min (g) 614 min and (h) 1011 min

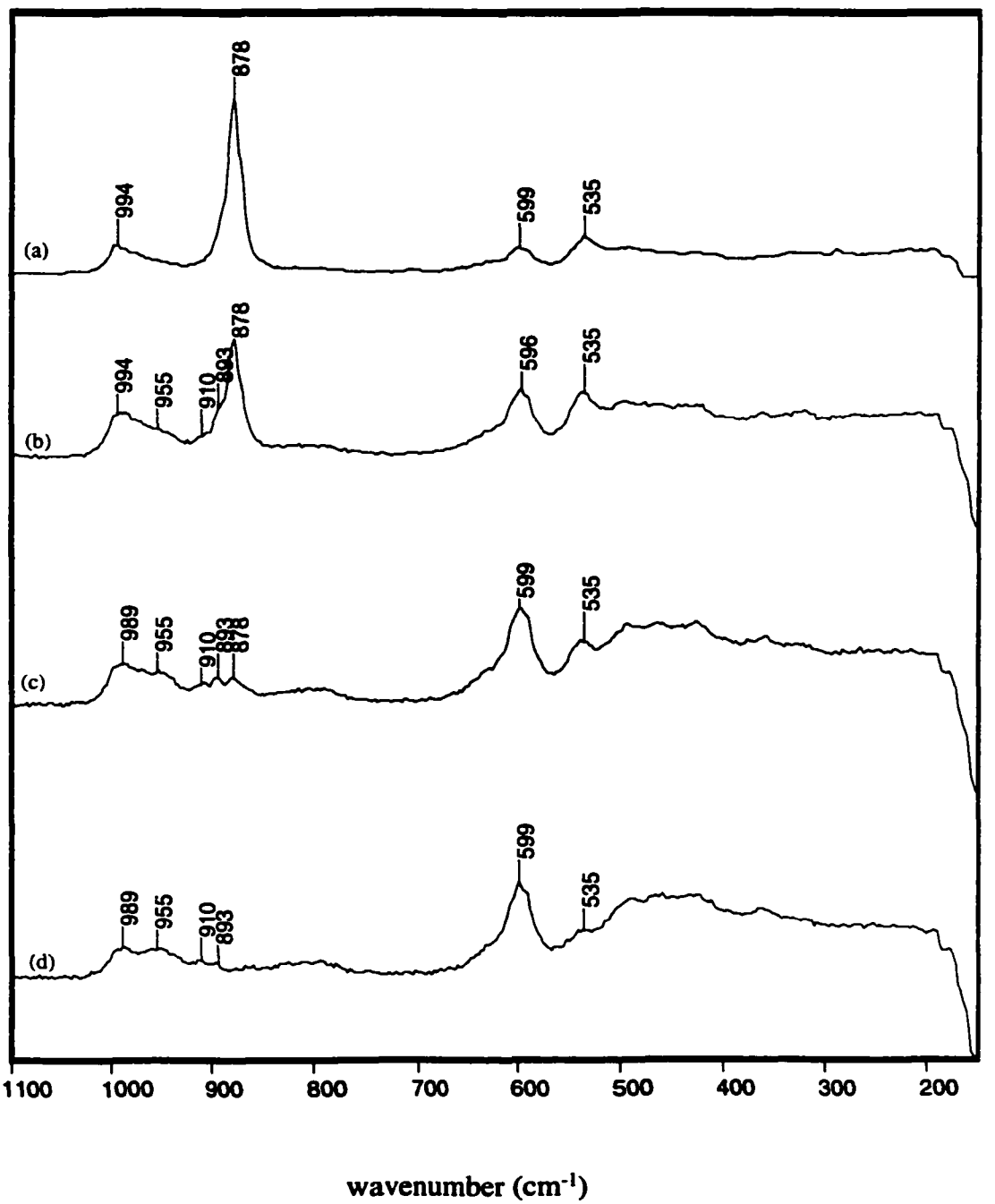

Figure 8. Laser Raman Spectra of Sample C taken at time: (a.) 5 minutes (b) 174 minutes (c) 341 minutes and (d) 393 minutes.

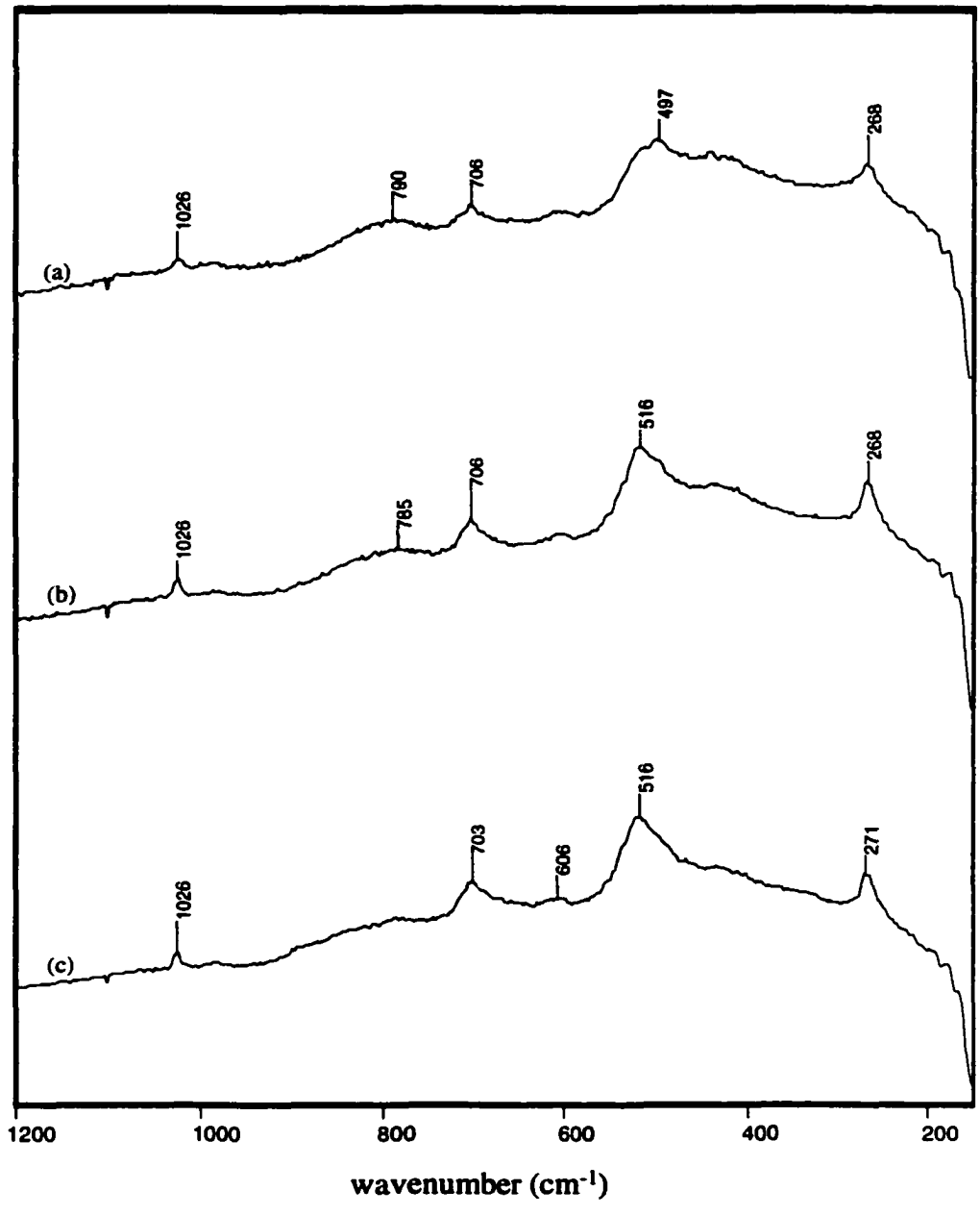

Figure 9. Laser Raman Spectra of Sample C taken at time: (a.) 415 minutes (b) 485 minutes and (c) 1523 minutes.

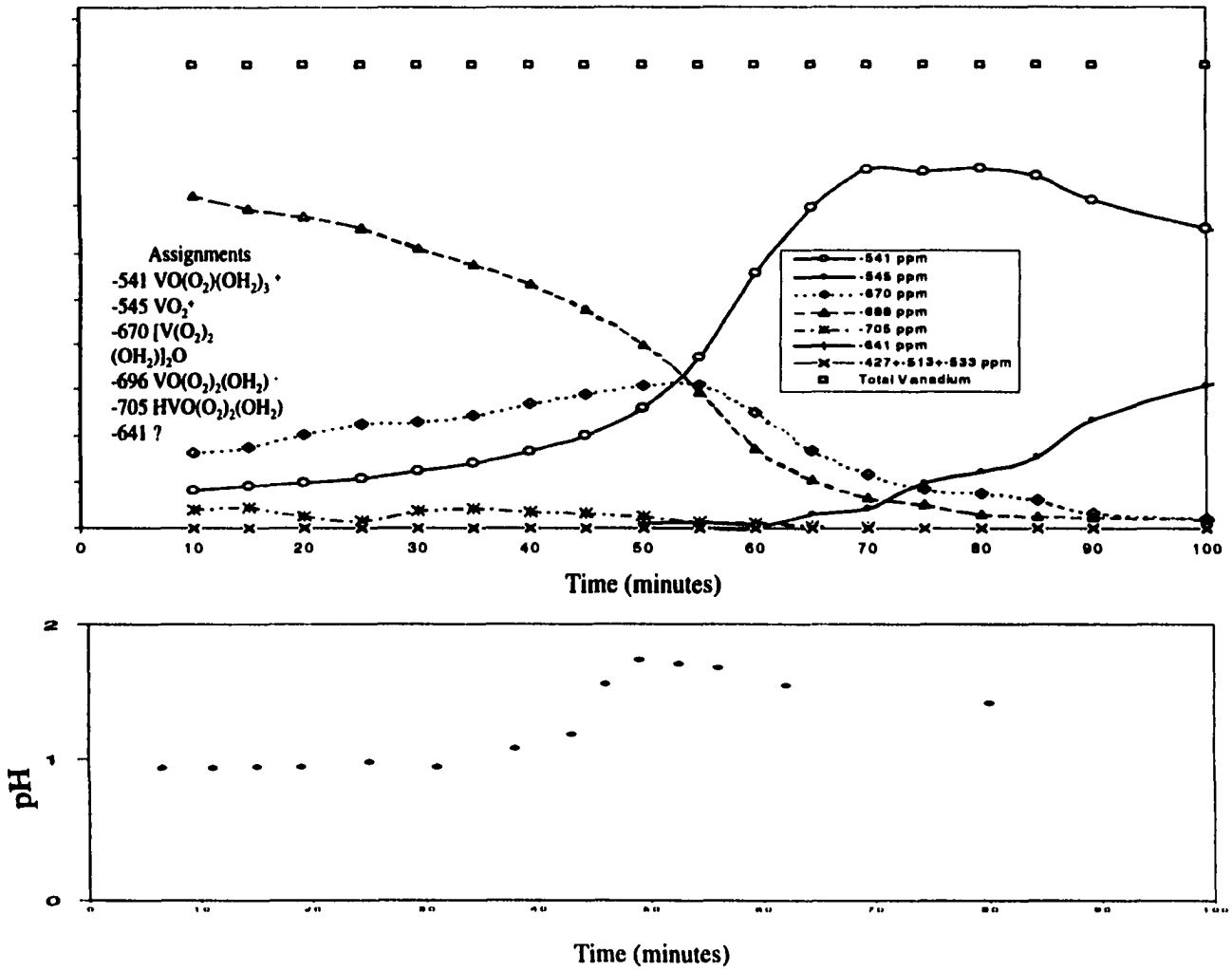

Figure 10. ^{51}V NMR and pH vs time for sample A.

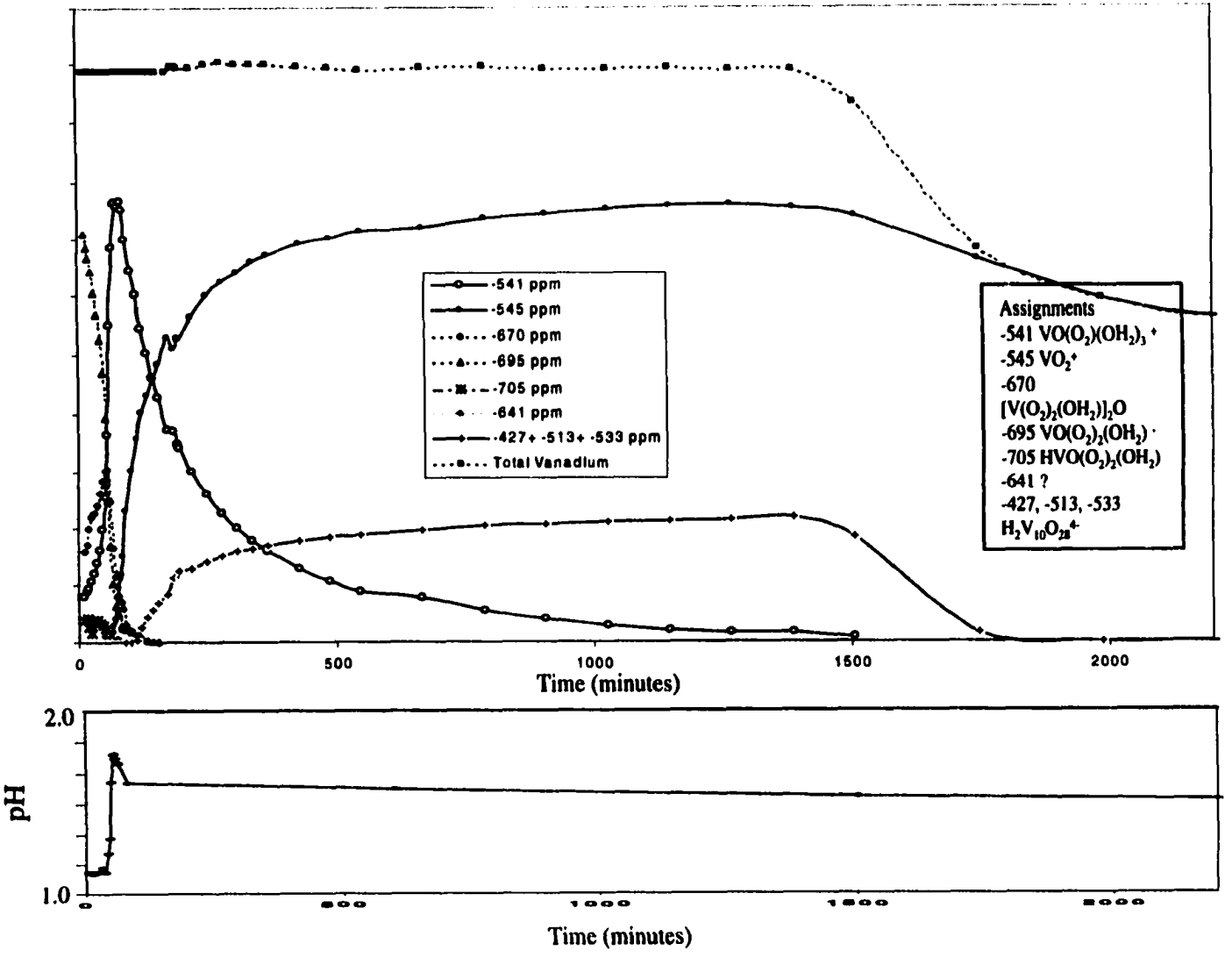

Figure 11. ^{51}V Solution NMR vs time and pH vs time for sample A.

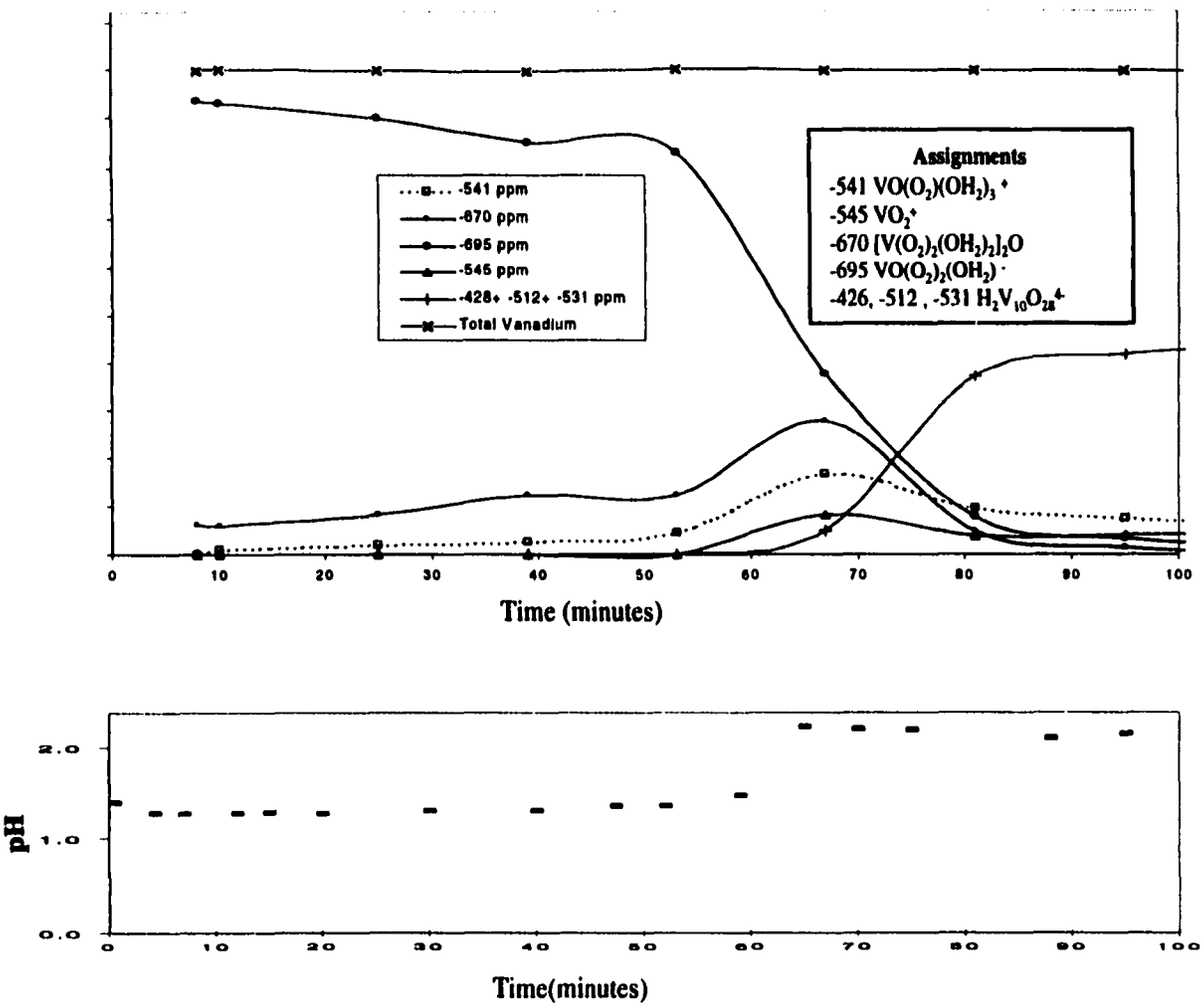

Figure 12. ^{51}V NMR and pH vs time for sample B.

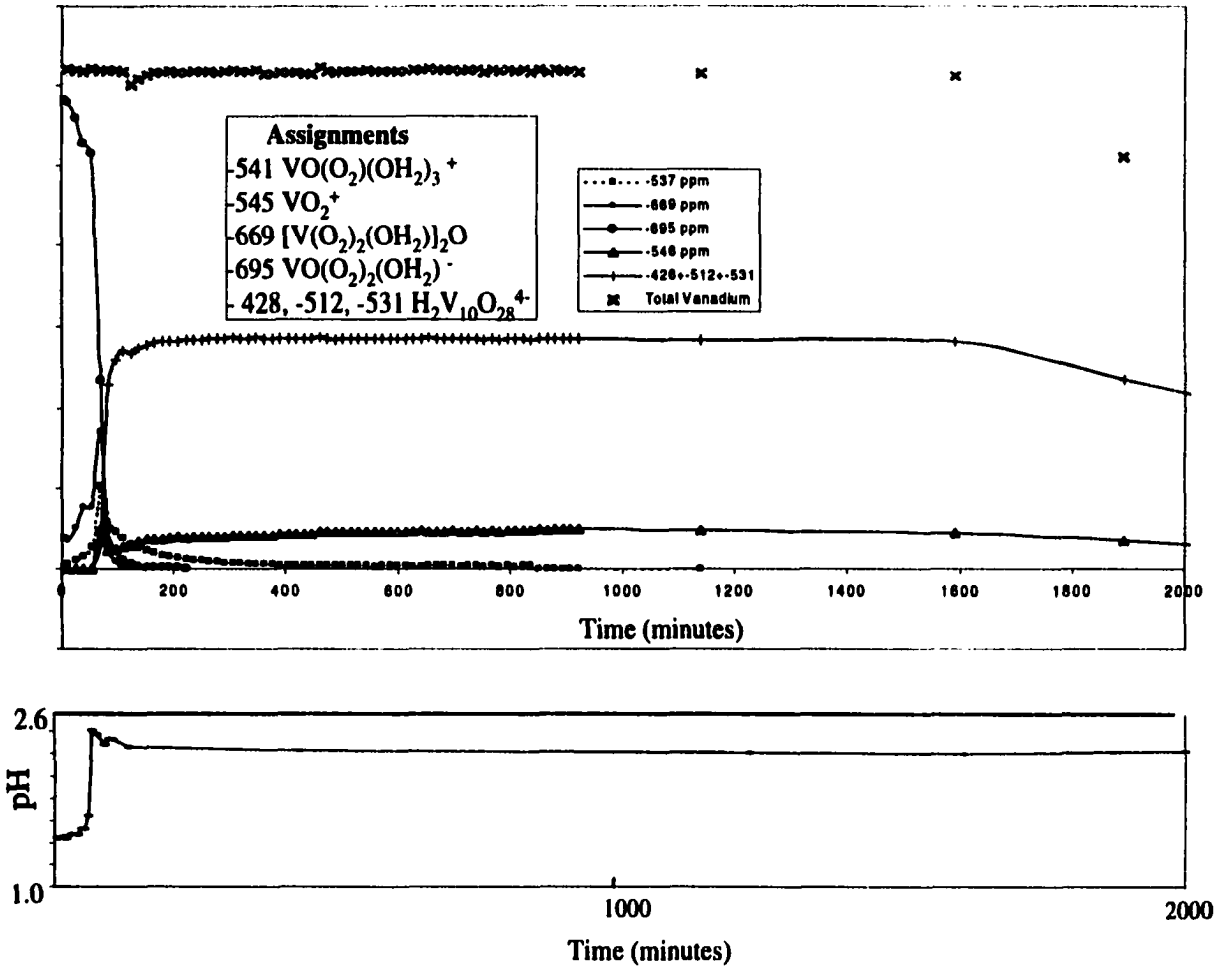

Figure 13. ^{51}V Solution NMR vs time and pH vs time for sample B.

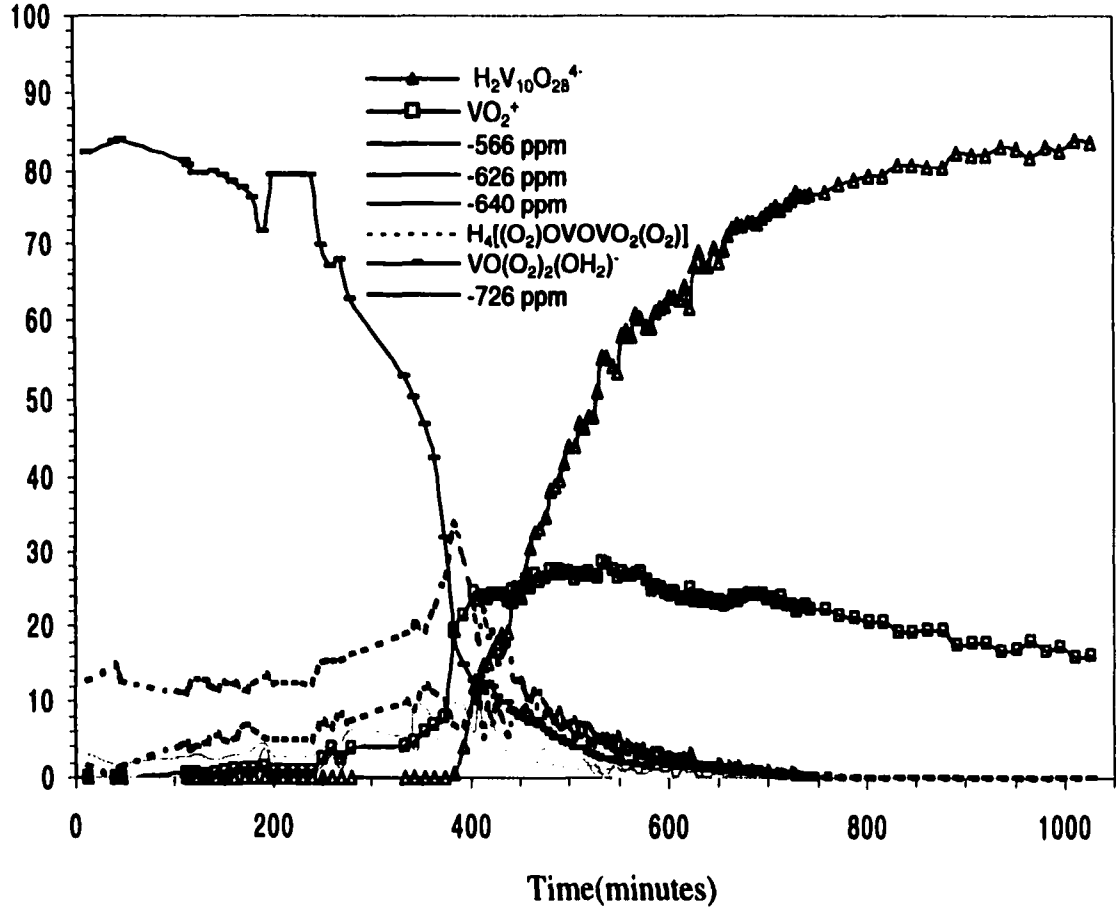

Figure 14. ^{51}V NMR vs time for sample C [normalized to total vanadium in solution]

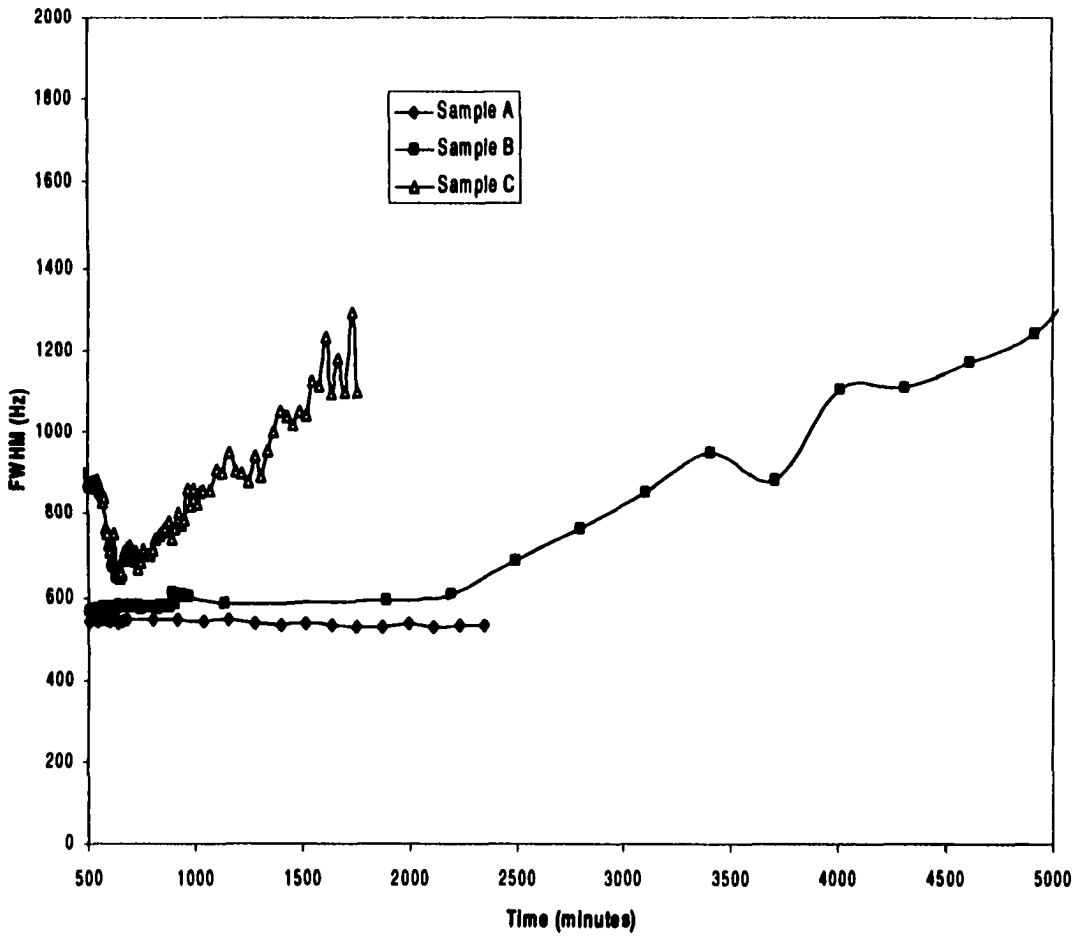

Figure 15. ^{51}V NMR peak width broadening of the VO_2^+ peak in (a) sample A (b) sample B and (c) sample C

Table 1. Summary of Sample Preparation Parameters

Sample	Vanadium Concentration (mol/dm^3)	Temperature(°C)	$n(H_2O_2):n(V)$ Ratio	Initial pH	Final pH	pH adjusted
A	0.11	25	7.9	0.95	1.47	0.58 mL HCl
B	0.11	25	7.9	1.28	2.31	n/a
C	0.11	25	7.9	5.35	7.39	0.85 mL NH_4OH
D	0.50	5	25	0.80	n/a	n/a

Table 2. Laser Raman and ^{51}V NMR Characterization of Species Observed in Peroxovanadate Solutions

	Species		Raman Shift (cm^{-1})	^{51}V NMR Shifts (ppm)	Observed in Sample
1	monperoxovanadate cation	$VO(O_2)(OH_2)_3$ +	977, 891, 542, 314 [977, 890, 540, 320]	-541 [-540]	A,B,D
2	diperoxovanadate anion	$VO(O_2)_2(OH_2)^-$	985, 891, 633, 537 314 [985, 890, 640, 540 320]	-695 (-711) [-692]	A,B,C,D
3	protonated diperoxovanadate	$HVO(O_2)_2$	--	-705 [-702]	A
4	NH_3-ligated diperoxovanadate	$VO(O_2)_2(NH_3)^-$	--	-749 [-746]	C
5	symmetric dimer	$[VO(O_2)_2]O(H_2O)_2$	960, 910, 864, 598	-670 [-670]	A,B
6	asymmetric dimer	$H_4[(O_2)_2OVOVO_2(O_2)]$	955, 910, 599, 490-410	-669, -674 [-670.6, -674]	D
7	decavanadate ion	$V_{10}O_{28}^{6-}$	[991, 960, 955, 910, 840, 595, 543, 463, 356, 322]	-425 [-420] -502 [-495] -518 [-510]	C
8	diprotonated decavanadate ion	$H_2V_{10}O_{28}^{4-}$	1007, 980, 935, 836, 547, 314 [1005, 981, 935, 850, 595, 550, 450 , 320]	-426 - -428 (-426) [-426] -512 - -513 (-509) [-512] -531 - -533 (-532) [-531]	A,B,D
9	dioxovanadium cation	VO_2^+	940 [940, 910]	-545 [-545]	A,B,D
10	diprotonated pyrovanadate	$H_2V_2O_7^{2-}$	--	-574 [-573.6]	C
11	metavanadate	$V_4O_{12}^{4-}$	948, 900, 635, 490, 360 [945, 905, 630, 490, 360]	-577 [-577.6]	C
12	metavanadate	$V_3O_{15}^{5-}$	[945, 905, 630, 490, 360]	-584 [-586]	C
13	--	$[H(VO_3)_2O]^{3-}$	--	-561 [-562]	C
14	--	$[VO_2(O_2)_2]^{3-}$	--	-754 [-760]	C
15	--	?	--	-613	C
16	--	?	--	-641	A,D
17	--	?	--	-720	D

( ) at 5 °C
[ ] Previous literature

CHAPTER 4

Vanadia Gel Synthesis via Peroxovanadate Precursors. Part II. Characterization of the Gels

C.J. Fontenot*+, J.W. Wiench+, M. Pruski+, and G.L. Schrader*+#

A Manuscript Published in the Journal of Physical Chemistry B (2001), 105, 10496

Department of Chemical Engineering and*
Ames Laboratory – USDOE+
Iowa State University
Ames, IA 50011

Abstract

Vanadium oxide gels derived from the reaction of H_2O_2 and V_2O_5 have been investigated using ^{51}V MAS NMR, TGA, XRD, SEM and laser Raman spectroscopy. Based primarily on the ^{51}V MAS NMR and TGA results, the coordination of five distinct vanadia sites has been detailed, which possibly include a previously unreported dimer. The relative concentration of these sites changed as dehydration progressed, and a model of this process has been proposed based on the numerical analysis of the NMR MAS spectra. In addition, the coordination of the most tightly bound water has been postulated. Depending on sample treatment, it was possible to synthesize both layered and non-layered materials. The laser Raman spectra revealed differences between layered and non-layered materials. These differences have been attributed to the interaction of coordinated water molecules, which were trapped between layers and held firmly in place, thus restricting or altering certain Raman-active vibrations.

key words: V_2O_5 gels, ^{51}V MAS NMR spectroscopy

\# *author to whom correspondence should be addressed.*

4.1 Introduction

Vanadia gels have been prepared by polymerizing decavanadic acid, dissolving amorphous V_2O_5 in water, hydrolyzing alkoxides, and ion exchanging a $NaVO_3$ solution.[1] Recently, a sol-gel peroxovanadate route based on the reaction of H_2O_2 with V_2O_5 has been used to prepare these materials.[2, 3] In our previous publication, *in situ* laser Raman and ^{51}V NMR spectroscopic characterization of this gelation process was reported.[3] The chemistry of the gelation was elaborated: the role of various peroxovandate species and the effects of initial H_2O_2/V molar ratio and total V concentration on the reaction pathway were examined. Amorphous and layered materials could be produced by this sol-gel route. In this paper, characterization of the solid (dried) gels is reported using techniques such as ^{51}V NMR spectroscopy, laser Raman spectroscopy (LRS), X-ray diffraction (XRD), scanning electron microscopy (SEM), and thermogravimetric analysis (TGA). Detailed structural information about these gels has been revealed by this characterization.

Aldebert et al. investigated layered gels prepared by the polymerization of a decavanadic acid solution.[4] XRD characterization revealed a strong 00l reflection due to well-organized layers, and the interlayer spacing depended on water content. At room temperature, the separation of layers was near 11.55 Å ($V_2O_5 \cdot 1.6\ H_2O$); after heating to 120° C, layer separation was 8.75 Å ($V_2O_5 \cdot 0.5\ H_2O$). A cross-linked fibrous texture could be observed which was consistent with a well-ordered structure. These researchers also reported vibrational spectroscopic characterization of amorphous gels prepared by grinding amorphous V_2O_5 with water. They reported that the short-range structure of the amorphous V_2O_5 was similar to crystalline (orthorhombic) V_2O_5, and that the addition of

water to the gel drastically modified the Raman spectrum: a shift of the 995 cm^{-1} band to 890 cm^{-1} occurred, and a new band appeared at 711 cm^{-1}. Water solvation was believed to be responsible for the shift of the V=O band to lower frequencies, and the appearance of a new mode was attributed to a V—OH_2 stretch. The general shift of vibrational bands to lower frequencies was associated with weakened V—O bonds which indicated that the 3-dimensional nature of the amorphous oxide had been structurally modified. Formation of molecular or macromolecular species was postulated, although the short-range order of the gel was still believed to be quite well-defined. Preparation of vanadia gels by the dissolution of amorphous V_2O_5 in water was also examined by these researchers.[5] The infrared and Raman spectra of these materials were consistent with prior results: formation of V—OH_2 bonds was proposed, and two different water species were identified, including one which was almost free of hydrogen bonding. Initial adsorption of water was believed to occur on V^{4+} sites. Gharbi et al. considered V^{4+} and V^{5+} species formed by the polymerization of decavanadic acid.[6] Coordination of the V^{4+} species involved six (rather than five) oxygen ions, and solvation by water was believed to be strong.

Abello et al. examined the vibrational spectra of gels having the formula $V_2O_5 \cdot n\ H_2O$, where n = 0.3, 0.4, 0.6, 1.2, and 1.6.[7] All materials were layered, and the short range order was closely related to crystalline V_2O_5. The lowest levels of water were removed at 510 K, just prior to crystallization; therefore, this water was likely strongly bonded or trapped during the dehydration process. For n = 0.6, an interlayer spacing of 8.75 Å was related to the loss of V=O···V bridges, so that the layers were nearly structurally independent. Significant changes in the spectra were observed at this

composition, and an additional type of water coordination to vanadium was postulated. For $0.6 < n < 1.4$, three types of molecular coordination were considered. For $n = 1.6$, filling of the interlayer space with water was likely, with excess water surrounding the gel ribbons or fibers. Further work by this group involved a normal coordinate analysis of the infrared and Raman spectra.[8] Several structural models were considered: 1) a two-dimensional V_2O_5 layer corresponding to crystalline vanadia; 2) a similar two-dimensional layer with all vanadium atoms coordinated to water; 3) a two-dimensional fibril. Changes in the vibrational spectra for the gels were attributed to the creation of terminal bonds on the sides of the fibrils and to the coordination of water molecules to vanadium. These researchers proposed that the existence of a V—OH_2 bond with a force constant of 1 mdyn·Å^{-1} created a bonding environment very different from that for crystalline V_2O_5.

Further work by Livage et al. discussed amorphous materials prepared by rapid quenching of V_2O_5 melts, including reaction with water.[9] Unpaired electrons were believed to be localized on V^{4+} sites surrounded by five oxygen atoms, and the ESR spectra were drastically modified by the adsorption of water. These researchers were among the first to report ^{51}V NMR characterization of vanadia gels: a peak at about -650 ppm disappeared with hydration, but a new peak developed near -340 ppm. Coordination of both V^{4+} and V^{5+} species were modified upon hydration, resulting in an octahedral ligand field with a short V—O bond along the z axis and a weakly bonded water molecule along the same axis in the opposite direction.

Hibino et al. prepared V_2O_5 by reaction of vanadium metal powder with an aqueous solution of H_2O_2.[10] A "two-dimensional" V_2O_5 gel was formed which lost

weight by heating in nearly one step. The structure of the 100°C-treated sample was believed to involve lamella consisting of three a-b planes of orthorhombic V_2O_5 in a parallel and equidistant arrangement; random translation parallel to the layers (for the central plane) and rotation around the c axis was postulated.

Mege et al. prepared thin films of vanadia gels by alkoxide hydrolysis including the use of nonylphenol surfactants to better control the deposition rate.[11] ^{51}V NMR characterization of the wet gels revealed broad peaks at -512 and -532 ppm which were attributed to protonated decavanadate anions, $H_xV_{10}O_{28}^{(6-x)-}$. Other NMR peaks were attributed to several possible precursors/hydrolyzed intermediates or to the surfactant.

McCormick et al. also conducted ^{51}V and ^{17}O NMR studies of V_2O_5 gels prepared by the acidification of metavanadate salt solutions and suggested that polymeric chains of vanadate octahedra were formed.[12,13] Only a single resonance in the ^{51}V MAS NMR spectrum of the wet gel was reported at –547 ppm; no spinning sidebands were observed. These results were consistent with a mobile polymeric chain model in which hydrogen bonding occurred between chains. Luca and Hook, however, did report spinning sidebands for a specific vanadia gel prepared for a study of mesostructured vanadium oxides.[14]

In the current study, we report further characterization of vanadia gels prepared by a sol-gel route involving H_2O_2 and V_2O_5.[3] The use of several complementary techniques has revealed new structural information about these materials. ^{51}V NMR techniques (including modeling of the spectra) has been particularly useful in identifying vanadium environments that previously were not characterized.

4.2 Experimental

4.2.1 Sample Preparation

Samples were prepared as reported previously (summary provided in Table 1).[3] Both non-layered (sample B) and layered (sample B') materials could be produced. For example, if the reacting solution was covered and unstirred, the resulting solid remained suspended in solution; removal of the mother liquor before drying produced a material that had a broad X-ray diffraction pattern. In contrast, if the liquid volume was reduced and stirring was continued during gelation, the material tended to form layers that were oriented parallel to the surface of a substrate or the synthesis vessel.

Spin counting of the ^{51}V nuclei by NMR spectroscopy corresponded well with the total vanadium content determined by inductively coupled plasma-mass spectroscopy (ICP-MS): 95 ± 4 % of the vanadium could be accounted for by NMR (V^{5+}). This is consistent with previous reports that these gels may contain only about 1 % of the vanadium as a V^{4+} species.[15]

4.2.2 Surface Area

Surface areas were determined using the BET method (N_2 adsorption) with a Micromeritics ASAP 2000 instrument.

4.2.3 Laser Raman Spectroscopy

Laser Raman spectra were obtained using a Coherent 532-50 diode-pumped laser (532 nm, 50 mW at the source) and were collected at 180° using a Kaiser probe head coupled via fiber optics to a Kaiser Holospec f/1.8 spectrometer.

4.2.4 Solid State NMR

The solid state NMR spectra of ^{51}V were obtained at room temperature using a Chemagnetics Infinity spectrometer operated at 9.4 T (105.17 MHz). Gels were dried at room temperature, placed in 3.2-mm rotors, and spun at 20 kHz in a Chemagnetics magic angle spinning (MAS) probe. Samples prepared in conjunction with TGA were examined under the same condistions following transfer of the sample to the probe within a glove box under N_2. Wet gels were spun at 10 kHz in a 5-mm MAS probe available from Chemagnetics. The resolution limit for the MAS characterization has also been examined by spinning at 30 kHz in a 2.5-mm MAS probe using a Bruker ASX400 spectrometer.

Static and MAS NMR spectra of ^{51}V were obtained using a Hahn echo sequence ($\frac{1}{2}\pi - \tau - \pi - \tau$ - acquisition) and a high RF field (100 kHz). Additional experiments performed at lower RF fields, with and without the use of an echo, assured us that no distortions were present in these spectra. Typically, 1000 scans were accumulated using a relaxation delay of 0.2 s. Approximate values for the ^{51}V T_1 relaxation times were 30 ms for sample B′ and 15 ms for samples A, B, and C. Quantitative measurement of vanadium content in the gels was performed by extrapolating the intensity of the Hahn echo to $\tau = 0$ and referring it to a known standard (aqueous solution of ammonium vanadate, NH_4VO_3) examined at the same experimental conditions. MAS spectra, which exhibited superimposed, wide patterns of spinning sidebands were analyzed using the QUASAR simulation program.[16] Both central and satellite transitions were taken into account during numerical simulations of the experimental data. The ^{51}V NMR shifts are reported using the δ scale, with positive values being downfield and referenced to $VOCl_3$.

4.2.5 X-ray Powder Diffraction

X-ray powder diffraction data were obtained using (Cu K_α radiation) and a Seimens D500 (50 kV, 27 mA) diffractometer equipped with a diffracted beam monochromator. The detector slit width was 0.05 %, the step size was 0.02, and the dwell time was 1 s.

4.2.6 Scanning Electron Microscopy.

Secondary electron images were obtained on a JEOL 6100 instrument using an accelerating voltage of 15 kV.

4.2.7Thermogravimetric Analysis.

Samples were analyzed using a Perkin Elmer TGA 7 instrument. Heating rates were 1 °C/min in N_2, although selected samples were examined at rates as low as 0.5 °C/min to confirm the procedure.

4.3 Results

^{51}V NMR spectra of as-prepared gels A, B, B', and C (Figure 1) had similar features, both under static and MAS conditions. For all samples, the MAS spectra consisted of superimposed patterns of spinning sidebands representing at least four distinct sites, as most clearly recognized in the spectrum of sample B' (Figure 1c). However, line shape simulations unambiguously indicated that the same resonances were present in all spectra (Figure 1a, 1b and 1d). The center bands for all patterns were positioned near -600 ppm, which is characteristic of vanadates.[17] Simulations of these patterns included the effects of chemical shift anisotropy (CSA) as well as first- and second-order quadrupolar interaction on central and satellite transitions. Several line shape parameters describing these interactions have been

determined by fitting the relative intensity, the quadrupole coupling constant (C_Q), the asymmetry parameter (η_Q), the isotropic chemical shift (δ_{iso}), the CSA ($\Delta\delta_{CSA}$) and the CSA asymmetry parameter (η_{CSA}) for each site. An example of a simulated MAS spectrum is given in Figure 2. The results obtained for sample B' at different temperatures of dehydration are shown in Table 2. The principal components of the CSA tensors (δ_{ii}, i = 1,2,3) are also listed in the table. We note that the simulations included the Euler angles α, β and γ between the CSA and quadrupolar tensors (not shown). However, only angle β, describing the relative orientation of the z axes of the two tensors had a marked effect on the simulated spectra. Thus, we reduced the number of variable parameters by using $\alpha = \gamma = 0$ throughout, in spite of the reports that these two angles may have non-zero values.[18-22] For all sites, the best fits were obtained within the range $53° < \beta < 79°$. For example, for crystalline V_2O_5 we obtained $\beta = 53°$, which is in excellent agreement with reference 18. The relative distributions (%) of each vanadium site (V_i) based on simulations of the MAS spectra are given in Table 3, along with the corresponding amount of coordinated water based on TGA measurements. Broad features present in the baseline of the MAS spectra of Figure 1a, b, and d did not reveal an additional vanadium site: rather, they were due to partial overlap of neighboring sidebands, as confirmed by MAS measurements for sample A at a sample rotation rate of 30 kHz. While this spectrum (not shown) exhibited similar spectral resolution, the broad feature disappeared due to the increased spacing between the sidebands. This broad baseline feature was not observed for the layered sample B' (Figure 1c).

^{51}V MAS NMR characterization was also performed for sample A in a wet gel state (Figure 3). In addition to the solution state resonances for VO_2^+ (at -545 ppm) and $H_2V_{10}O_{28}^{4-}$

(at -426, -516 and -530 ppm), isotropic peaks and corresponding sidebands were observed for several of the solid state sites between -550 and -680 ppm.

TGA of samples A, B, B′, and C (Figure 4) revealed that the weight percentages of water were 18.6, 17.1, 19.2 and 18.6 % respectively, corresponding to n = 2.3, 2.1, 2.4 and 2.3 for $V_2O_5 \cdot n\ H_2O$.

In order to more clearly distinguish the vanadium sites, ^{51}V MAS NMR spectra were obtained for sample B′ after various stages of dehydration following TGA (Figure 5a). The temperature was ramped at a rate of 1 °C/min to temperatures approximately corresponding to the endpoints of the linear regions of the weight loss curve during TGA (Figure 5b). For the as-prepared gel at 25 °C, four vanadium sites were determined to be present (V_1, V_3, V_4, and V_5) ; no changes in the NMR spectra were observed up to 100 °C. However, after heating to 215 °C, an additional site (V_2) was revealed; simultaneously, the NMR characterization indicated that V_3 disappeared completely, V_4 decreased slightly, and V_5 decreased substantially. Heating to 224 °C resulted in an increase of V_1 and V_2 while V_4 and V_5 continued to decrease. V_1 and V_2 were the only sites observed after heating to 272 °C, and V_1 was the only site detected after heating to 550 °C. The relative distribution (%) of these sites at each stage of hydration is provided in Table 3.

The Raman spectra of the non-layered vanadia gels (samples A, B and C) were very similar (Figure 6a, b, and d). A strong band was observed at approximately 998 cm^{-1} with a shoulder at 1008 cm^{-1}, and relatively weak bands were detected around 700, 532, 416 and 291 cm^{-1}. A shoulder feature at about 305 cm^{-1} was observed for each sample. The Raman spectrum of sample B' differed (Figure 6c): the strongest bands were observed at 704 and 668 cm^{-1}, and broad bands were observed at 892 and 512 cm^{-1}. Weak bands were observed at

1027, 1019, and 349 cm^{-1}. The δ (V_2O_b) band, observed at 404 cm^{-1} for crystalline V_2O_5, was not present.[23] No change in the spectrum was observed after heating this sample to 100° C (Figure 7b). However, after heating to 215° C, several spectral changes were observed (Figure 7c). Bands appeared at 995 and 407 cm^{-1}, which were associated with vibrations for V=O and V_2O_b (where O_b is the bridging oxygen), respectively. After heating to 226 ° C, the spectrum was similar to that of V_2O_5 (Figure 7d).

Powder x-ray diffraction (Figure 8) of samples A, B and C showed only broad, weak diffraction peaks with some variation in intensities. Sample B' had very strong reflections corresponding to the 00l planes, indicating a basal plane orientation of the material. The d-spacing of the repeating unit was determined to be approximately 13.2 Å.

The BET surface areas for samples A, B, B' and C were, 1.3, 1.7, 2.0 and 1.7 m^2/g, respectively. Since the surface areas were very low, most of the vanadium can be considered to be in the bulk state, although formation of internal surfaces is quite common in gels.[24]

The SEM micrographs revealed differences in sample morphology. Samples A (Figure 9a) and B had rough surfaces with sharp or abrupt edges. Void spaces having a diameter of approximately 10 μm were apparent. The micrograph of sample B' (Figure 9b) showed orientation of the layers parallel to the substrate surface, and large voids were not present. Sample C (Figure 9c) had a rough surface with smooth edges; voids on the order of 10 μm were observed.

4.4 Discussion

Measurements of the vanadium content of the samples as determined by NMR and ICP-MS were in agreement within experimental error. Thus, the vanadium species

were predominantly in the V^{5+} oxidation state, and the following discussion of the solid state data would be relevant to most of vanadium present in these samples. However, the presence of a small concentration (no more than few percent) of paramagnetic V^{4+} species was likely, as indicated by short relaxation time T_1 of the ^{51}V nuclei. Nayeem and Yesionowski[25] have shown that the dipolar interaction of a nucleus with a thermally averaged magnetic moment $\bar{\mu}_e$ of a paramagnetic electron can produce a powder pattern equivalent to that of a CSA tensor. This effect would influence the intensities of MAS sidebands and could, therefore, influence the results of line shape analysis as summarized in Table 2. However, two experiments were performed that dismissed this possibility. First, additional MAS spectra were obtained between 20 and 150 °C. Analysis of these spectra revealed that the sideband patterns for the gels were not temperature dependent. Since $\bar{\mu}_e$ would be inversely proportional to the temperature (CSA and quadrupolar interactions would not), a narrowing of the MAS sideband pattern should be observed if the paramagnetic coupling was effective. Second, a series of MAS spectra were obtained using a reduced pulse delay between consecutive scans, to approximately one tenth of the average T_1 value. This experiment would selectively increase the contribution of ^{51}V nuclei with shortest T_1, which are expected to reside in the vicinity of unpaired electrons. Again, no changes were observed. Finally, the results of Table 2 were well within the range expected for diamagnetic ^{51}V nuclei.[17] For example, the vanadium site corresponding to a V_2O_5-like structure (see the discussion below) had the same line shape parameters as found for crystalline V_2O_5 by Fernandez et al.[18] No paramagnetic species were present in this material.[26]

Static ^{51}V NMR spectra (Figure 1) revealed that the vanadia gels exhibited large anisotropic broadening. Numerical simulations of such spectra were not feasible because of the similarity and strong overlap of the CSA and quadrupolar powder patterns corresponding to different vanadium sites. However, simulations could be performed using the sideband patterns obtained from the MAS NMR technique for both as-synthesized and thermally treated samples. Sample B' exhibited the best resolution under MAS measurements (Figure 1c), and numerical analysis revealed the full set of line shape parameters for at least four sites (see Table 2). The quality of the fit is clearly demonstrated in Figure 2. Reliable fits for the spectra of other samples could then be obtained by fixing these values and varying only the relative intensities. The chemical shifts (δ_{iso}) were determined to be -623 ppm (V_1), -664 ppm (V_3), -593 ppm (V_4) and -572 ppm (V_5) (Table 2). An additional site (V_2) was evident at –597 ppm after thermal treatment of sample B´ at 272 °C (Figure 5). However, its presence at room temperature was not likely, although this could not be conclusively confirmed because of the proximity to V_4. Therefore, V_2 and V_4 were treated jointly for the simulations.

We note that the above strategy produced remarkably unambiguous sets of line shape parameters, which were verified by conducting extensive searches for other possible minima in the simulation error. The patterns of spinning side bands representing different sites were sufficiently resolved to allow for independent searches of best fitting parameters for each site. Also, we have verified that the error introduced by varying the parameters related to one of the interactions (CSA or quadrupolar) could not be compensated by changing any of the remaining constraints.

In agreement with other studies, the ^{51}V MAS spectra for the gels were dominated by the anisotropy of the chemical shift tensor.[17,18,27] The CSA parameter ($\Delta\delta_{CSA}$) for all vanadium resonances should on the order of 1000 ppm to be consistent with strongly distorted octahedral coordination.[17] Clearly, this is the case for all sites identified in our study. Tetrahedral vanadium sites should be inherently more symmetric so that $\Delta\delta_{CSA}$ would be less than 500 ppm even in the presence of strong distortion.

The V_1 site was readily associated with a V_2O_5-type structure, as depicted in Figure 10a. Values for δ_{iso} and $\Delta\delta_{CSA}$ (Table 2) were similar to those previously reported in single crystal[19] and polycrystalline[18,20-22] studies of V_2O_5. Furthermore, V_1 was the only site observed after complete dehydration and crystallization of sample B´ at 550° C (Figure 5). The charge distribution at this site was dependent on the temperature of thermal treatment, as evidenced by changes in C_Q, η_Q and η_{CSA}. As sample B´ was further dehydrated, these parameters approached those previously reported for crystalline V_2O_5. For example, the symmetry of the charge distribution increased after thermal treatment to higher temperatures (demonstrated by decreasing values for C_Q, η_Q and η_{CSA}) because less water was present to separate adjacent planes. Shifts of the layers relative to each other have also been previously reported in the XRD studies of Hibino et al.[10]

The V_2 site also did not have associated water. TGA indicated that after heating to 272 °C, the dehydration was complete. The corresponding MAS NMR spectrum showed that a resonance at -597 ppm (V_2) was still present (Figure 5a). This site had the largest $\Delta\delta_{CSA}$ and η_{CSA} parameters (see Table 2): therefore, a highly distorted symmetry,

consistent with the proposed coordination (Figure 10b), was present. Apparently, removal of water from the gel resulted in the distorted V_2 sites being created.

Correlation of the TGA data with the relative abundance of sites V_3, V_4 and V_5 revealed that the differences in the local environment of these sites were due to variations in their coordination with water. Four different slopes were apparent in the TGA data for sample B′, which indicated four temperature regions for water loss (Figure 5b). Correlation of these regions with the corresponding MAS spectra was possible, as shown in Figure 5a, and the structure of sites V_3, V_4 and V_5 could be inferred. The chemical shift for site V_3 was close to that for the diperoxovanadate dimer observed in solution.[3] This site might be associated with a similar dimer (Figure 10c) having one water molecule per vanadium and a bridging oxygen atom between the V_3 sites. The lower value obtained for C_Q is consistent with the presence of a water molecule *trans* to the bridging oxygen of the dimer. In addition, the larger value obtained for η_Q could indicate this dimer was located in a terminal position in the layer (i.e. η^2–peroxo ligand on the terminal side). However, definitive evidence, such as Raman bands, for the presence of η^2–peroxo ligands in the gel could not be obtained. This is not surprising, as the dimer site was present in small amounts (~5 %). Still, we cannot rule out the possibility of the oxygen atoms being coordinated to other vanadium sites in a 'dimer-like' environment, rather than as a η^2–peroxo ligand structure. The V_3 site was fairly unstable, and this coordination disappeared after dehydration at 215 °C. The charge distribution around site V_4 was comparable to that for V_1, as indicated by similar values of C_Q and η_Q (Table 2). However, the δ_{33} component of the CSA tensor was much larger for V_4, which could be due to the presence of a water molecule coordinated to the vanadyl oxygen via a hydrogen bond

(Figure 10d). Previous solution-phase studies using ^{51}V NMR have revealed that protonation of an oxygen atom or the presence of a hydrogen-bonded water molecule should not change the vanadium chemical shift by more than 5 ppm.[28] Thus, the 25-30 ppm shift difference observed between sites V_1 and V_4 must be attributed to different interlayer structures, as was postulated for site V_2. The V_5 site had nearly the same C_Q value as V_3 and also had the smallest asymmetry parameters. The most likely assignment of this resonance was a vanadium with the oxygen atom of the water molecule directly coordinated in a *trans* position relative to the vanadyl group, as shown in Figure 10e. However, a structure having an additional water molecule coordinated to the vanadyl oxygen (see Figure 10f) could not be rejected.

The NMR spectral assignments were corroborated by comparing the concentrations of the various detected sites relative to the amount of water lost at various temperatures (see Table 3). Since the ^{51}V MAS spectra of sample B' did not change after heating from 25 to 100 °C (as for the Raman spectra), water lost below this temperature was not chemically bound. Normal tangent procedures were used to analyze the weight loss curves during TGA (Figure 5), and the percentage of water associated with each region of weight loss was determined. The water lost from 100 – 215 °C corresponded to 39% of the bound water present initially; the water lost from 215 – 224 °C corresponded to 51%; and the water lost from 224 – 272 °C corresponded to approximately 10%.

The relative distribution of sites at each temperature as determined by ^{51}V MAS NMR could be successfully correlated with these results, and a comprehensive pathway for the dehydration process was developed (Figure 11). Sites V_2 and V_4 were treated jointly in the QUASAR simulations. However, their presence is clearly supported by the NMR and TGA data, even though they could not be reliably separated using QUASAR due to their proximity.

First, as noted previously, site V_2 (observed at -597 ppm after dehydration at 272 °C) did not have coordinated water. To account for the amount of water determined by TGA at lower temperatures, a water-containing site (V_4) had to be present at around -593 ppm. Indeed, closer examination of ^{51}V MAS NMR spectra revealed that the resonance representing these sites shifted between -593 ppm and -597 ppm as the dehydration progressed. This observation further supported the argument that two vanadium species contributed to this resonance. Second, by using the small changes in the observed shift and the overall stoichiometry as a guide, a consistent description of the dehydration process could be obtained. By assuming that a decrease in the water-containing site concentrations must be associated with a corresponding increase in the water-free site concentrations as dehydration progressed and that no V_2 sites existed below 100 °C, the following contributions of the resonance at around -595 ppm were apparent: 0% V_2 and 45% V_4 below 100 °C, 32% V_2 and 41% V_4 at 215 °C, 57% V_2 and 6% V_4 at 224 °C. This composition was consistent with one water molecule shared between two V_4 sites and one V_5 site and two water molecules being shared between three adjacent V_4 sites and two adjacent V_5 sites.

The ^{51}V MAS NMR spectrum obtained after heating the sample to 215 °C showed that the water-coordinated sites decreased in concentration as a new water-free site (V_2) appeared. After heating to 224 °C, the same trend was observed although this time the site corresponding to crystalline V_2O_5 (V_1) also increased. At this stage, TGA revealed that only 0.03 moles of water per mole vanadium were present. The relative site distribution indicated that these water molecules were most likely shared between two V_4 sites and one V_5 site (Figure 12). To accommodate this type of shared water coordination, one layer would have to shift slightly in the a-b plane. This shift was consistent with the observation of V_2 sites. After

heating to 272 °C, only V_1 and V_2 sites were detected. TGA indicated all water had departed by this temperature, and therefore no water was associated with these sites. Finally, after heating to 550 °C, only V_1 sites resembling crystalline V_2O_5 were observed.

Discrepancies do exist in the literature with respect to the number of moles of water present at each level of gel dehydration for specific desorption temperatures.[7,29,30] Abello et. al[7] suggested that these discrepancies may be attributed to the various heating rates. TGA was performed with sample B´ for heating rates as slow as 0.5 °C/min, but no changes resulted. Our work generally agrees with the report by Aldebert and Livage,[30] although their desorption temperatures were slightly higher. These temperature disparities may be a result of mass transfer limitations imposed by variations in the extent of sample layering. In agreement with earlier studies,[29] the powder XRD pattern for sample B´ revealed significant long-range order, consistent with extended layering. A large percentage of the vanadium was involved in this long-range layering since the diffraction peaks were quite strong relative to the other samples. Apparently, water molecules could be more readily removed from this structure, and linear weight loss slopes were observed during TGA. A random orientation of smaller one-dimensional crystallites would probably introduce some diffusional limitations which could affect the TGA curves for the non-layered samples (Figure 4). The diffraction patterns observed for samples A, B and D were consistent with a layered structure in which one plane was shifted along the a-b plane.[10] However, the intensity of the diffraction peaks was much less than that observed for sample B´, indicating that a smaller percentage (probably less than 10%) of the vanadium participated in this long-range ordered structure.

Previous literature has indicated that the interlayer distance between planes was 11.55 Å for gels produced by the polymerization of decavanadic acid.[4] Another group has reported

two dimensional ordering involving three layers per repeating unit, corresponding to a unit cell size of 11.5 Å; these materials were produced by reacting metallic vanadium powder with H_2O_2 .[10] The repeating unit distance for the layered materials produced in our study was 13.2 Å, although it was not clear if this corresponded to an interlayer distance or if an incommensurate layer was present.

The above ^{51}V NMR results are distinctly different from those reported previously for V_2O_5-based gels. Nabavi and Livage recorded static ^{51}V NMR spectra of amorphous gels produced by rapidly quenching V_2O_5 melts.[9] Resonances were only detected at –328 and –658 ppm which were assigned to five- and four-coordinated sites, respectively. After hydration, only one resonance was present at –340 ppm.[9] ^{51}V MAS spectra of gels formed via ion exchange of a metavanadate solution, as discussed by Pozarnsky and McCormick, only showed a single broad resonance at –547 ppm; no spinning sidebands were observed.[12] In contrast, the ^{51}V MAS NMR spectra (Figure 3) of wet gels prepared in the current study revealed several solid state signals due to the presence of corresponding spinning sidebands. Luca and Hook reported an MAS spectrum composed of a broad pattern of spinning sidebands centered at -559 ppm (assigned to the vanadia gel) and a weak feature (assigned to an ammonium hexavanadate impurity).[14] Discrepancies in the NMR results reported by these researchers cannot be readily explained; clearly, their synthesis procedures produced different gels.

Despite these differences in the NMR results, the laser Raman characterization was quite similar to that reported by Sanchez et al.[31] The Raman spectra for hydrated amorphous vanadia produced by cooling the molten oxide were nearly identical to the Raman spectra reported for the non-layered samples in our study. The Raman spectra obtained for the

layered sample (B´) were very different from those obtained from the non-layered samples but were nearly identical to those reported for amorphous V_2O_5 which was hydrated by grinding with a known amount of water.[31] Sanchez et al. concluded that the differences in the Raman could be attributed to the manner or extent in which water had modified the vanadium coordination. However, the same differences were observed in the Raman spectra reported here but ^{51}V MAS NMR showed no evidence of the uniqueness of this sample. In fact, the NMR clearly showed that water was coordinated in the same fashion in all of the gels. NMR spectroscopy is regarded as providing short-range order information and Raman spectroscopy generally provides short- to medium-range order information: therefore the two spectroscopic techniques would be expected to be consistent. A possible explanation for the discrepancies is that water molecules trapped between the layers were held firmly in place so that they might constrict or alter certain bond vibrations. This model is supported by correlating the Raman spectra of sample B´ with the ^{51}V MAS NMR results. At 100 °C, a Raman band at 672 cm^{-1} (Figure 7b) was observed. Previous work has assigned this band to a V-OH_2 vibration.[4] After heating to 215 °C, this band had nearly disappeared. The corresponding ^{51}V MAS NMR spectra (Figure 5) showed that V_5 was the only site to decrease significantly during this period. Since we know that the same V_5 site is present in both the layered and non-layered materials, the observed band at 672 cm^{-1} in the layered sample might be attributed to a V-OH_2 group, with the water molecule held firmly in position (as it would be if shared between V_4 and V_5 sites) and thereby creating a link between layers. A similar analogy can be drawn looking at the Raman and ^{51}V MAS NMR data at 215 °C and 224 °C (Figure 7c and d). At 215 °C, a Raman band was observed at 1028 cm^{-1}. After heating to 224 °C, this band had disappeared. The corresponding ^{51}V MAS spectra (Figure 5) revealed that after thermal treatment from 215

°C to 224 °C, V_4 was the only site that had decreased substantially. Therefore, the band at 1028 cm^{-1} can likely be assigned to this site. If hydrogen-bonded water coordinated to V_4 was held firmly in place (trapped between layers) and thus restricted the V=O vibration, the frequency of the observed Raman band might be shifted.

4.5 Conclusion

Prior to dehydration of the vanadia gel, ^{51}V MAS NMR revealed the presence of at least four ordered vanadium chemical environments, several of which have not been previously detected in vanadia gels. The key difference in many of these sites was the manner in which water is coordinated. The line shape parameters and the relative intensities of these sites were obtained from the simulation of MAS NMR spectra. The sites present before dehydration corresponded to: 1) vanadium with a water molecule coordinated *trans* to V=O; 2) vanadium with a water molecule coordinated with the oxygen of the V=O; 3) vanadium in a "crystalline V_2O_5" environment; and 4) vanadium in a 'dimer-like' environment. The distribution of these sites changed as dehydration progressed and a new site not involving coordinated water was observed by ^{51}V NMR at -597 ppm. This site appeared during gel dehydration and was present until the material crystallized to form V_2O_5. Based on the numerical analysis of MAS NMR spectra, a detailed model of the transformation of the gel structure during dehydration was proposed. The Raman spectra of the layered and non-layered samples were different. Since the MAS NMR results indicated that the electronic environments around the vanadium nuclei were similar in both the layered and non-layered samples, the differences in the observed Raman bands may have been caused by interaction of the coordinated water molecules which were trapped between the vanadia layers. This

interaction may have constricted the V=O and $\delta(V_2O)$ vibrations. There was no evidence for this interaction for the non-layered samples.

Acknowledgment. This research was supported at Ames Laboratory by the U.S. Department of Energy, Office of Basic Energy Sciences, Division of Chemical Sciences, under Contract W-7405-Eng-82. The authors would like to thank Dr. R.S. Houk for completing the ICP-MS measurements, Drs J.-P. Amoureux and C. Fernandez for providing the QUASAR simulation program and Drs. O. Lapina and J.P. Yesionowski for helpful discussions. We also thank Mr. A. Bailly for assistance with the MAS experiment at 30 kHz.

4.6 List of Figures

Figure 1. Static and MAS ^{51}V NMR spectra of (a) sample A, (b) sample B, (c) sample B´ and (d) sample C, taken at 25 °C.

Figure 2. Representative sample of numerical line shape simulation (QUASAR) vs. experimental data.

Figure 3. (a) ^{51}V MAS NMR spectrum of the wet gel (sample B) taken at 10 kHz. (b) Spectral region between -200 and -1000 ppm with superimposed liquid species (•) and MAS sideband patterns. Spinning sidebands are marked with asterisks (*).

Figure 4. Results of thermogravimetric analysis for the studied gels (1 °C/min).

Figure 5. (a) ^{51}V MAS NMR spectra (isotropic region) of sample B´ at various degrees of hydration and (b) TGA weight loss curve for sample B´.

Figure 6. Laser Raman spectra of (a) sample A, (b) sample B, (c) sample B´ (d) sample C and (e) crystalline V_2O_5.

Figure 7. Laser Raman spectra of sample B´ at (a) 25°C, (b) 100 °C, (c) 215 °C and (d) 226 °C.

Figure 8. Powder XRD patterns of dried samples: (a) sample B´, (b) sample B and (c) sample C. The XRD pattern of sample A was nearly identical to that of sample B.

Figure 9. SEM micrographs of (a) sample A, (b) sample B´ and (c) sample C. The micrograph of sample B was nearly identical to that of sample A.

Figure 10. Postulated structures of vanadium sites: (a) vanadium pentoxide (V_1), (b) vanadium pentoxide with shifted sub-unit below (V_2), (c) vanadium dimer with a water molecule coordinated to each V site (V_3), (d) vanadium oxide with one water molecule hydrogen-bonded to the vanadyl oxygen (V_4), (e) vanadium oxide with one water molecule coordinated trans to the vanadyl oxygen (V_5) and (f) vanadium oxide with two water molecules, one hydrogen-bonded and one trans-coordinated to the vanadyl oxygen.

Figure 11. Relative concentration of vanadia sites during dehydration (%).

Figure 12. Postulated coordination of most tightly bound water.

4.7 List of Tables

Table 1. Sample preparation

Table 2. Quadrupole coupling constant (C_Q in MHz), quadrupolar asymmetry parameter (η_Q), isotropic chemical shift (δ_{iso} in ppm), chemical shift anisotropy ($\Delta\delta_{CSA}$ in ppm), and CSA asymmetry parameter (η_{CSA}) obtained by QUASAR simulations[a] of ^{51}V MAS NMR spectra for sample B´.

Table 3. Relative concentrations of V_i sites and number (n) of coordinated H_2O molecules per V_2O_5 in the vanadia gels obtained by QUASAR calculations of ^{51}V MAS spectra and TGA, respectively.

4.8 References

[1] Livage, J. *Chem. Mater.* **1991**, 3, 578.
[2] Alonso, B.; Livage, J. *J. Solid State Chem.* **1999**, 148, 16.
[3] Fontenot, C.J.; Wiench, J.W., Pruski, M., Schrader, G.L. *J. Phys. Chem. B*, **2000**, 104, 11622.

[4] Aldebert, P.; Baffier, N.; Gharbi, N.; Livage, *J. Mat. Res. Bull.* **1981**, 16, 669.
[5] Sanchez, C.; Livage, J.; Lucazeau, G. *J. Raman Spectosc.*, **1982**, 12, 1, 68.
[6] Gharbi, N.; Sanchez, C.; Livage, J.; Lemerle, L. Nejem, L.; Lefebvre, J. *Inorg. Chem.* **1982**, 21, 2758.
[7] Abello, L.; Husson, E.; Repelin, Y.; Lucazeau, G. *J. Solid State Chem.* **1985**, 56, 379.
[8] Repellin, Y.; Husson, E.; Abello, L.; Lucazeau, G. *Spectr Acta* **1985**, 41A, 8.
[9] Nabavi, M.; Sanchez, C.; Livage, J. *Phil. Mag. B* **1991**, 63, 4, 941.
[10] Hibino, M.; Ugaji, M.; Kishimoto, A.; Kudo, T. *Solid. State Ionics* **1995** , 79, 239.
[11] Mege, S.; Verelst, M.; Lecante, P.; Perez, E.; Ansart, F.; Savariault, J.M. *J Non-Cryst. Solids* **1998**, 238, 37.
[12] Pozarnsky, G.A.; McCormick, A.V.; *Chem. Mater.* **1994**, 6, 380.
[13] Pozarnsky, G.A.; McCormick, A.V.; *J. Mater. Chem.* **1994**, 4, 11, 1749.
[14] V. Luca, J.M. Hook, *Chem. Mater.***1997**, 9, 2731.
[15] Gharbi, N.; Sanchez, C.; Livage, J.; Lemerle, J.; Nejem, L.; Lefebvre, J. *J. Inorg. Chem.* **1982**, 21, 2758.
[16] Amoureux, P.; Fernandez, C.; Dumazy, Y. *37th Rocky Mountain Conference*, Denver, **1995**, Abstract, No. 264.
[17] Mastikhin V.M.; Lapina, O. "Vanadium Catalysts:Solid State NMR", in 'Encyclopedia of Magnetic Resonance', eds. D.M. Grant and R.K. Harris, John Wiley & Sons, Chichester, 1996, Vol. 3.
[18] Fernandez, C.; Bodart, P.; Amoureux, J.-P. *Solid State NMR*, **1994**, 3, 79
[19] Gornostansky, S.D.; Stager, C.V. *J. Chem. Phys.* **1967**, 46, 4959
[20] France, P.W. *J. Magn. Reson.* **1991**, 92, 30.
[21] Skibsted, J.; Nielsen, N.Chr.; Bildsøe, H.; Jakobsen, H.J. *Chem. Phys. Lett.* **1992**, 188, 405.
[22] Marichal, C.; Kempf, J.-Y.; Maigret, B.; Hirschinger, J. *Solid State NMR* **1997**, 8, 33.
[23] Abello, L.; Husson, E.;Repelin, Y.;Lucazeau,G.; *Spectrochemica Acta* **1983**, 39A,7.
[24] Paulik, F., Special Trends in Thermal Analysis, 1995, p.130.
[25] Nayeem, A.; Yesionowski, J.P. *J. Chem. Phys.* **1988**, 89, 4600.
[26] After publishing reference 21, the authors have examined their sample by EPR spectroscopy. No signal has been detected (J.-P. Amoureux, private communication).
[27] Mastikhin, V.M.; Lapina, O.B.; Krasilnikow, V.N., Ivakin, A.A. *React. Kinet. Catal. Lett.*, **1984**, 24, 119.
[28] Rehder, D. *Bull. Magn. Reson.* **1982**, 4, 33.
[29] Abello, L.; Pommier, C. *J. Chimie. Phys.* **1983**, 80, 373
[30] Aldebert, P.; Baffier, N.; Gharbi, N.; Livage, *J. Mat. Res. Bull.* **1981**, 16, 669
[31] Sanchez, C.; Livage, J.; Lucazeau, G. *J. Raman. Spec.* **1982**, 12, 1, 68

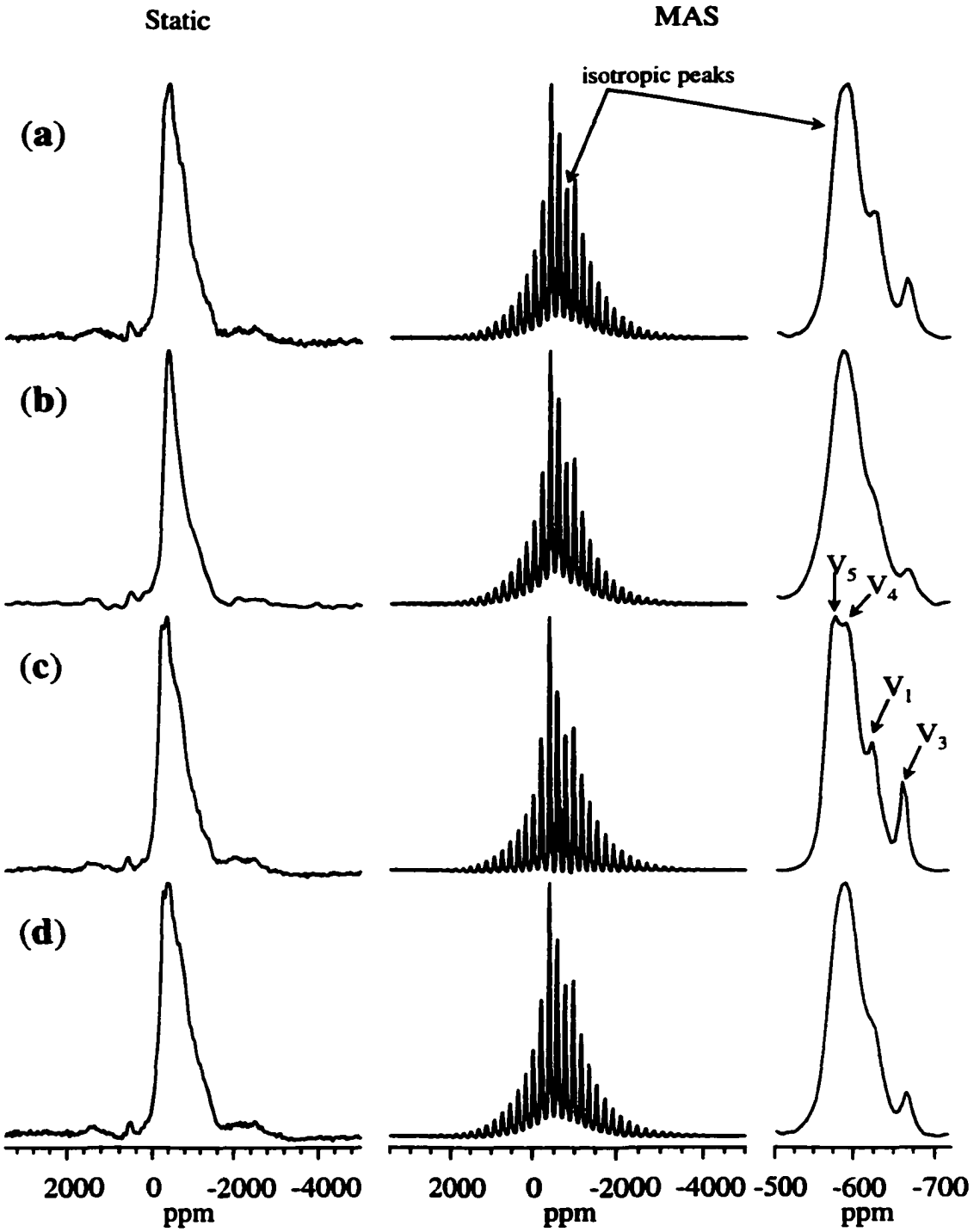

Figure 1. Static and MAS ^{51}V NMR spectra of (a) sample A, (b) sample B, (c) sample B′ and (d) sample C, taken at 25 °C.

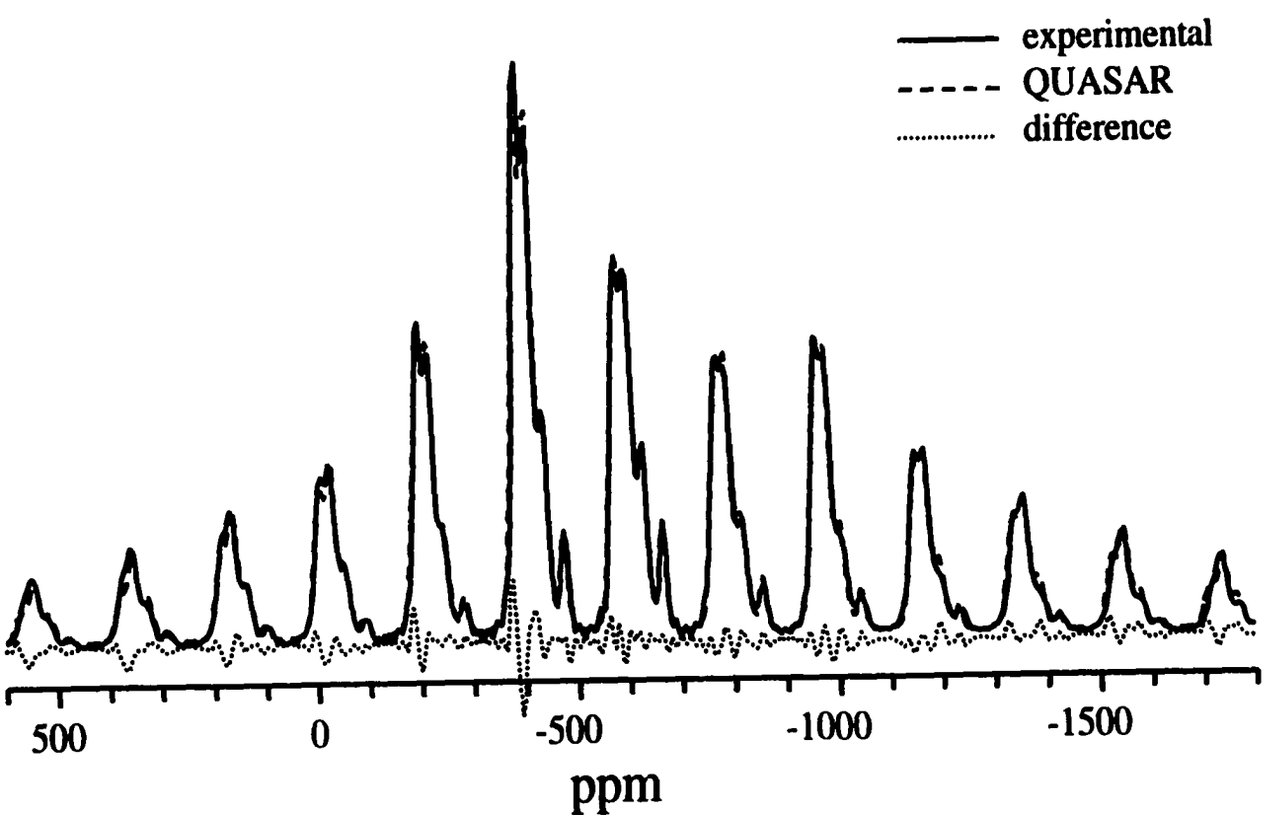

Figure 2. Representative sample of numerical line shape simulation (QUASAR) vs. experimental data.

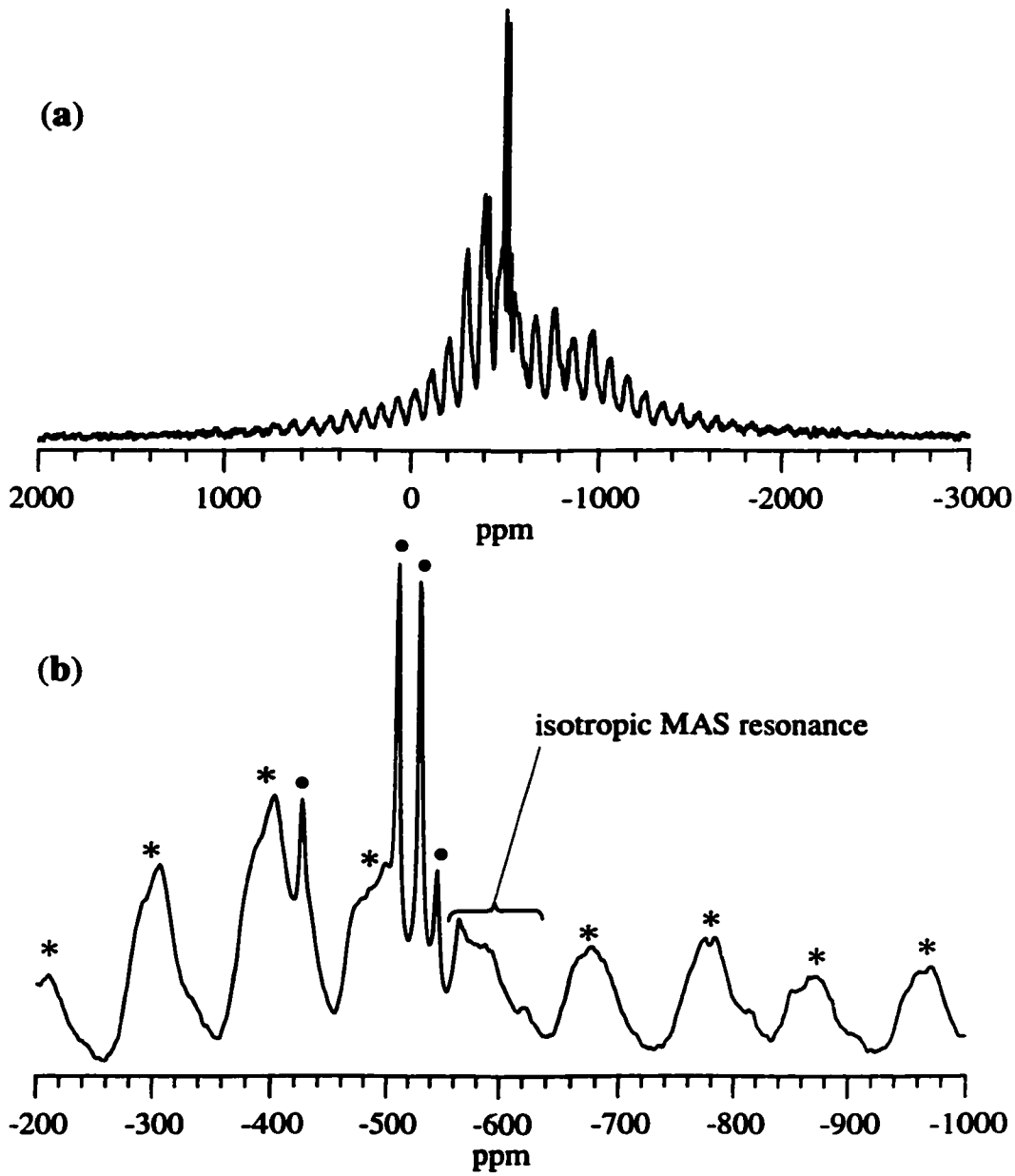

Figure 3. (a) ^{51}V MAS NMR spectrum of the wet gel (sample B) taken at 10 kHz. (b) Spectral region between -200 and -1000 ppm with superimposed liquid species (•) and MAS sideband patterns. Spinning sidebands are marked with asterisks (*).

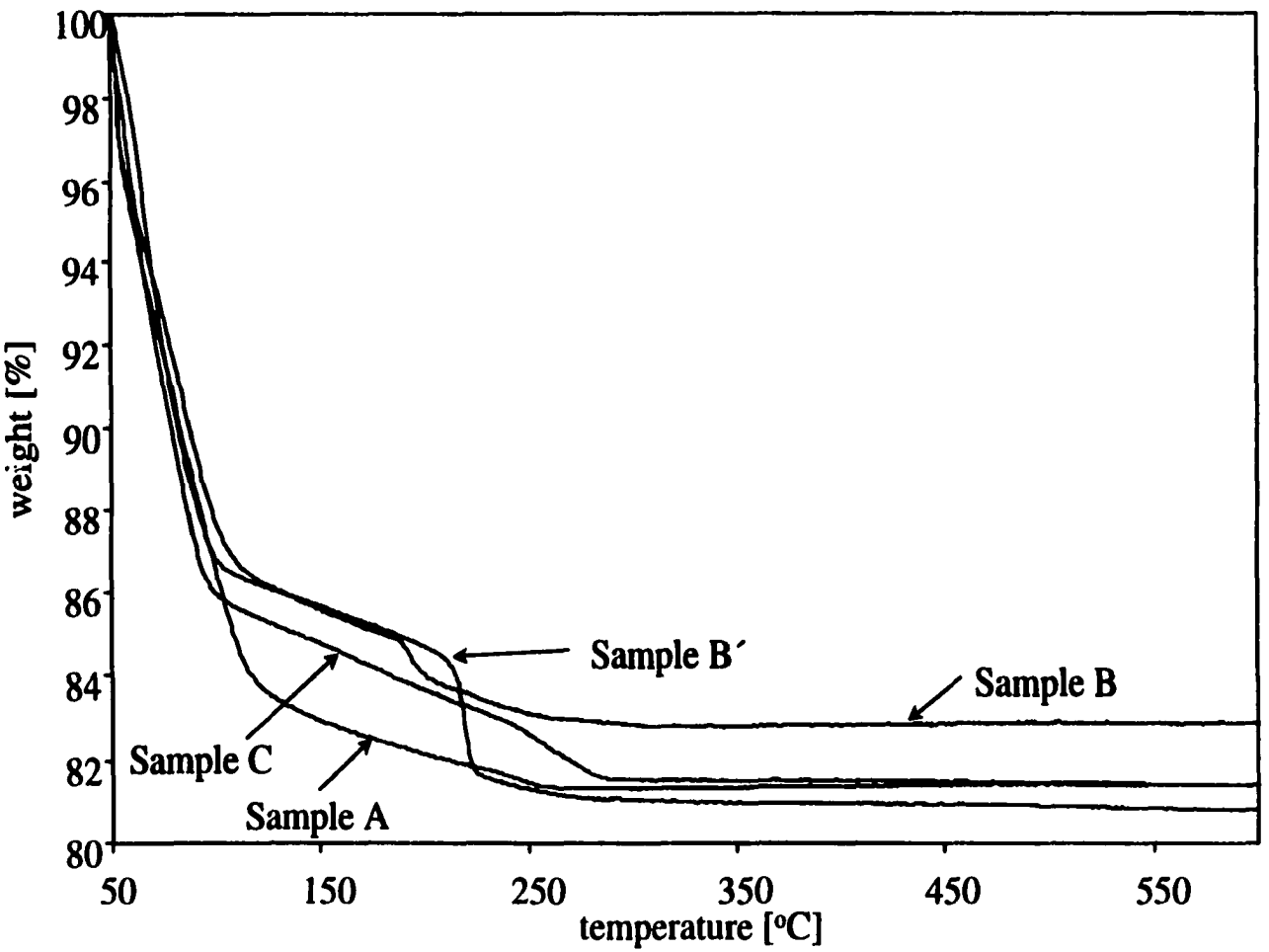

Figure 4. Results of thermogravimetric analysis for the studied gels (1 °C/min).

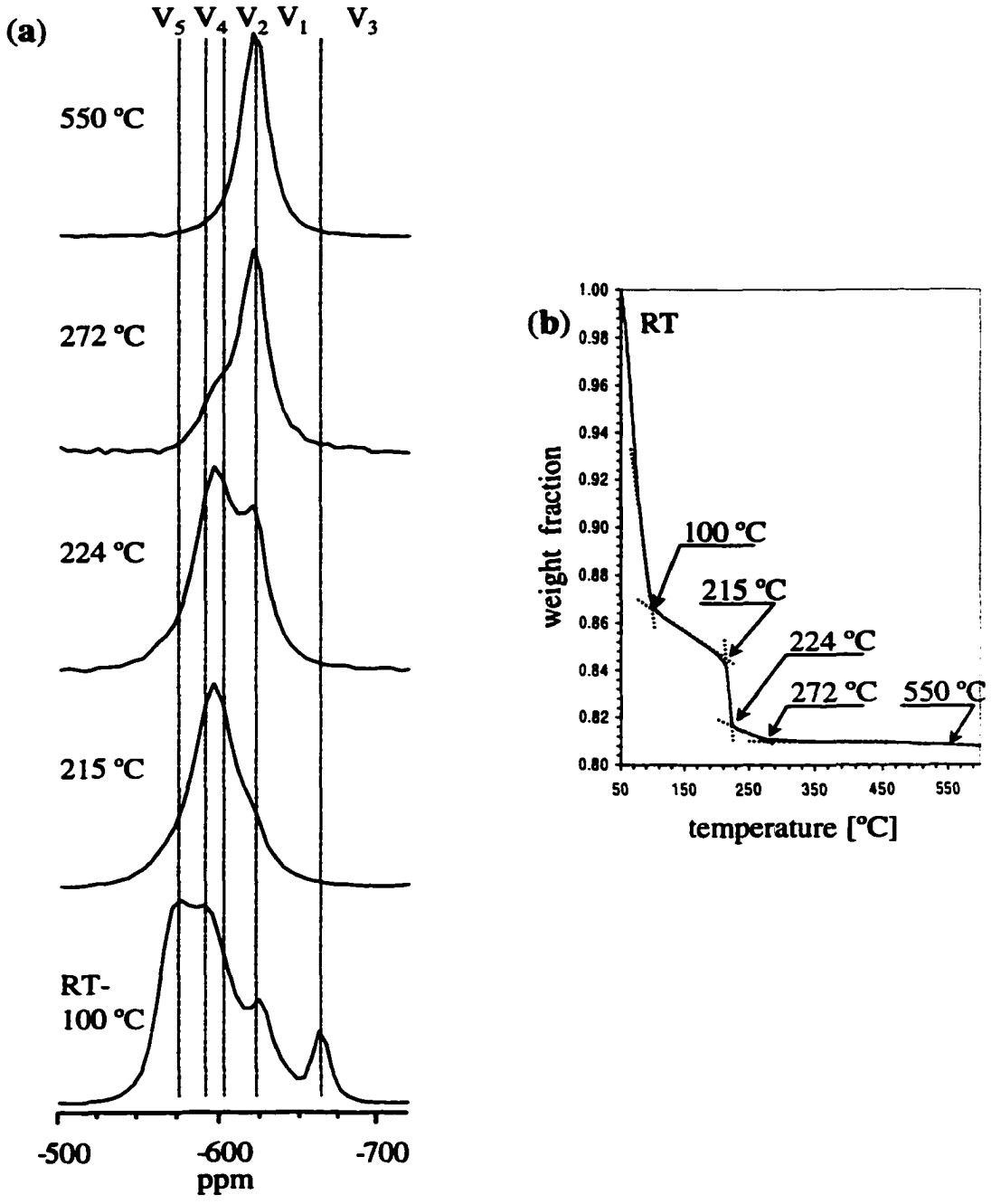

Figure 5. (a) ^{51}V MAS NMR spectra (isotropic region) of sample B′ at various degrees of hydration and (b) TGA weight loss curve for sample B′.

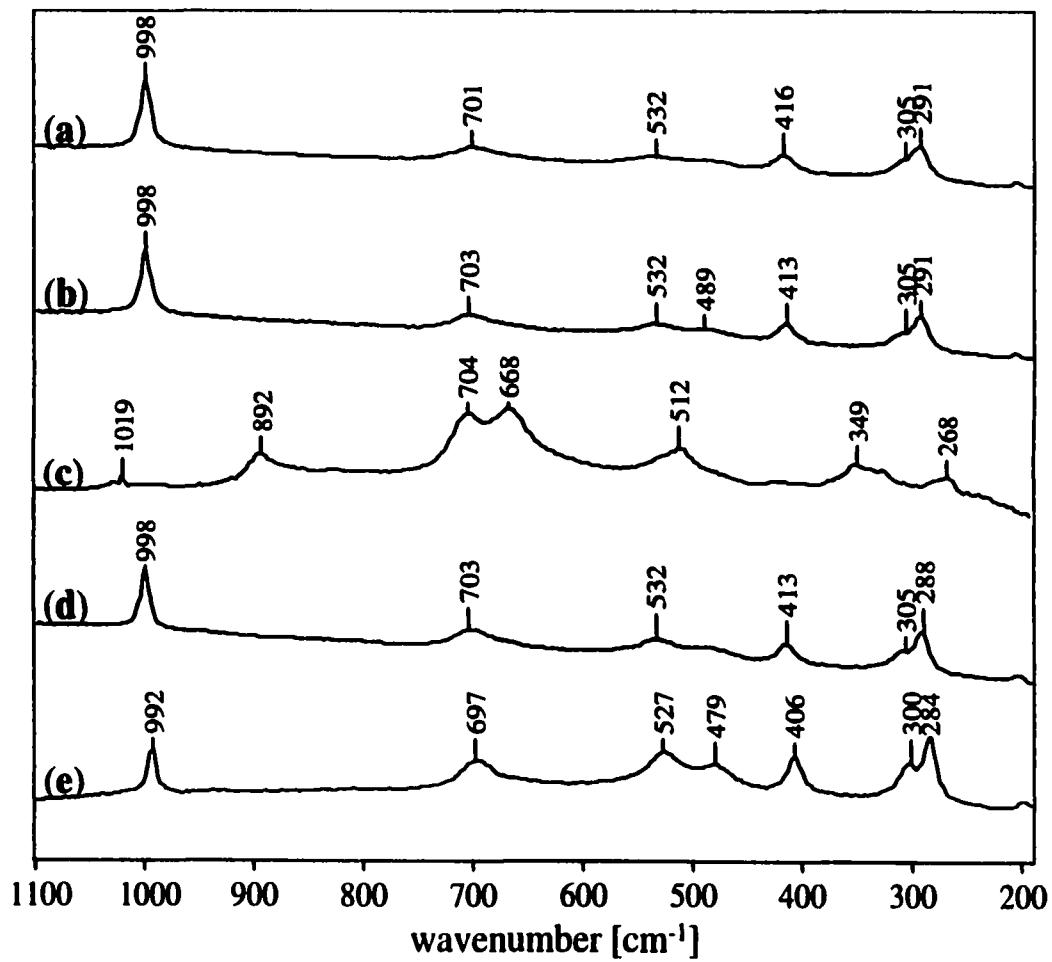

Figure 6. Laser Raman spectra of (a) sample A, (b) sample B, (c) sample B′ (d) sample C and (e) crystalline V_2O_5.

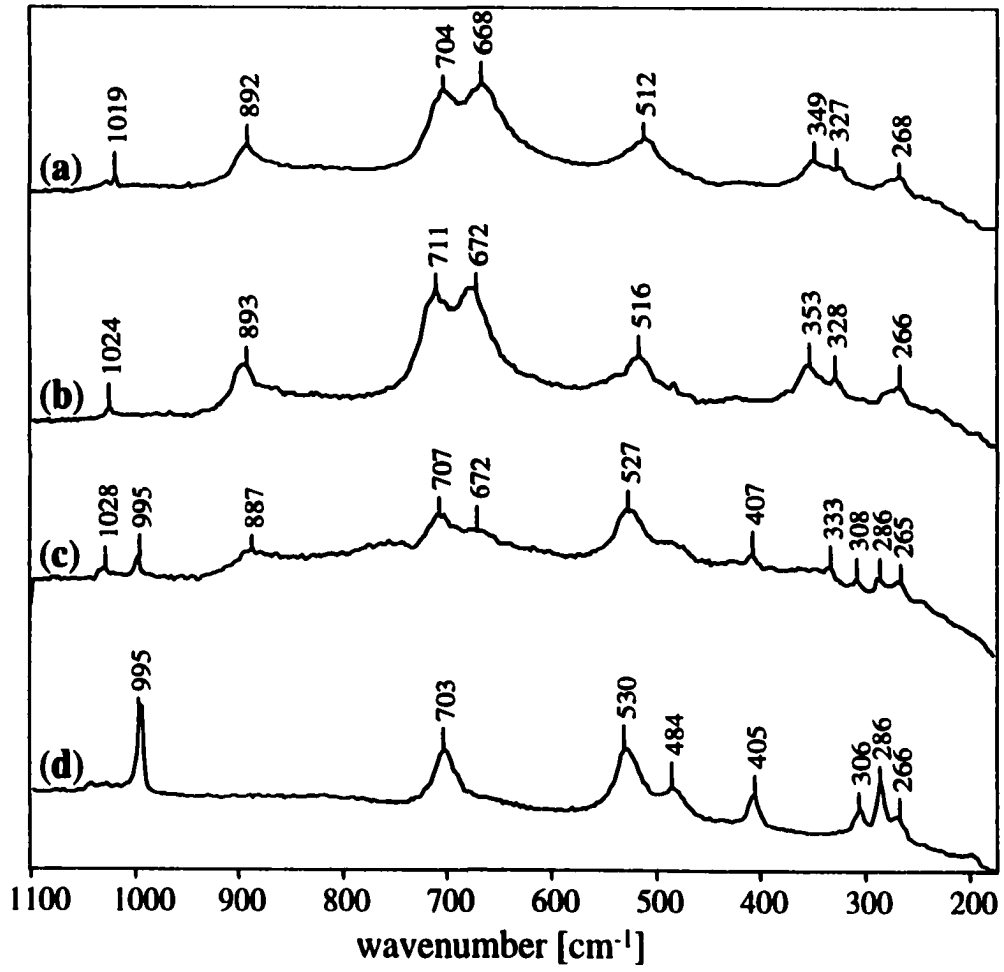

Figure 7. Laser Raman spectra of sample B´ at (a) 25°C, (b) 100 °C, (c) 215 °C and (d) 226 °C.

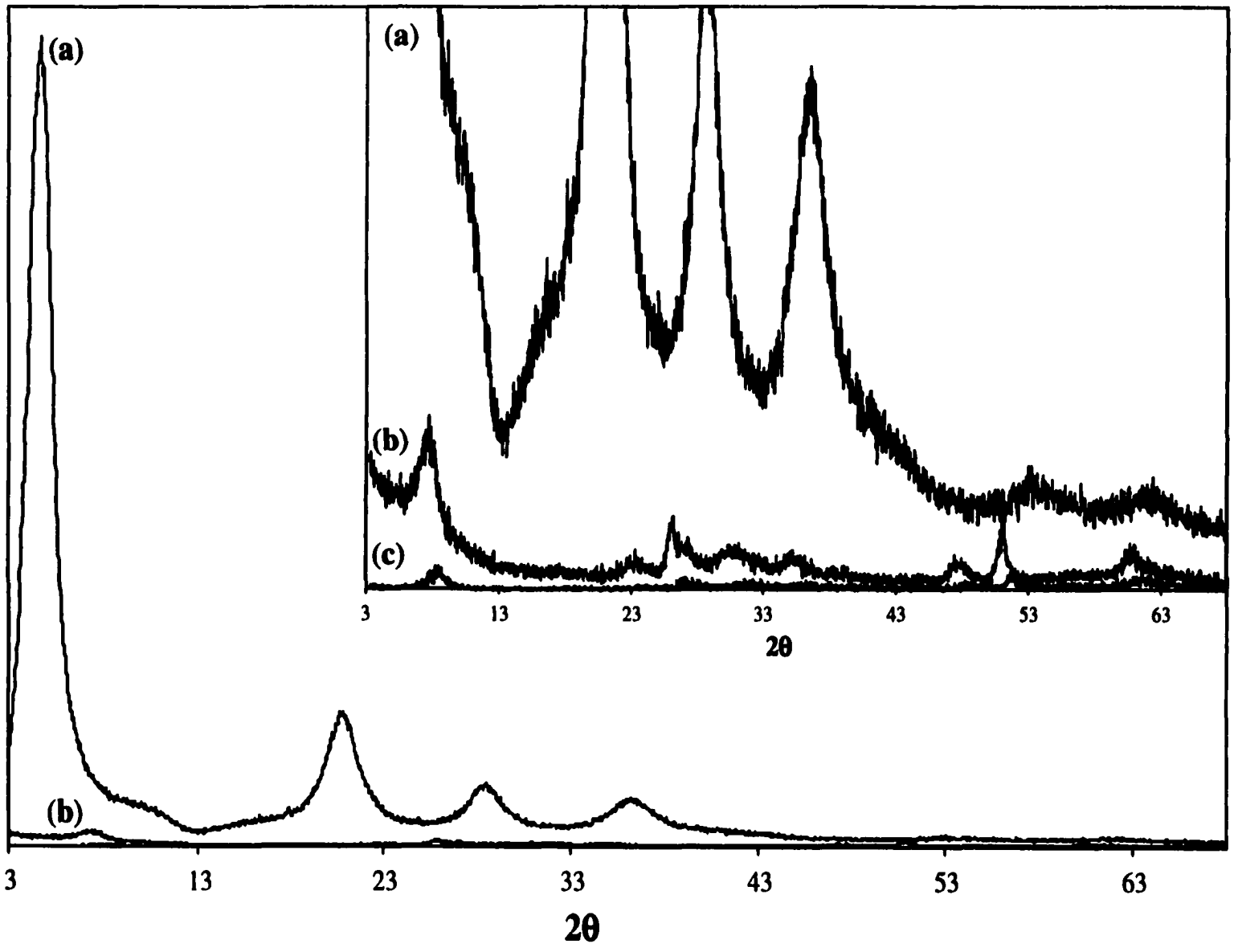

Figure 8. Powder XRD patterns of dried samples: (a) sample B′, (b) sample B and (c) sample C. The XRD pattern of sample A was nearly identical to that of sample B.

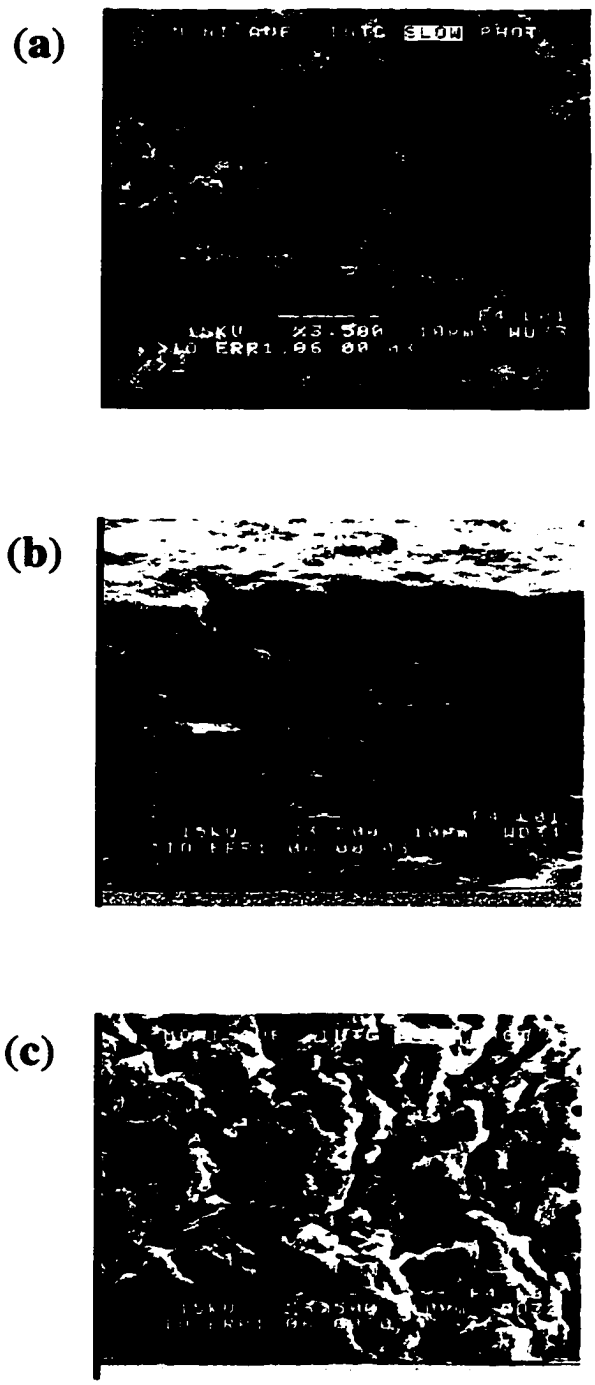

Figure 9. SEM micrographs of (a) sample A, (b) sample B´ and (c) sample C. The micrograph of sample B was nearly identical to that of sample A.

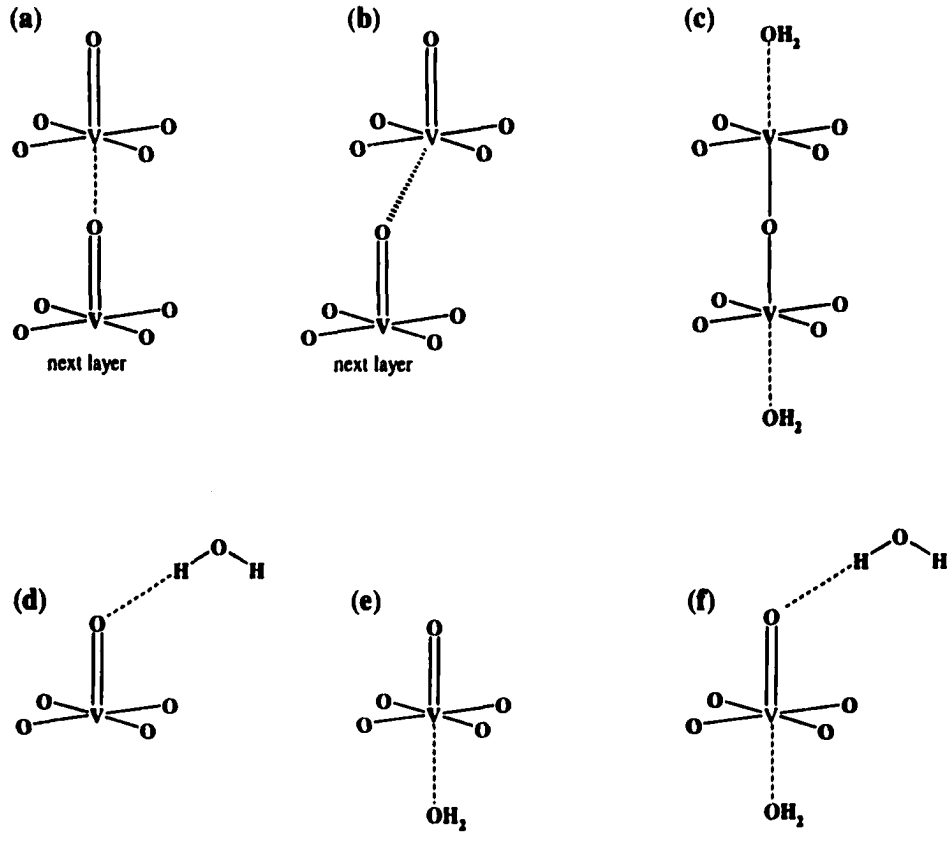

Figure 10. Postulated structures of vanadium sites: (a) vanadium pentoxide (V_1), (b) vanadium pentoxide with shifted sub-unit below (V_2), (c) vanadium dimer with a water molecule coordinated to each V site (V_3), (d) vanadium oxide with one water molecule hydrogen-bonded to the vanadyl oxygen (V_4), (e) vanadium oxide with one water molecule coordinated trans to the vanadyl oxygen (V_5) and (f) vanadium oxide with two water molecules, one hydrogen-bonded and one trans-coordinated to the vanadyl oxygen.

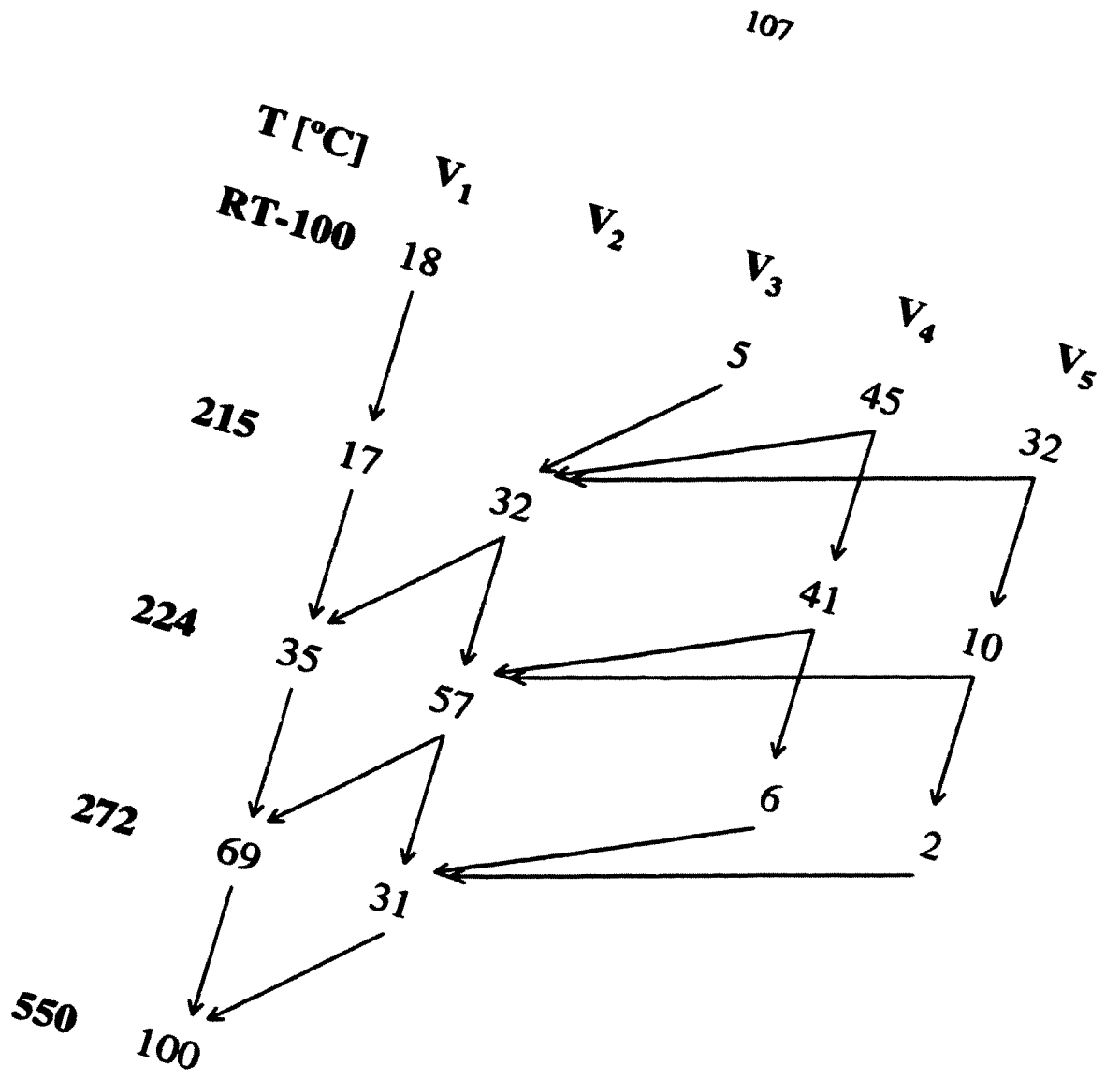

Figure 11. Relative concentration of vanadia sites during dehydration (%).

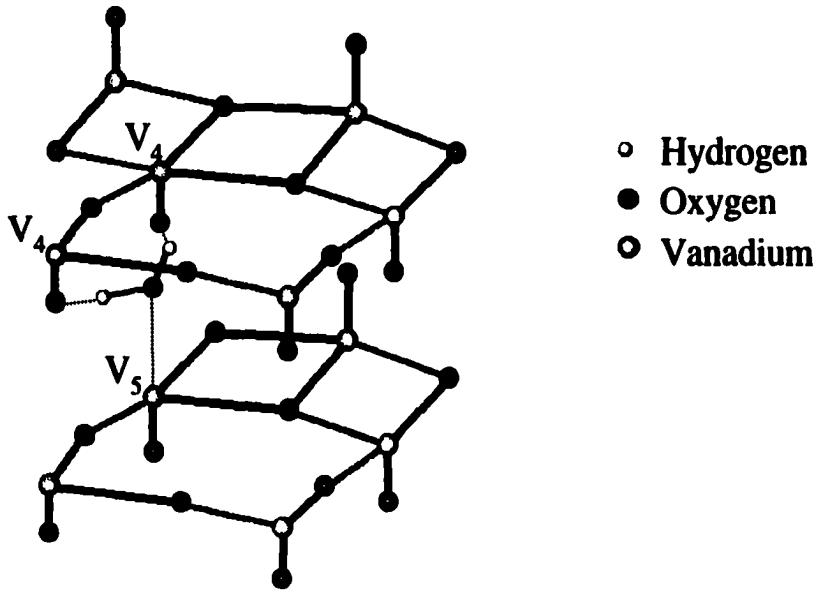

Figure 12. Postulated coordination of most tightly bound water

Table 1. Sample preparation

Sample	C_v	Temperature(°C)	$n(H_2O_2)/n(V)$	Initial pH	Final pH	Sample History	Solid Formed	Surface Area (m^2/g)
A	0.11	25	7.9	0.95	1.47	Decanted/ without stirring	amorphous	1-2
B	0.11	25	7.9	1.28	2.31	Decanted/ without stirring	amorphous	1-2
B´	0.11	25	7.9	1.28	2.31	Stirred and volume reduced	layered	1-2
C	0.50	5	25	0.80	n/a	Decanted/ without stirring	amorphous	1-2

Table 2. Quadrupole coupling constant (C_Q in MHz), quadrupolar asymmetry parameter (η_Q), isotropic chemical shift (δ_{iso} in ppm), chemical shift anisotropy ($\Delta\delta_{CSA}$ in ppm), and CSA asymmetry parameter (η_{CSA}) obtained by QUASAR simulations[a] of ^{51}V MAS NMR spectra for sample B´.

Site	Temp[°C]	C_Q	η_Q	δ_{iso}[b]	$\Delta\delta_{CSA}$[b]	η_{CSA}[b]	δ_{11}[b]	δ_{22}[b]	δ_{33}[b]
V_1	25-100	1.34	0.70	-622.5	-862	0.49	-194	-476	-1197
	215	1.33	0.45	-618.5	-917	0.51	-157	-469	-1230
	224	1.33	0.45	-618.9	-917	0.51	-157	-469	-1230
	272	0.83	0.08	-619.4	-920	0.00	-313	-313	-1233
	550	0.86	0.10	-619.4	-960	0.00	-299	-299	-1259
$V_2 + V_4$	25-100[c]	1.39	0.60	-593.2	-1180	0.62	45	-444	-1380
	215	1.71	1.00	-592.6	-1000	0.30	-159	-359	-1259
	224	1.70	1.00	-594.6	-887	0.15	-255	-343	-1186
	272[d]	1.61	0.98	-597.2	-1583	0.81	358	-497	-1653
V_3	25-100	0.76	0.94	-663.6	-1096	0.53	-105	-492	-1394
V_5	25-100	0.73	0.31	572.3	-1069	0.14	-166	-266	-1285
V_2O_5	25[e]	0.81	0.04	-609.0	-890	0.20	-252	-372	-1202
	25[f]	0.83	0.06	-609.0	-956	0.24	-214	-367	-1246

a) The data were obtained with the following accuracy: C_Q: ± 0.05 MHz; η_Q and η_{CSA}: ± 0.05; δ_{iso}: ± 1.0 ppm; $\Delta\delta_{CSA}$ and δ_{ii}: ± 5 ppm.

b) Chemical shift tensor parameters δ_{iso}, $\Delta\delta_{CSA}$, η_{CSA}, and δ_{ii} are related as follows: $\delta_{iso} = {}^1/_3\cdot(\delta_{11} + \delta_{22} + \delta_{33})$; $\Delta\delta_{CSA} = {}^3/_2\cdot(\delta_{33} - \delta_{iso})$; $\eta_{CSA} = (\delta_{22} - \delta_{11})/(\delta_{33} - \delta_{iso})$ assuming $|\delta_{33} - \delta_{iso}| \geq |\delta_{11} - \delta_{iso}| \geq |\delta_{22} - \delta_{iso}|$.

c) assuming V_4 only.

d) V_2 only.

e) reference 20.

f) reference 23.

Table 3. Relative concentrations of V_i sites and number (n) of coordinated H_2O molecules per V_2O_5 in the vanadia gels obtained by QUASAR calculations of ^{51}V MAS spectra and TGA, respectively.

Sample	Temp[°C]	n	V_1	$V_2 + V_4$	V_3	V_5
A	25	2.30	16.3	54.8	3.7	25.2
B	25	2.10	20.4	49.5	4.1	25.9
B'	25	2.40	18.1	44.7[a]	4.7	32.5
	100	0.69	18.1	44.7[a]	4.7	32.5
	215	0.40	17.4	72.1	0.0	10.4
	224	0.06	35.1	62.7	0.0	2.2
	272	0.00	69.3	30.7[b]	0.0	0.0
	550	0.00	100.0	0.0	0.0	0.0
C	25	2.30	16.9	50.9	3.8	28.3

a) V_4 only;
b) V_2 only.

CHAPTER 5

^{17}O MAS and 3QMAS NMR Investigation of Crystalline V_2O_5 and Layered $V_2O_5 \cdot nH_2O$ Gels

C. J. Fontenot*+, J. W. Wiench+, G. L. Schrader*+ , and M. Pruski+#

Department of Chemical Engineering* and
Ames Laboratory – USDOE+
Iowa State University
Ames, IA 50011

Abstract

The environments of oxygen sites in crystalline V_2O_5 and in vanadia produced via sol-gel synthesis have been investigated using ^{17}O MAS and 3QMAS NMR. For crystalline V_2O_5, three sites were observed: V=O (vanadyl), V_2O (bridging), and V_3O (corner-sharing). Line shape parameters for these sites were determined from numerical simulation of the MAS spectrum. For the vanadia gel, assignments have been proposed for several oxygen sites including: at least two vanadyl sites, two bridging oxygens and two corner-sharing oxygens. Based on the ^{17}O MQMAS and ^{51}V MAS NMR results, the coordination of the water sites has been detailed, and the evolution of these sites during dehydration has been established. Upon re-hydration of the layered gel, a preferred site for initial water re-adsorption was observed. Surprisingly, the oxygen atoms of these re-adsorbed water molecules readily exchanged into all of the oxygen sites of the gel even at room temperature. These oxygen-exchanged sites in the gel persisted upon thermal treatment to 550 °C.

key words: V_2O_5 gels, ^{17}O MAS/MQMAS NMR spectroscopy

author to whom correspondence should be addressed

5.1 Introduction

Metal oxide applications include semiconductor components, as well as various types of catalysts and ceramics. The role of oxygen in the applications of these materials is frequently of great importance: for example, for oxidation by reducible metal oxides, the reactive lattice oxygen species directly participates in the catalysis. Our group recently reported results for the selective oxidation of 1,3-butadiene over vanadia-molybdena oxide gels,[1,2] which were prepared via the peroxo sol-gel method.[3-5] We found that that even at relatively low temperatures (275 °C) these catalytic materials were active, and such products as maleic anhydride, furan, crotanaldehyde and epoxybutene could be formed.

Often, metal oxides are utilized in a non-crystalline state, which can make their characterization challenging. Recent advances in solid state NMR allow for better characterization of disordered materials, such as gels or glasses. Magic-angle spinning (MAS) and various RF driven manipulations of spins can be used to average the first-order interactions that broaden the observed line shapes (mainly chemical shift anisotropy, CSA, and the dipolar coupling). Examination of half-integer quadrupolar nuclei such as ^{17}O (I = 5/2) requires the use of more complex techniques, including multiple-quantum magic angle spinning (MQMAS) NMR,[6-10] so that second-order quadrupolar broadening can be eliminated the high resolution (isotropic) spectra can be obtained. In addition to site resolution, the quadrupolar parameters, such as the quadrupole induced shift (QIS), can be obtained using these techniques.

Although MQMAS measurements of oxygen are challenging due to the very low natural abundance of ^{17}O nuclei (<0.03%), most samples can be enriched and studied

under appropriate conditions. The majority of solid state ^{17}O NMR studies have focused on materials containing Si and/or Al. Several studies report the detection of OH groups, but there are few reports of observing chemisorbed water. The sites of water adsorption in catalysts are of particular interest in light of reports which have indicated that water addition to hydrocarbon feedstocks can significantly alter both the activity and selectivity of several metal oxide catalysts,[11-13] including those prepared from vanadia gels.[1,2] Several TPD[14,15] and computational[16,17] studies of water adsorption on crystalline V_2O_5 have been reported. The only ^{17}O NMR investigation of vanadia gels published to date, by McCormick *et al.*,[18] investigated gels formed by the acidification of metavanadate salt solutions. Although the same species were present in solution at the time of gelation, their gels were quite different than those prepared for this study by the peroxo-method. They concluded that mobile polymeric chains of vanadate octahedra were formed as the gelation progressed and that hydrogen bonding occurred between these chains. Several resonances in the ^{17}O MAS NMR spectrum of the wet gel were identified and assigned to V=O, V-O-V, V-OH, and one type of V-OH_2 site.

Oxygen exchange from water into solid state sites has been previously reported for several oxides, although usually a large amount of thermal energy was required for the exchange to occur. For example, the exchange of ^{18}O from adsorbed water into ZSM-5 was investigated by von Ballmoos et al.[19] Nearly all sites oxygen sites were observed to exchange within one hour under steaming conditions at 873 K. The water-induced cleavage of Si-O-Si and Si-O-Al bonds was thought to give rise to the formation of hydroxyl groups. The exchange of ^{18}O from adsorbed CO_2 into zeolite A and $AlPO_4$-5, was reported by Endoh et al.[20] and Taksihiet al.,[21] respectively. They concluded that the

highly reactive oxygen sites in the zeolites were associated with defects or amorphous regions.

We have previously reported studies of the peroxo-based sol-gel synthesis of vanadia gels using ^{51}V liquid state NMR and Raman spectroscopy.[3] Subsequent characterization of the hydrated gels used solid state ^{51}V NMR and TGA.[22] In the current work, we use recently developed ^{17}O NMR techniques to elucidate the structural role of oxygen in crystalline V_2O_5 and vanadia gels. Sites for water coordination in the hydrated gel and the role of re-adsorbed water were investigated. Based mainly on NMR results, supporting evidence has been obtained that is consistent with previously proposed[22] sites for water adsorption. In addition, evidence was obtained for room temperature oxygen exchange between re-adsorbed water and several oxygen sites of the gel matrix.

5.2 Experimental Section

Results are reported for two layered samples prepared using $H_2{}^{17}O$ (sample I) and $H_2{}^{16}O$ (sample II). The synthesis method used for sample II has been reported previously:[22] a 0.1 M peroxovanadate solution was prepared by addition of 30% H_2O_2 (Fisher Chemicals) to a 0.1 M slurry of de-ionized non-enriched water and V_2O_5 (Alpha Aesar) at 25 °C. In order to minimize the dilution of ^{17}O nuclei in the gel and to conserve ^{17}O-enriched water during the synthesis of sample I, 50% H_2O_2 was added to a slurry of V_2O_5 in 40% $H_2{}^{17}O$ (Isotec) and held at a constant temperature of 2 °C. Thus, the resulting H_2O_2/V and $H_2{}^{17}O/V$ molar ratios were 3.5 and 11.5, respectively. For the subsequent dehydration experiments, sample I was theated to the desired temperature, then cooled to room temperature under N_2. The sample was loaded into the NMR rotor under N_2.

For the rehydration experiments, sample II was prepared as described above (without $H_2{}^{17}O$). The sample was heated to 224 °C in flowing N_2, cooled to room temperature (under N_2), and placed in a N_2 environment enriched with $H_2{}^{17}O$ vapor. The sample was kept in this environment at 20 °C for 2 days so that re-adsorption of $H_2{}^{17}O$ could occur.

5.2.1 Solid State NMR Spectroscopy. Solid state NMR spectra of ^{51}V and ^{17}O were obtained using a Chemagnetics Infinity spectrometer operated at 105.17 MHz and 54.2 MHz, respectively. Samples were placed in 3.2-mm rotors and spun at 20 kHz in a Chemagnetics MAS probe. All of the experiments were performed at room temperature following transfer of the thermally treated samples to the probe within a glove box under dry N_2. Shifts are reported using the δ scale, with positive values being downfield as referenced to $VOCl_3$ and water for ^{51}V and ^{17}O, respectively.

^{51}V MAS NMR spectra were obtained using the Hahn echo sequence ($\frac{1}{2}\pi - \tau - \pi - \tau$ - acquisition) and a high RF field of 100 kHz. Additional experiments performed at lower RF fields, with and without the use of an echo, ensured that no distortions were present in the reported spectra. Typically, 1000 scans were accumulated using a relaxation delay of 0.2 s.

The ^{17}O MAS experiments used an extended Hahn echo pulse sequence with 16 phase cycling to eliminate acoustic ringing.[23] A delay of 2 s between the scans was required to ensure complete relaxation for all resonances in these experiments. For the two-dimensional experiments (3QMAS), a delay of 500 ms was sufficient for the sites being examined and thus was used in order to shorten the over-all acquisition time. Still,

due to the small concentration of ^{17}O nuclei and the limited overall efficiency of the 3QMAS experiment, acquisition times of up to 3 days were required. The 3QMAS experiments employed the standard Z-filtered method.[24]

Numerical simulations of the ^{17}O and ^{51}V MAS spectra of crystalline V_2O_5 were performed using QUASAR.[25] These simulations included the effects of the chemical shift anisotropy (CSA) as well as first- and second-order quadrupolar interactions; both central and satellite transitions were considered. Several line shape parameters describing these interactions have been determined, including the quadrupole coupling constant (C_Q), the asymmetry parameter (η_Q), the isotropic chemical shift (δ_{iso}), the CSA ($\Delta\delta_{CSA}$), and the CSA asymmetry parameter (η_{CSA}). In addition, the isotropic chemical shifts were determined directly from the ^{17}O 3QMAS spectra.[26]

5.2.2 Thermogravimetric Analysis. Samples were analyzed using a Perkin Elmer TGA 7 instrument. Heating rates were 5 °C/min in N_2.

5.3 Results

5.3.1 ^{51}V NMR. For all samples, the ^{51}V MAS spectra consisted of superimposed patterns of spinning sidebands representing up to five sites (V_i, i = 1, 2 ...5). The previously proposed[22] coordination for these sites has been provided in Figure 1. The resonances present in sample I (Figure 2a) were consistent with those reported and discussed in the previous study.[22] Both the site distribution and the corresponding line shape parameters were determined based on simulations of the MAS spectra (Table 1). However, the different synthesis procedure (compared to our previous studies) used for sample I resulted in some differences in both the TGA weight-loss curves and the relative concentrations of vanadium sites. For sample I, resonances at –580, -593, -620 and –660

ppm were observed at 25 °C (see Figure 2a). These were previously assigned[22] to V_5, V_4, V_1 and V_3 sites, respectively. Following the thermal treatment to 224 °C, the resonance corresponding to the V_3 site vanished while an additional resonance, previously ascribed[22] to the V_2 site, was observed at –597 ppm (Figure 2a). Although the V_2 and V_4 sites could not be resolved by ^{51}V NMR, strong evidence for the presence of two sites in this region (only one of which was coordinated with water) has been previously discussed.[22] The ^{51}V spectrum obtained after heating to 272 °C contained resonances at –580, -597 and –620 ppm, and corresponded to V_5, V_4+V_2 and V_1 sites, respectively (Figure 2a). Following thermal treatment to 350 °C, only one resonance at –620 ppm remained (Figure 2a), which was assigned to vanadium sites similar to those for crystalline V_2O_5 (V_1).

Prior to rehydration of sample II, the ^{51}V NMR characterization (not shown) and TGA analyses (Figure 3c, as synthesized) were identical to those reported earlier.[22] However, rehydration was not reversible in the sense that it resulted in a different distribution of sites and a different response to further thermal treatment (Figure 3a, 3c and Table 2). TGA for samples I and II in their as-prepared state indicated 16 to 17 wt. % water, corresponding to $V_2O_5 \cdot 2.0\ H_2O$. Only half of that amount (8.5 %) was found in sample II following thermal treatment to 224 °C and subsequent rehydration (Figure 3c). The TGA results were consistent with ^{51}V MAS NMR characterization that indicated (Figure 3a) the V_1 sites did not fully rehydrate and were the predominant species at 25 °C (Table 2). Among the water coordinating sites, V_5 was the most abundant: the preferred site for readsorption of water under these conditions apparently was *trans* to the vanadyl oxygen. Again, in agreement with the previous work, the concentration of this site decreases first; although in these studies it declined at temperatures less than 100 °C. As

expected, the V_2, V_3 and V_4 sites gradually transformed to V_1 sites upon further heating to 350 °C.

5.3.2 ^{17}O NMR. To facilitate identification of the ^{17}O NMR assignments, the oxygen sites have been labeled O_{ij}, where i = 1, 2, ...5 denotes the corresponding vanadium site (as discussed above) and j = A, B, ... F indicates the type of oxygen site, (A = singly coordinated, B = doubly coordinated, C = triply coordinated, D and E being the linear bridging and η^2-peroxo of the dimer and F the coordinated water, as shown in Figure 1). Nearly all assignments were made based on the spectra of sample I; scrambling may have occurred during thermal treatment of sample II, and only low temperature (25 and 70 °C) sample spectra were considered in making the ^{17}O assignments. A total of ten different oxygen species were observed including the oxygen of chemisorbed water. A summary of the assignments and corresponding ranges for the observed shifts has been provided in Table 3.

Oxygen sites were distinguished using ^{17}O MAS (Figures 2b and 3b) and 3QMAS (Figures 4 and 5) NMR. The ^{17}O MAS NMR spectra consisted of superimposed patterns of spinning side bands representing several oxygen sites with wide CSA patterns. The center bands for the different sites were present in three general regions: 1400-1100 ppm, 800-700 ppm, and 600-200 ppm. A previous ^{17}O NMR HETCOR study of the decavanadate anion in solution[27] and a ^{17}O MAS NMR investigation of a chain-structured vanadia gel[18] indicated that the V=O, V_2O and V_3O resonances for those materials were observed in the 1450-1050, 800-700 and 500-400 ppm regions, respectively. In our studies only resonances between 600 and 200 ppm were detectable for the 3QMAS experiments. Most likely, the spectral region between 1400 and 1100 ppm unobservable

due to small C_Q values for the vanadyl sites; resonances for the bridging oxygen sites expected between 800 and 700 ppm were not detected due to large CSA values. The C_Q and CSA values obtained for these sites from the simulation of the ^{17}O MAS spectrum of crystalline V_2O_5 were consistent with this explanation, as indicated in Table 4 (O_{1A} and O_{1B}).

For the as-prepared sample I, several oxygen resonances were observed in the vanadyl region of the MAS spectrum (Figure 2b). Other resonances were observed at 700 ppm and in the 600-200 ppm range. The number of sites contributing to the spectrum between 600 and 200 ppm could not be determined from the MAS spectrum alone, as it contained a number of superimposed powder patterns representing the central transition of several resonances. Surprisingly, a minimum of five sites in this region was revealed by the 3QMAS method (see the isotropic dimension in the spectrum of Figure 4 and Table 4). The isotropic chemical shifts corresponding to these sites were 328, 343, 377, 410, 474 and 507 ppm. No changes were observed in the MAS or 3QMAS spectra following heating of sample I to 100 °C. However, after heating to 224 °C, the changes had occurred in the general line shape of the V=O region, and a new peak was observed at about 1350 ppm (see Figure 2b). Resonances at 780, 705 and between 600 and 200 ppm were still present. The corresponding 3QMAS spectrum revealed that the resonances previously observed at 343, 377 and 474 ppm had decreased (see Figure 4). After thermal treatment to 272 °C, vanadyl resonances in the ^{17}O MAS spectrum were observed at 1326 and 1210 ppm (Figure 2b). The resonances at 700 and between 600-200 ppm were still quite strong, while the center band corresponding to 787 ppm had weakened. Resonances were observed in the 3QMAS experiments at 331, 375, 413, 460 and 511

ppm (Figure 4). After heating to 325 °C, resonances in the MAS spectrum were observed at 1337, 1211, 792, 700 and between 600 and 200 ppm (Figure 2b). At this stage, the 3QMAS spectrum revealed strong peaks at 462 and 408 ppm along with a weaker resonance at 375 ppm (Figure 4). Following heating to 350 °C, the MAS spectrum contained resonances at 1211, 795 and 444 ppm (Figure 2b). After heating to 550 °C, these same resonances were observed although the FWHM of each peak had decreased, which was consistent with a crystallization process. During the dehydration process, the lineshape corresponding to the vanadyl region of the ^{17}O MAS spectra changed (Figure 2b). This is likely due to changes in the lineshape parameters for these sites. This is consistent with our previously reported ^{51}V MAS NMR study, which indicated that the lineshape parameters of the corresponding vanadia sites had also changed during this process.[22]

The ^{17}O MAS and 3QMAS NMR spectra of rehydrated sample II were surprisingly similar to the corresponding spectra of sample I (comparisons of Figures 2b and 3b and Figures 4 and 5). The main differences involved the signal at 377 ppm (only observed in the 3QMAS spectrum of sample I) and the signal at –602 ppm (only observed in the 3QMAS spectrum of sample II at low temperatures). The similarity of these results indicated that 1) incorporation of ^{17}O nuclei from $H_2{}^{17}O$ took place under the mild conditions used during rehydration, and 2) oxygen had apparently exchanged into all sites in the gel. However, it should be acknowledged that during the subsequent thermal treatment, further oxygen scrambling was possible.

3QMAS experiments do not always yield reliable quantitative information since changes in the quadrupolar coupling constant C_Q, the asymmetry parameter η and CSA

can affect the efficiency of multiple quantum transfers. However, the values for the quadrupolar product $P_Q = C_Q(1 + \eta^2/3)^{1/2}$, as determined from the MQMAS spectra, were between 3.0 and 4.2 MHz for the observed sites. Since $0 \leq \eta \leq 1$, the C_Q values for each site should be within 1.6 MHz of each other. Assuming no large changes in the CSA, the expected efficiency for each site should be within about 20% for the experimental conditions used in our work. Using these assumptions, the observed intensities yielded a semi-qualitative representation of the site populations.

5.4 Discussion

Previous reports have indicated that the amorphous vanadia gels crystallize into orthorhombic V_2O_5 following thermal treatment at 350 °C.[28] Our assignments and discussion focus first on this material since its structure is well understood. The X-ray diffraction studies of crystalline V_2O_5 indicated that only one type of vanadium site (V_1) and three different oxygen sites (see Figures 6a,b) exist.[29] The ^{51}V MAS spectrum of our sample treated at 350 °C (Figure 6c) was consistent with this structure, and the QUASAR simulation yielded line shape parameters similar to those published earlier.[30,31] The corresponding ^{17}O MAS NMR spectra and line shape simulations (Figure 2b and Figure 6d) clearly revealed three distinct resonances at 1214, 833 and 480 ppm. Based on the liquid state NMR studies of similar oxygen environments,[26] these resonances have been assigned to the vanadyl oxygen (O_{1A}), the doubly coordinated bridging oxygen (O_{1B}) and the triply coordinated oxygen (O_{1C}), respectively, as shown in Figures 6a,b. For the V=O and V_2O oxygen gel sites, our assignments are similar to those made by McCormick et al. in a solid state NMR study of a chain structured vanadia gel.[18] However, McCormick et al. did not observe any V_3O oxygen sites. The large CSA value for the vandyl oxygen

(O_{1A}) obtained via the simulations of the ^{17}O MAS spectrum (Table 4) was consistent with previous studies of organic doubly-bonded oxygen compounds.[32] The C_Q values calculated for each oxygen site were found to be in the order: $O_{1B} > O_{1C} > O_{1A}$. Interestingly, this trend was consistent with the calculated populations of the p_z orbitals [perpendicular to the (001) plane] of these nuclei in crystalline V_2O_5.[33]

Only V_1 and V_2 sites were present in sample I after thermal treatment to 325 °C (Figure 2a). The ^{17}O MAS and 3QMAS NMR spectra (Figures 2b and 4) revealed three new resonances at 1350 ppm, 700 ppm and 408 ppm, designated as O_{2A}, O_{2B} and O_{2C}, respectively. Thus, O_{2A}, O_{2B} and O_{2C} were assigned to the vanadyl, the doubly-coordinated and the triply-coordinated oxygen species of the V_2 site. Note that the O_{2A} species was not detected at 25 °C, which was consistent with our previous hypothesis[22] that V_2 sites were not present in as-prepared samples but were created at the expense of V_3, V_4 and V_5 sites as water molecules were released.

The strong resonance at around 700 ppm in the ^{17}O MAS spectrum was observed at temperatures ≤325 °C. At 325 °C it was assigned to O_{2B}, a site that does not exist at 25 °C. The presence of this peak at 25 °C can be reasonably explained by assigning it to similar types of oxygen sites, specifically O_{4B} and O_{5B}. The observed downfield shift of this resonance from 704 to 696 ppm with progressing dehydration reinforces the idea that it represents more than one species. A similar argument can be made for the resonance at around 400 ppm, which shifted between 400 and 420 ppm during dehydration. This resonance corresponded to O_{2C} at 325 °C, O_{4C} and O_{5C} at 25 °C, and a mixture of all three species (O_{2C}, O_{4C} and O_{5C}) at the intermediate stages of hydration.

Another resonance, at about 375 ppm, was identified in the 3QMAS spectra for sample I at 272 °C (Figure 4). It was previously proposed[22] that the water remaining at the last stage of hydration was shared between two V_4 sites and a V_5 site. Therefore, the ^{17}O resonance at 375 ppm was assigned to this species and labeled as O_{445F}. A residual amount of this species may still be observed under 3QMAS at 325 °C (Figure 4). Even at room temperature, this resonance was strong in sample I (Figure 4), indicating that this type of coordination was prevalent in the as-prepared gel.

Following heating of sample I from 25 to 224 °C, the most significant changes in the ^{51}V NMR spectra (Figure 2a) involved the V_3 and V_5 sites. The relative concentrations of V_3 and V_5 sites decreased from 11 to 0% and 38 to 10%, respectively (Table 1). Comparison of the ^{17}O 3QMAS spectra (Figure 4) obtained at these temperatures indicated that the resonances at 328, 343, 375 and 474 ppm had also decreased. The resonance at 375 ppm was already assigned to shared water O_{445F}. The resonance at 328 ppm can be most easily assigned by examining the rehydrated gel. The ^{51}V NMR spectrum of sample II at 25 °C (Figure 3a) indicated that, except for V_1, the most prevalent vanadium site was V_5. The corresponding 3QMAS spectrum revealed that the resonance at 328 ppm (O_{5F}) was also dominant. Upon heating sample II to 70 °C, both the V_5 site concentration and the intensity of the resonance at 328 ppm (Figure 5) decreased. This strongly suggested that the resonance at 328 ppm corresponded to water coordination at the V_5 site (O_{5F}). There is no spectroscopic evidence that this water is shared with any other V_i site.

The assignments of the remaining, relatively weak resonances at 343, 477 and 507 ppm in the 3QMAS spectra were less clear. The lines at 343 and 477 ppm vanished

between 25 and 224 °C (although the resonance for O_{1C} at 462 ppm made this determination somewhat ambiguous for the signal at 477 ppm), which was in concert with the dissapearance of the V_3 site. If our earlier assignment of the V_3 site to a dimer[18] was correct, the resonance at 477 ppm would correspond to a η^2-peroxo oxygen (O_{3E}) in the dimer. Two η^2-peroxo oxygen resonances of a similar diperoxovanadate species in solution were observed at 444 and 464 ppm in a previous study.[34] The resonance at 343 ppm might then be assigned to the expected coordinated water molecule of the dimer (O_{3F}). The peak corresponding to the bridging oxygen (O_{3D}) of the linear V-O-V group of this dimer might be expected in the vanadyl region (1500-1100 ppm) due to the possible π character of this bond.[3] However, this region was not resolvable in the ^{17}O MAS spectrum and thus more conclusive evidence for the presence of this bridging oxygen of the dimer was not obtained. The weak resonance at 507 ppm in the ^{17}O 3QMAS spectra for sample I decreased in intensity as dehydration progressed, which is a strong indication that this resonance was related to a site that contained water. Since this resonance was present after V_3 had disappeared and the oxygen sites associated with V_5 have been rather unambiguously assigned, association with those sites is very unlikely. The presence of the oxygen resonance at 507 ppm did coincide with the presence of the V_4 sites so a plausible explanation could involve water coordinated to a single V_4 site.

The ^{17}O signals for water coordinated to V^{5+} oxide species in solution were previously reported[35] in the 0-100 ppm region, while the signal for a triply coordinated water in the chain-structured vanadia gel was reported at 220 ppm.[18] The triply coordinated oxygen species present in decavanadate anions have been reported at about 440 ppm.[27] The signals for all of the coordinated water in our gels fell within the 300-500

ppm region, which seemed consistent with triply coordinated oxygen. Thus, it seems likely that the oxygen atom (O_{4F}) of the water molecule of the V_4 site was triply coordinated, most likely hydrogen-bonded to another bound water molecule. An example of such a hydrogen-bonded structure was proposed by Livage, [36] where one OH bond of water was in the same direction as the V=O bond.

The general types of water coordination proposed for the gel studied in this work are consistent with those predicted in the computational studies by Yin et al. of adsorbed water onto the most thermodynamically stable (010) plane of crystalline V_2O_5.[17] These simulations indicated two preferential adsorption sites for water: 1) water molecule hydrogen-bonded to (bridging) two vanadyl oxygens and 2) oxygen atom of water molecule coordinated directly to the vanadium atom. The additional water coordination sites we have proposed for our multi-layered gels include: a water molecule shared between two V_4 sites and a V_5 site, a water molecule associated with a dimer (V_3) and a water molecule shared between one V_4 site and a V_5 site. Additional adsorptive computational studies on the (001) plane reported by Ranea et al. concluded that the preferred site for water adsorption on crystalline V_2O_5 at room temperature involved the vanadyl oxygen.[16] Clearly, the gel layers cannot be considered to be exposed surfaces, and the adsorption sites may be expected to differ from those found in crystalline V_2O_5.

The rehydration experiments involving $H_2{}^{17}O$ were initially undertaken with the intent of simplifying the assignments of the water adsorption sites. The discovery that oxygen had exchanged under such mild conditions from adsorbed water to the oxygen sites in the gel was quite surprising. Except for the absence of the signal at 377 ppm (O_{445F}) in sample II, the ^{17}O MAS and 3QMAS spectra for samples I and II were nearly

identical at every stage, indicating that oxygen had exchanged into nearly all of the oxygen sites in the gel. The lack of oxygen exchange into the O_{445F} site at 25 °C was not surprising, since this was the only type of water not removed before rehydration. However, following thermal treatment of the rehydrated sample to 224 °C, this water site was detected, indicating that some form of mobile oxygen was present during thermal treatment. The ^{51}V MAS NMR results of sample H at 25 °C indicated that water preferentially re-adsorbed *trans* to the vanadyl oxygen, creating a V_5 site (Figure 3a, 25 °C). Since the V_1 sites might be expected to be fairly stable, and no V_2 sites were present following rehydration (no O_{2A} sites), the re-adsorbed water probably coordinated with a V_2 site, thereby creating a V_5 site. It is interesting that for the rehydrated gel (sample II), some of the water lost below 100 °C was chemisorbed (V_5 site). This was in contrast to sample I, where the water lost below 100 °C was solely physisorbed.

Several possible exchange mechanisms may be responsible. According to conductivity measurements,[37] the H^+ species in the layered gels are quite mobile. This would suggest a partial or complete dissociation process occurring with the adsorbed water. Partial dissociation:

$$H_2O \rightarrow H^+ + OH^-$$

yields OH^- and H^+ species. Complete dissociation:

$$H_2O \rightarrow H^+ + OH^-$$

$$OH^- \rightarrow H^+ + O^{2-}$$

results in O^{2-} and H^+ moieties being produced. Considering the reactivity of the oxygen species (i.e. the relative ease of oxygen exchange), the O^{2-} species, which is a product of complete dissociation, may be more likely. Since the O^{2-} species would be very unstable

(and therefore reactive), its existence would probably depend on the presence of a catalyzed process or a resonance structure. The presence of a coordinated water molecule *trans* to the vanadyl oxygen could give rise to a short-lived resonance structure, such as the one depicted in Figure 7. Since the coordinated water (O_{5F}) resonance of this structure was observed at about 320 ppm, and the V=O (O_{5A}) was thought to be observed at about 1100 ppm, an oxygen signal for such a resonance structure might be expected at about 700 ppm. An unassigned ^{17}O signal, which was observed only in sample II at 25 and 70 °C at approximately 602 ppm, may correspond to such a structure. These resonance stabilized oxygen atoms would conceivably be very reactive and might be expected to exchange into the gel oxygen sites.

The discovery that the oxygen of water exchanges so readily with the oxygen sites in the gel may indicate that these layered materials are suitable for very low temperature oxidation catalysis and work is underway to determine the activity of these materials. Using these ^{17}O labeled catalysts, it should now be possible to determine what oxygen site(s) are responsible for each insertion in the selectively oxidized products. Additional experiments are underway to examine the underlying fundamental phenomena (i.e. dissociation, competitive adsorption, changes in bond strength) which were found to result in improved catalyst activity and product selectivities caused by the addition of water to the feedstock.

Acknowledgment. This research was supported at Ames Laboratory by the U.S. Department of Energy, Office of Basic Energy Sciences, Division of Chemical Sciences, under Contract W-7405-Eng-82.

5.5 List of Figures

5.6 List of Tables

5.7 References:

[1] Schroeder, W.; Fontenot, C.J.; Schrader, G.L. *J. Cat.* **2001**, 203, 382

[2] Schroeder, W.D.; Schrader, G.L., submitted **2001**

[3] Fontenot, C.J.; Wiench, J.W.; Pruski, M.; Schrader, G.L. *J. Phys. Chem. B.*, **2000**, 104, 11622.

[4] Fontenot, C.J.; Schroeder, W.D.; Schrader G.L.; **2001**, submitted *Chemistry of Materials*

[5] Wiench, J.W.; Fontenot, C.J., Schrader, G.L., Larsen, S.; Pruski, M. **2001**, to be submitted

[6] Llor, A.; Virlet, J. *Chem. Phys. Letters*, **1988**, 152, 248.

[7] Chmelka, B.F.; Mueller, K.T.; Pines, A.; Stebbins, J.; Wu, Y.; Zwanziger, J.W. *Nature*, **1989**, 339, 42.

[8] Mueller, K.T.; Sun, B.Q.; Chingas, G.C.; Zwanziger, J.W.; Terao, T.; Pines, A. *J. Magn. Reson.*, **1990**, 86, 470.

[9] Frydman L.; Harwood, J.S. *J. Am. Chem. Soc.*, **1995**, 117, 5367.

[10] Medek, A.; Harwood, J.S.; Frydman, L. *J. Am. Chem. Soc.*, **1995**, 117, 12779.

[11] Park, Dae-Won; Kim, Dong-Uk; Woo, Hee-Chul; Cho, Young-Gu. Abstracts of Papers, 222nd ACS National Meeting, Chicago, IL, United States, **2001**, August 26-30.

[12] Hocevar, Stanko; Levec, Janez. Abstracts of Papers, 222nd ACS National Meeting, Chicago, IL, United States, **2001**, August 26-30.

[13] Henrich, V.E. Rep. Prog. Phys. 1985, 48, 1481

[14] Ranea, V.A.; Vicente, J.L.; Mola, E.E.;Arnal, P.;Thomas,H.;Gambaro, L. *Surface Science* **2000**, 115.

[15] Moshfegh, A.Z.; Ignatiev, A. *Surf. Sci. Letters* **1992**, L650.

[16] Ranea, V.A.; Vicente, J.L.; Mola, E.E.; Uyewa Mananu, R. *Surf. Sci.* **1999**, 442, 498.

[17] Yin, X.; Fahmi, A.; Han, H.; Endou, A.; Ammal, S.; Kubo, M.; Teraishi, K.; Miyamoto, A. *J. Phys. Chem B*, **1999**, 103, 3218

[18] Pozarnsky, G.A.; McCormick, A.V. *J. Mater. Chem.*, **1994**, 4(11), 1749.

[19] von Ballmoos, R. *The ^{18}O-exchange method in zeolite chemistry*, Otto Salle Verlag, Frankfurt, 1981.

[20] Endoh, A.; Mizoe, K.; Tsutsumi, K.; Takaishi, T. *J. Chem Soc., Faraday Trans.* **1989**, 85(6), 1327.

[21] Takaishi, T.; Endoh, A. *J. Chem Soc., Faraday Trans.*, **1987**, 83, 411.

[22] Fontenot, C.J.; Wiench, J.W.; Pruski, M.; Schrader, G.L. *J. Phys. Chem. B.*, **2001**, 105, 10496.

[23] Kunwar, A.C.; Turner, G.L.; Oldfield, E. *J. Magn. Reson.*, **1986**, 69, 124.

[24] Amoureux, J.-P.; Fernandez, C.; Steuernagel, S. *J. Magn. Reson.*, **1996**, 123, 116.

[25] Massiot, D.; Touzo, B.; Trumeau, D.; Coutures, J. P.; Virlet, J.; Florian, P.; Grandinetti, P. J. **1996**, *Solid State Nucl. Magn. Reson.*, 6(1), 73-83.

[26] Amoureux, P.; Fernandez, C.; Dumazy, Y. *37th Rocky Mountain Conference*, Denver, **1995**, Abstract, No. 264.

[27] Wagner, G.W. *Inorg. Chem.*, **1991**, 30, 1960.
[28] Aldebert, P.; Baffier, N.; Gharbi, N.; Livage, J. *Mater. Res Bull.*, **1981**, 16, 669.
[29] Bystrom, A.; Wilhelmi, K.A.; Brotzen, O. *Acta Chem. Scand.*, 1950, 4, 1119
[30] France, P.W. *J. Magn. Reson. 1991*, 92, 30.
[31] Skibsted, J.; Nielsen, N. Chr.; Bildsøe, H.; Jakobsen, H.J. *Chem. Phys. Lett.* **1992**, 188, 405
[32] Wu, G.; Dong. S. *Chem. Phys. Letters*, **2001**, 334, 265.
[33] Witko, M.; Tokarz,J.; Haber,J. *J Mol. Cat.*, **1991** 66, 205.[30] Reynolds, M.S.; Butler, A. *Inorg. Chem.*, **1996**, 35, 2378.
[34] Reynolds, M.S.; Butler, A. *Inorg. Chem.*, **1996**, 35, 2378.
[35] Harrison, A.T.; Howarth, O.W. *J. Chem. Soc. Dalton Trans.*, **1985**, 1173.
[36] Vandenborre, M.T.; Prost, R.; Huard, E.; Livage, J. *J. Mater. Res. Bull.*, **1983**, 18, 1133
[37] Barboux, P.; Morineau, R.; Livage, J. *Solid State Ionics*, **1988**, 27, 221

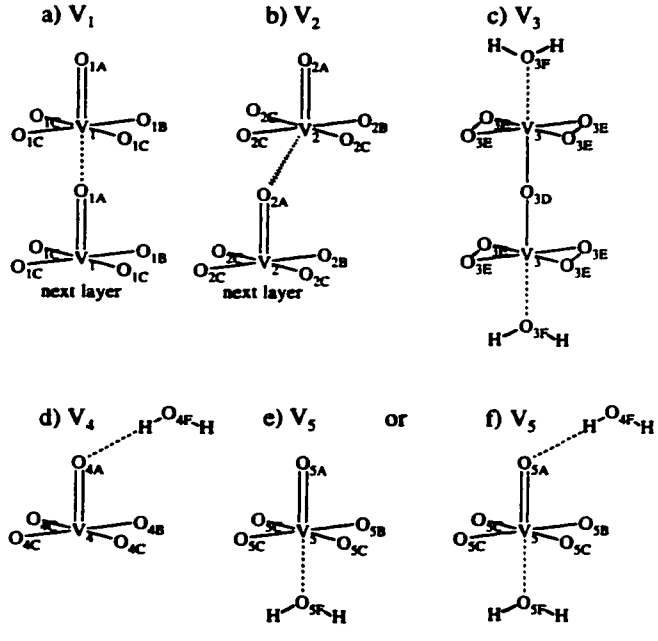

Figure 1.

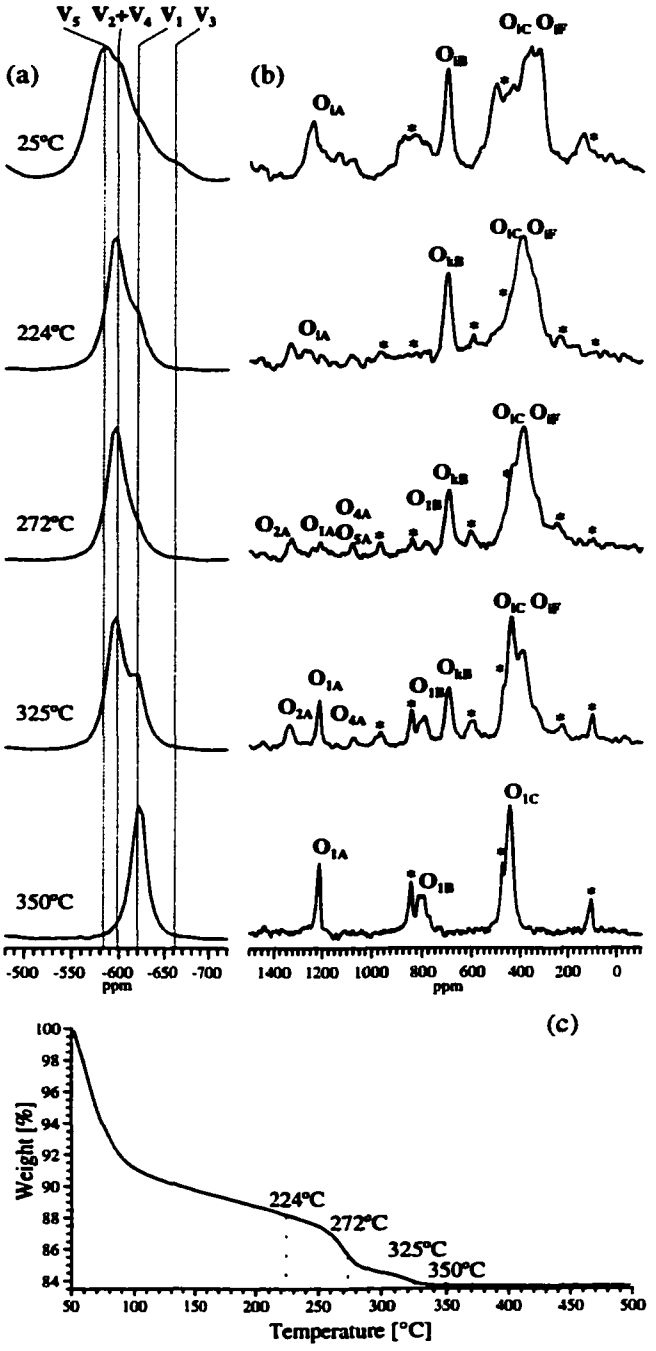
(a)
(b)
(c)
V5 V2+V4 V1 V3
25°C
224°C
272°C
325°C
350°C
O1A
O1B
O1C O1F
O2A
O4A
O5A
-500 -550 -600 -650 -700
ppm
1400 1200 1000 800 600 400 200 0
ppm
Weight [%]
Temperature [°C]
224°C
272°C
325°C
350°C

Figure 2.

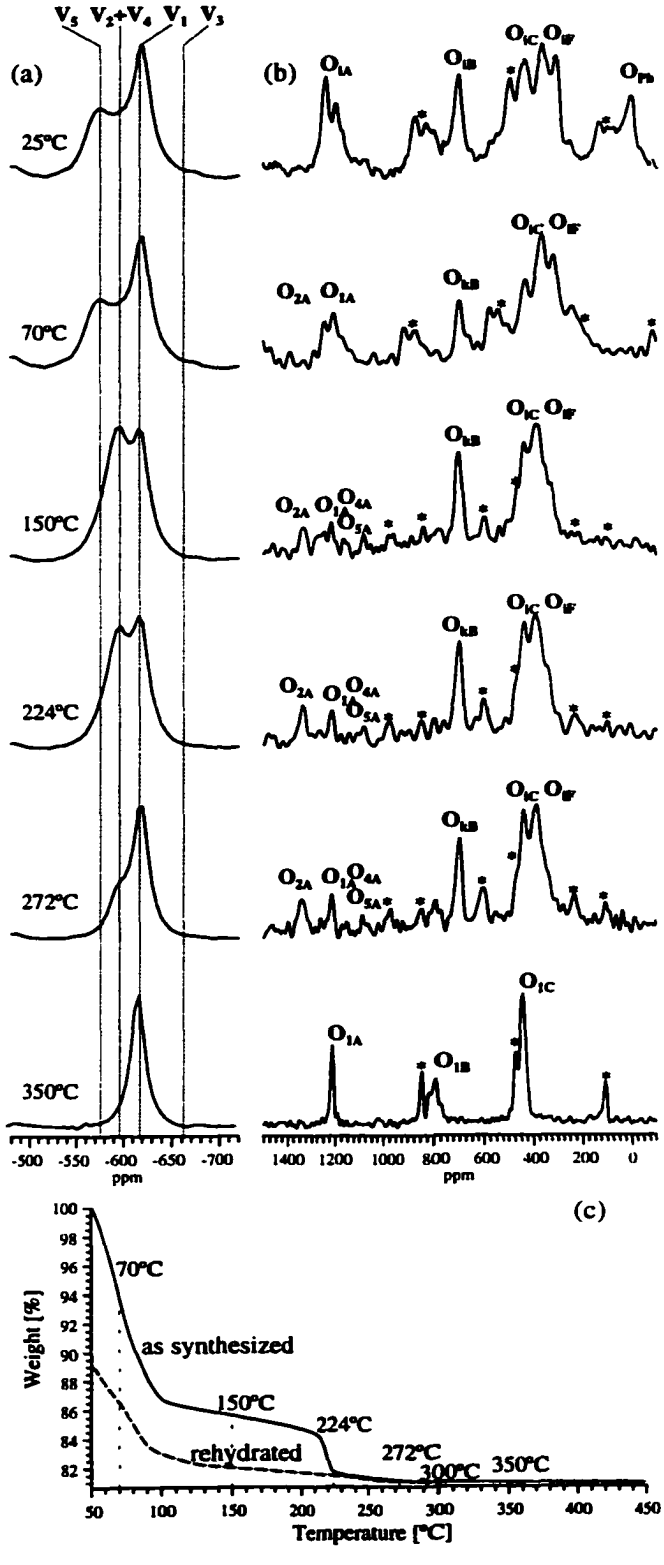
(a)
(b)
(c)
25°C
70°C
150°C
224°C
272°C
350°C
ppm
ppm
Weight [%]
Temperature [°C]
as synthesized
rehydrated
300°C

Figure 3.

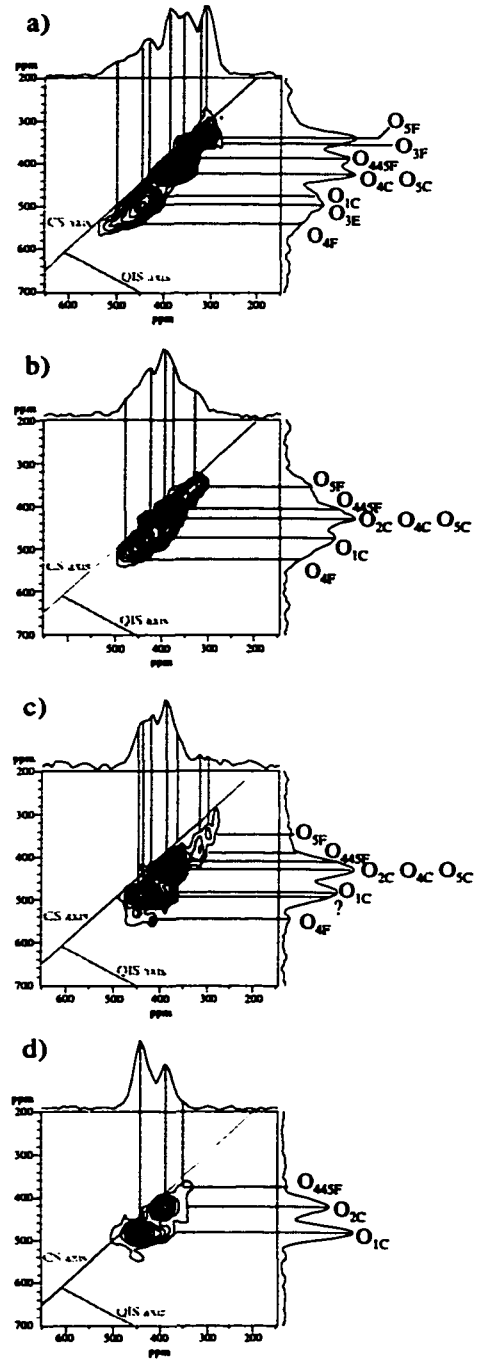
a)
O_{5F}
O_{3F}
O_{445F}
O_{4C} O_{5C}
O_{1C}
O_{3E}
O_{4F}
b)
O_{5F}
O_{445F}
O_{2C} O_{4C} O_{5C}
O_{1C}
O_{4F}
c)
O_{5F}
O_{445F}
O_{2C} O_{4C} O_{5C}
O_{1C}
?
O_{4F}
d)
O_{445F}
O_{2C}
O_{1C}

Figure 4.

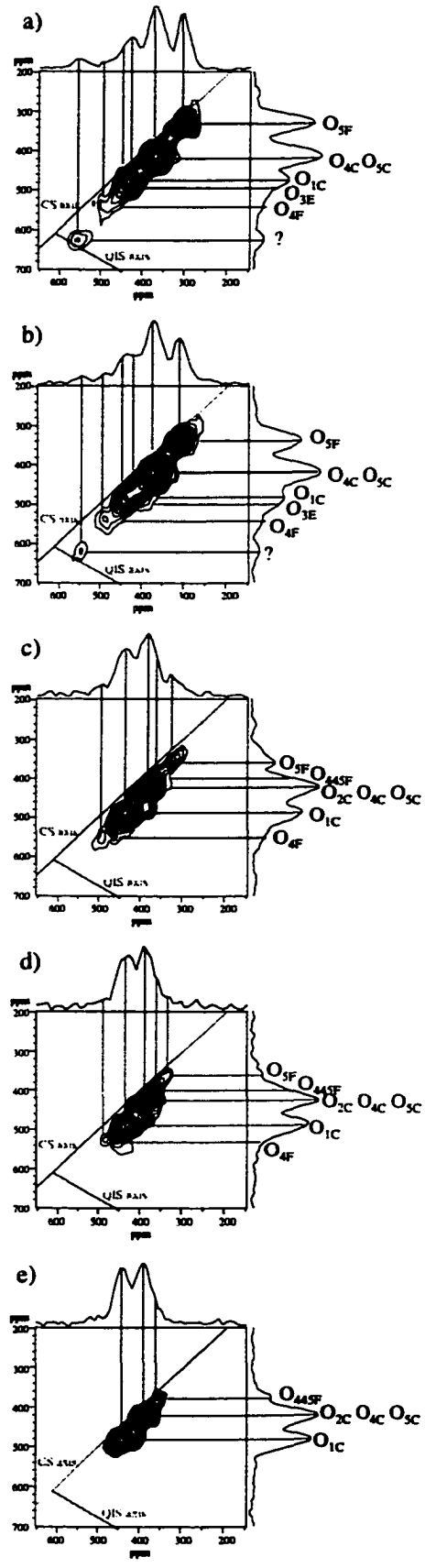
a)
O_{5F}
O_{4C} O_{5C}
O_{1C}
O_{3E}
O_{4F}
?
b)
O_{5F}
O_{4C} O_{5C}
O_{1C}
O_{3E}
O_{4F}
?
c)
O_{5F} O_{445F}
O_{2C} O_{4C} O_{5C}
O_{1C}
O_{4F}
d)
O_{5F} O_{445F}
O_{2C} O_{4C} O_{5C}
O_{1C}
O_{4F}
e)
O_{445F}
O_{2C} O_{4C} O_{5C}
O_{1C}

Figure 5.

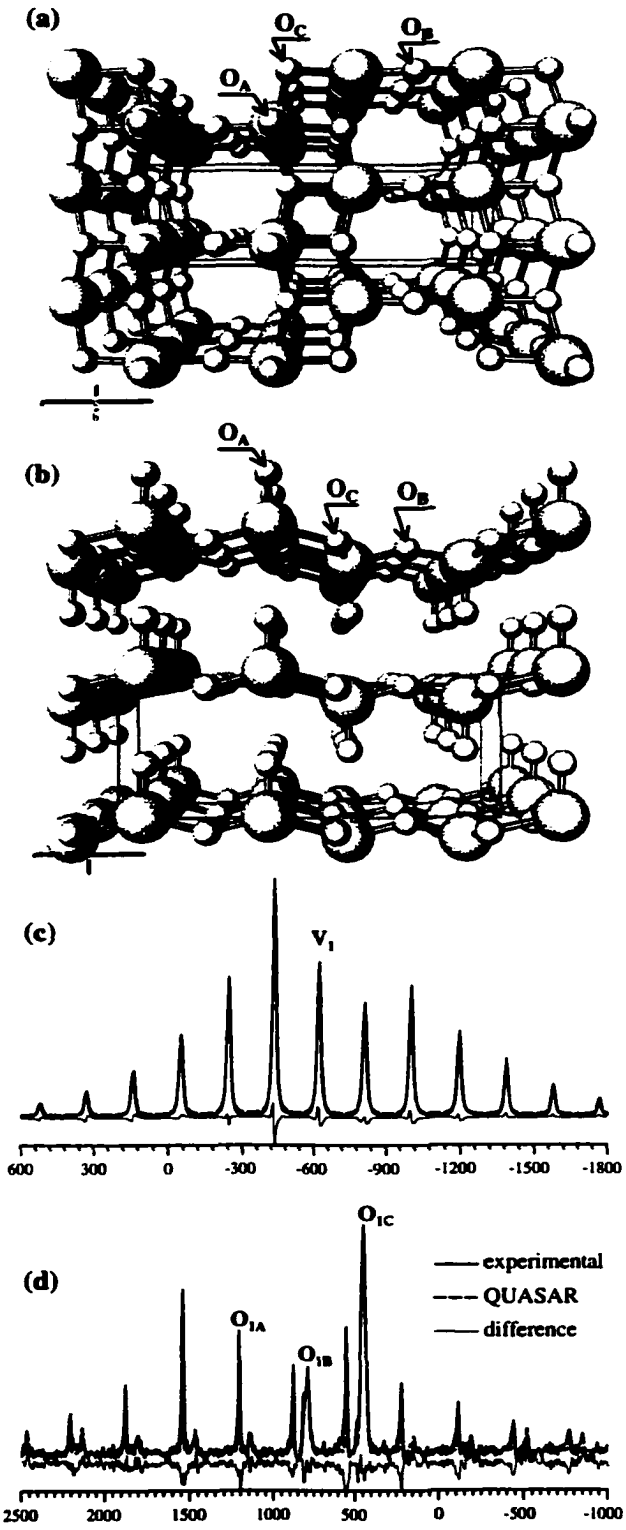
(a)
O_C
O_B
O_A
(b)
O_A
O_C
O_B
(c)
V_1
600
300
0
-300
-600
-900
-1200
-1500
-1800
(d)
O_{1C}
experimental
QUASAR
difference
O_{1A}
O_{1B}
2500
2000
1500
1000
500
0
-500
-1000

Figure 6.

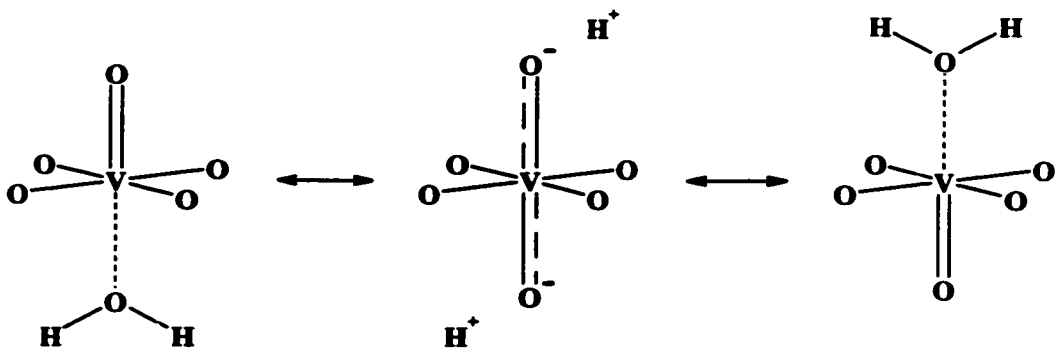

Figure 7.

Table 1. Sample I: Quadrupole coupling constant (C_Q in MHz), quadrupolar asymmetry parameter (η_Q), isotropic chemical shift (δ_{iso} in ppm), chemical shift anisotropy ($\Delta\delta_{CSA}$ in ppm), and CSA asymmetry parameter (η_{CSA}) obtained by QUASAR simulations[a,b] of ^{51}V MAS NMR spectra.

Temperature (°C)	V_i	%	δ_{iso}[c]	C_Q	η_Q	$\Delta\delta_{CSA}$[c]	η_{CSA}[c]
25	V_1	13.1	-625	0.86	0.05	-862	0.26
	V_2+V_4[d]	45.5	-594	1.44	1.00	-1032	0.62
	V_3	5.8	-661	1.20	0.66	-1096	0.20
	V_5	35.6	-574	1.32	0.00	-883	0.64
224	V_1	21.5	-616	0.86	0.01	-960	0.24
	V_2+V_4	74.2	-593	1.70	0.79	-848	0.50
	V_5	4.3	-574	1.32	0.00	-883	0.64
272	V_1	13.6	-620	0.79	0.18	-960	0.24
	V_2+V_4	81.4	-593	1.19	0.71	-825	0.31
	V_5	5.0	-574	1.32	0.00	-883	0.64
325	V_1	28.6	-620	0.79	0.18	-960	0.24
	V_2+V_4[e]	71.4	-593	1.45	0.63	-887	0.58
350	V_1	100	-623	0.86	0.10	-960	0.00

a) The data were obtained with the following accuracy: C_Q: ± 0.05 MHz; η_Q and η_{CSA}: ± 0.05; δ_{iso}: ± 0.5 ppm; $\Delta\delta_{CSA}$ and δ_{ii}: ± 5 ppm.

b) Euler angels between CSA and Q tensors (α, β, γ in degrees) reported in literature for V_2O_5 are varying between 0 and 180 degrees, which has been explained elsewhere.[29] For our results, the β angle was found to be in the range 53-79 deg., while α and γ were kept at 0.

c) Chemical shift tensor parameters δ_{iso}, $\Delta\delta_{CSA}$, η_{CSA}, and δ_{ii} are related as follows: $\delta_{iso} = {}^1/_3\cdot(\delta_{11} + \delta_{22} + \delta_{33})$; $\Delta\delta_{CSA} = {}^3/_2\cdot(\delta_{33} - \delta_{iso})$; $\eta_{CSA} = (\delta_{22} - \delta_{11})/(\delta_{33} - \delta_{iso})$ assuming $|\delta_{33} - \delta_{iso}| \geq |\delta_{11} - \delta_{iso}| \geq |\delta_{22} - \delta_{iso}|$.

d) V_4 only.

e) V_2 only.

Table 2. Sample II: Quadrupole coupling constant (C_Q in MHz), quadrupolar asymmetry parameter (η_Q), isotropic chemical shift (δ_{iso} in ppm), chemical shift anisotropy ($\Delta\delta_{CSA}$ in ppm), and CSA asymmetry parameter (η_{CSA}) obtained by QUASAR simulations[a,b] of ^{51}V MAS NMR spectra.

Temperature (°C)	V_i	%	δ_{iso}[c]	C_Q	η_Q	$\Delta\delta_{CSA}$[c]	η_{CSA}[c]
25	V_1	31.6	-616	1.44	0.39	-857	0.54
	V_2+V_4[d]	19.3	-593	1.40	0.56	-1020	0.73
	V_3	7.9	-659	1.20	0.66	-885	0.20
	V_5	41.5	-569	1.43	0.44	-1096	0.99
150	V_1	20.7	-618	1.33	0.55	-846	0.54
	V_2+V_4	66.9	-594	1.38	0.50	-1004	0.74
	V_3	2.1	-659	1.20	0.66	-885	0.20
	V_5	10.3	-569	1.43	0.44	-1096	0.99
224	V_1	26.0	-617	1.55	0.64	-855	0.54
	V_2+V_4	67.4	-593	1.44	0.56	-1019	0.73
	V_5	6.5	-569	1.43	0.44	-1096	0.99
272	V_1	64.7	-616	0.74	0.03	-980	0.13
	V_2+V_4	33.8	-592	1.70	1.00	-1054	0.46
	V_5	1.5	-569	1.43	0.44	-1096	0.99
350	V_1	100	-623	0.86	0.10	-960	0.00

a) The data were obtained with the following accuracy: C_Q: ± 0.05 MHz; η_Q and η_{CSA}: ± 0.05; δ_{iso}: ± 0.5 ppm; $\Delta\delta_{CSA}$ and δ_{ii}: ± 5 ppm.

b) Euler angels between CSA and Q tensors (α, β, γ in degrees) reported in literature for V_2O_5 are varying between 0 and 180 degrees, which has been explained elsewhere.[29] Therefore, we used β angle in the range 53-79 deg., while α and γ were kept at 0.

c) Chemical shift tensor parameters δ_{iso}, $\Delta\delta_{CSA}$, η_{CSA}, and δ_{ii} are related as follows: $\delta_{iso} = {}^1/_3\cdot(\delta_{11} + \delta_{22} + \delta_{33})$; $\Delta\delta_{CSA} = {}^3/_2\cdot(\delta_{33} - \delta_{iso})$; $\eta_{CSA} = (\delta_{22} - \delta_{11})/(\delta_{33} - \delta_{iso})$ assuming $|\delta_{33} - \delta_{iso}| \geq |\delta_{11} - \delta_{iso}| \geq |\delta_{22} - \delta_{iso}|$.

d) V_4 only.

Table 3. Isotropic chemical shifts and P_Q values for samples I and II determined from ^{17}O 3QMAS NMR spectra

site	chemical shift (ppm) range	P_Q (MHz) range
O_{1C}	460-471	3.5-4.0
O_{2C} O_{4C} O_{5C}	400-420	2.9-3.5
O_{3E}	474	4.3
O_{3F}	343	
O_{4F}	507-515	
O_{5F}	328-332	
O_{445}	375-377	
?	602	

Table 4. Results of numerical simulation (QUASAR) of ^{17}O MAS spectrum of crystalline V_2O_5.

	δ_{iso}	$\Delta\delta_{CSA}$	η_{CSA}	C_Q	η_Q
V_1	-620	960	0.2	0.9	0.1
O_{1A}	1213	2600	1.0	0.9	0.6
O_{1B}	824	450	0.4	4.0	0.7
O_{1C}	474	0	0.0	3.3	0.6

CHAPTER 6

VMoO Gel-Based Materials Synthesized via Peroxovanadate Precursors. 1. Evidence for a Supersaturated Solid Solution.

A Manuscript Submitted to Chemistry of Materials (2001)

Craig J. Fontenot*+, W.D. Schroeder*+, and G. L. Schrader*+#

Department of Chemical Engineering* and
Ames Laboratory – USDOE+
Iowa State University
Ames, IA 50011

Abstract

Vanadium-molybdenum oxide gels derived from the reaction of mono- and diperoxovanadates with an ammonium molybdate solution have been investigated using XRD, laser Raman spectroscopy, TGA, and TPD. Based on the laser Raman and powder x-ray diffraction results at intermediate stages of thermal treatment, evidence for the presence of a supersaturated solid solution phase is reported. Surface areas could be increased by exchanging the water trapped in the gel matrix with a lower surface tension solvent.

key words: vanadium oxide gels, molybdenum oxide gels, XRD, laser Raman, solid solution

author to whom correspondence should be addressed

6.1 Introduction

Mixed metal oxide are known to have interesting catalytic properties, and in several cases, the formation of solid solutions has been shown to be important for superior catalytic performance.[1-6] Previous research has demonstrated that the relative concentration of each component can be optimized to achieve improved activity and/or selectivity. Some catalyst preparation techniques, such as precipitation/calcination or solid-state synthesis may produce established equilibrium phases. However, sol-gel synthesis techniques offer an opportunity to produce new materials which may include metastable or supersaturated phases. In our research, we have been investigating new catalytic materials which may be promising for the low temperature selective oxidation of hydrocarbons such as 1,3-butadiene.

In our previous publications, *in situ* laser Raman and ^{51}V NMR spectroscopic characterization of the synthesis of vanadia gels by a peroxo-based process was reported along with characterization of the subsequent vanadia gels.[7-9] The nature of the vanadium-oxygen coordination was determined, and the coordination of water had a significant role in the modification of these vanadia gel sites. Our group has recently reported an investigation of the selective oxidation of 1,3-butadiene over VMoO gel-based materials prepared via the peroxo method.[4,5] The selectivity to maleic anhydride increased as more molybdenum was incorporated into the solid solution phase, but the concentration of molybdenum in the solid solution has been reported to be limited to 10-16 mole % at equilibrium.[10,11] However, our work suggested that if this solubility limit was surpassed, higher selectivities to desired selective oxidation products was obtainable.

Several methods for the addition of molybdenum to these vanadia oxide gels has been reported, along with limited characterization of the resulting materials. However, studies of the gel to crystalline phase transformation and the effect of molybdenum concentration on the structure have not been reported in the literature. Layered VMoO gels having the stoichiometry $H_2V_{12-x}Mo_xO_{31 \pm y} \cdot nH_2O$ (x = 0, 0.5, 1, 2, and 3) were made by Zacharova et al. by reacting a mixture of molybdenum acid ($H_2MoO_4 \cdot 1.3\ H_2O$) and V_2O_5 with H_2O_2.[12] Their work examined the frequency dependence of the conductance and capacitance and determined values for the carrier mobilities. Mobility in the direction parallel to the VMoO layers was reported to be 4 orders of magnitude greater than the mobility perpendicular to these planes. They also reported that the conductance and capacitance depended on the relative humidity of the surrounding environment, but only when some molybdenum had been incorporated into the vanadium gels.

Another route to layered VMoO gel materials was reported by Dingsan et al. using peroxovanadate precursors and molybdenum metal.[13] They reported synthesizing thin films of hydrated VMoO gels having the stoichiometry $H_2V_{12-x}Mo_xO_{31 \pm y} \cdot nH_2O$ (x=0.25). The TGA and XRD results indicated that the compounds had a layered structure with V^{5+} and Mo^{6+} ions being well distributed in the films. The humidity sensing properties of this film were evaluated and the conductance and capacitance was reported to increase in an exponential fashion with increasing relative humidity. They also reported that the sensor had excellent long-term stability, reversibility, and reproducibility.

Dunn et. al reported synthesizing aerogel-like VMoO gels using alkoxide precursors.[14] This study focused on an ambient pressure drying technique which replaced the water molecules trapped in the gel matrix with a lower surface tension solvent.

In the current work, laser Raman spectroscopy (LRS), powder x-ray diffraction (XRD), temperature programmed desorption (TPD) and thermogravimetric analysis (TGA) were employed to characterize VMoO gels of varying composition. Detailed structural information about these gels has been revealed by this characterization along with the temperatures of water and ammonia desorption.

6.2 Experimental

6.2.1 Sample Preparation

Samples A-D were prepared by reacting an aqueous peroxovanadate solution with a molybdate solution at room temperature. The 0.26 M peroxovanadate solutions were prepared by reacting crystalline V_2O_5 (Alfa) with 30% wt. H_2O_2 (Fisher) using a H_2O_2:V_2O_5 molar ratio of 25. Prior characterization has revealed that these solutions consisted mostly of the diperoxovanadium anion, although small amounts of the monoperovanadium cation and the neutral diperoxovanadate dimer were also present. The molybdate solutions were prepared by dissolving ammonium molybdate [$(NH_4)_2MoO_4$] in de-ionized water. Results are reported for four samples having 3.3, 14.0, 26.4, and 45.5 mole % MoO_3 in V_2O_5 and will be referred to as samples A, B, C and D, respectively. The molar percent of MoO_3 in the samples was calculated as: moles MoO_3/ (moles MoO_3 + moles V_2O_5) to facilitate comparison with the published equilibrium phase diagrams.[10,11] The stoichiometry of the as-prepared samples as described by the general formula $(NH_4^+)_{2y}\ H_nV_{12-y}\ Mo_yO_{30+n/2}$ has been provided in Table 1.

Unless otherwise specified, the thermally treated samples were heated in N_2 and then cooled quickly in N_2.

6.2.2 Laser Raman Spectroscopy.

Laser Raman spectra were obtained using a Coherent 532-50 diode-pumped laser (532 nm, 50 mW at the source) and were collected at 180° using a Kaiser probe head coupled via fiber optics to a Kaiser Holospec f/1.8 spectrometer.

6.2.3 X-ray Powder Diffraction.

X-ray powder diffraction data was obtained using a Seimens D500 (50 kV, 27 mA) diffractometer equipped with a diffracted beam monochromator (Cu K_α radiation). The detector slit width was 0.05 %, the step size was 0.02, and the dwell time was 1 s.

6.2.4 Thermogravimetric Analysis.

Samples were analyzed using a Perkin Elmer TGA 7 instrument. Heating rates were 5 °C/min in N_2, although selected samples were examined at rates as low as 2 °C/min to confirm the procedure.

6.2.5 Differential Scanning Calorimetry

Samples were analyzed using a Perkin Elmer DSC 7. Heating rates were 5 °C/min.

6.2.6 Temperature Programmed Desorption

Samples were analyzed in a quartz micro-reactor using a helium purge rate of 40 sccm. A Varian 3600 gas chromatograph with a PorapakQ 80/100 column was used to separate the water and ammonia peaks. The column, TCD detector filament and TCD detector were held at 150 °C, 275 °C and 200 °C, respectively.

6.2.7 Surface Area.

Surface areas were determined by the BET method (N_2 adsorption) and the pore size distribution was determined by the BJH method. A Micromeritics ASAP 2000 instrument was used for both measurements.

6.3 Results

Laser Raman characterization of the as-prepared samples (Figure 1) revealed that sample A had a spectrum similar to a previously reported layered V_2O_5 gel.[9, 15] Raman spectra for samples B and C were similar to each other and showed very broad bands consistent with a disordered V_2O_5-like material.[8] The spectrum for sample D clearly differed from the other samples and contained even broader bands; the strongest having a maximum at about 730 cm^{-1}.

Laser Raman spectra for the samples calcined at 350°C/ 4h in dry air (Figure 2). revealed band positions that were similar to that of both crystalline V_2O_5[16] and amorphous V_2O_5[15] although the bands were weaker and slightly broader. As the molybdenum loading was increased a shift was observed for the vanadyl band, (992 cm^{-1} in crystalline V_2O_5) as illustrated in Figure 3.

In general, the powder x-ray diffraction results for all as-prepared samples (Figure 4) revealed weak peaks that were consistent with a previously reported mixed phase vanadia gel containing a layered phase and an amorphous phase.[8] However, Sample D differed slightly and contained several additional peaks around $2\theta = 28°$. X-ray data was also collected for samples B and D after successive stages of thermal treatment in N_2. For sample B (Figure 5), after each progressive stage of heating up to 325 °C, the diffraction patterns remained relatively similar. However, after thermal treatment to 400 °C, the diffraction peaks

corresponding to a Mo-substituted V_2O_5 solid solution appeared. Upon further thermal treatment, these features became more distinct, until the expected equilibrium solid solution phase was identified at 570 °C. For sample D (Figure 6), thermal treatment to 300 °C resulted in the appearance of diffraction peaks that were consistent with V_2MoO_8 and/or $V_2MoO_{7.5}$.[17] Also, the presence of the peak at $2\theta = 10.7°$ for sample D at 300 °C was consistent with the presence of an intermediate layered phase having a d-spacing of 8.3 Å. Upon further heating, additional diffraction peaks appeared that were consistent with both a Mo-substituted V_2O_5 solid solution and V_2MoO_8 and/or $V_2MoO_{7.5}$.

The x-ray data for samples thermally treated at 350 °C for 4 h in dry air indicated (Figure 7) that some crystallization had occurred. Comparison of the x-ray diffraction patterns corresponding to samples A-D indicated that more more distinct diffraction peaks could be observed for the samples containing less amounts of molybdenum (samples A and B), while the samples containing higher concentrations of Mo (samples C and D) showed relatively weaker peak intensities and broader features. Powder x-ray data was also collected for each sample after thermal treatment at 570 °C for 10 h; solid solution formation was apparent for samples A and B and a mixed phase of a solid solution with V_2MoO_8 and/or $V_2MoO_{7.5}$ for samples C and D was detected.

Temperature programmed desorption (TPD) studies indicated that both water and ammonia desorbed during thermal treatment. For all samples, ammonia desorbed from 100 - 450 °C with a maximum at 360 °C and water desorbed in two regions: below 150 °C and from 350 - 380 °C with a maximum around 360 °C.

Thermogravimetric analysis (TGA) of samples A-D (Figure 8) revealed a decrease of between 12-14 wt. % upon heating to 550 °C. Generally, there seemed to be four regions of

weight loss: the first at less than 125 °C, the second from 125 - 285 °C, the third from 285 - 340 °C, and the fourth from 340 - 375 °C. Differential scanning calorimetry (DSC) analysis results were similar for each sample; a large endothermic peak was observed around 350 °C and a smaller exothermic peak around 570 °C.

Following thermal treatment to 100 °C for 4 h. samples A, B, C and D had surface areas of 1 - 2 m^2/g. Surface area analysis after solvent exchange with n-pentane for 10 days followed by thermal treatment at 350 °C for 4 hours showed that the surface areas for samples A, B, C and D had increased to 3.3, 12.6, 6.1 and 15.5 m^2/g, respectively. Pore size distribution analysis (BJH method) for these solvent-exchanged samples indicated a bi-modal distribution with one maxima between 100-150 Å and the other < 17Å.

6.4 Discussion

Previous reports have indicated that VMoO solid solutions are expected at MoO_3 concentrations of less than either 10 mole %[10] or 16 mole %[11] MoO_3. The solid solution phase has been shown to be substitutional, in which Mo^{6+} directly replaces V^{5+} in the orthorhombic V_2O_5 crystal structure. In this solid solution, charge neutrality is maintained as V^{5+} reduces to V^{4+} when Mo^{6+} is substituted into the lattice. When the concentration of molybdenum exceeds the solid solution solubility limit, an additional phase appears. There is discrepancy in the literature as to the composition of this additional phase, but either V_2MoO_8 [18] or $V_6Mo_9O_{40}$ [10,11] have been reportedly observed.

For the reaction of V_2O_5 + MoO_3, Volkov et al. reported that the source of the V^{4+} was the solid state reaction:[19]

$$V_2O_5 + ye^- \rightarrow V_2O_{5-y} + y\,O^-$$

and

$$(V_{1-x}Mo_x)_2O_{5+y} + ze^- \rightarrow (V_{1-x}Mo_x)_2O_{5+y-z} + z\,O^-$$

However, since ammonium and water were present in these materials, the redox chemistry may have been more complex. Nevertheless, EPR studies of these gel-based materials did indicate the presence of V^{4+}, as we will discuss in a subsequent publication.[20]

Additional XRD characterization was performed on samples B and D after successive stages of thermal treatment in N_2 since these fell on each side of the solid solution limit. For the as prepared sample B (Figure 5), the diffraction pattern was consistent with a layered structure. As thermal treatment progressed to 325 °C, the peak at about $2\theta = 8.2°$ began to increase in intensity and to shift to smaller scattering angles. This shift, which indicated an increase in the interlayer distance, was surprising since previous reports of similar layered $V_2O_5 \cdot nH_2O$ gels indicated that the interlayer distance decreased as water was driven out upon heating. At temperatures greater than 325 °C, peaks corresponding to the presence of the solid solution appeared and became more intense. The XRD results for the as prepared sample D (Figure 6) indicated that as thermal treatment progressed, a relatively strong peak appeared at $2\theta = 10.7°$, which probably was a more pronounced indication that the layered structure had formed (d = 8.3 Å). At this stage, other peaks had appeared that corresponded to V_2MoO_8 or $V_2MoO_{7.5}$. At higher temperatures, crystalline phases begin to form in this sample, mostly V_2MoO_8 or $V_2MoO_{7.5}$ and a small amount of the solid solution. These high temperature results were consistent with the equilibrium phase diagram.

Interestingly, the XRD results for the samples heated in dry air (Figure 7) were somewhat different from those heated in N_2 (Figures 5 and 6). This is readily apparent for

sample D where more crystallization occurred when the same sample was heated in N_2 at 300 °C, than when the sample was heated in air for 4 h at 350 °C. This seems to indicate that for these gels, the presence of oxygen plays a significant role in the crystalline phase formation. Morette et al.[21] previously reported the reduction of V_2MoO_8 with H_2: reduction may also occur due to the presence of NH_4^+ in these materials.

Previous laser Raman characterization of VMoO solid solution behavior revealed that the vanadyl band shifted to lower wavenumbers as the concentration of MoO_3 was increased.[22] Furthermore, this trend was shown to be linear in the solid solution regime which provides another indication of solid solution formation for the gel samples. The Raman spectra for the samples calcined at 350 °C for 4 h in dry air (Figure 2) revealed that the vanadyl band shifted to lower wavenumbers as a function of the molybdenum concentration. The plot of the observed V=O Raman band versus mole % MoO_3 clearly revealed a linear trend, at least up to 26 mole % MoO_3 (Figure 3). This exceeds the previously reported limits at 10-16 mole % MoO_3, and thus the phase can probably be considered to be supersaturated.

Further evidence for a supersaturated phase was obtained from the x-ray data. Comparison of the diffraction patterns (Figure 7) of the thermally treated (350 °C for 4 h in air) reveals two distinct trends as the molybdenum concentration was increased: (1) the degree of crystallinity decreased, and (2) the diffraction peaks also shifted. In addition, the x-ray data for sample D (Figure 7) revealed additional peaks at $2\theta = 11.3°$ and around $2\theta = 28.3°$, which indicates that the layered structure is still present at this intermediate temperature. Previous reports have indicated that for VMoO solid solutions, the peak positions shift to reflect changes in the d-spacing which occurs during the incorporation of the larger Mo^{6+} ion into the V_2O_5 framework.[10] Furthermore, in the solid solution regime this change was reported to

increase linearly with the incorporation of molybdenum. Following thermal treatment to 350 °C for 4 h in dry air, the peak maxima locations corresponding to the 101 plane ($2\theta = 21.7°$) and the 110 ($2\theta = 26.1°$) were consistent with this linear trend (Figure 9), even up to 45.5 mole % MoO_3 (sample D). This suggests that the crystalline portion of this material was a supersaturated solid solution. The peaks for sample D might also be assigned to the V_2MoO_8 or $V_2MoO_{7.5}$ phases [17,18] (Figure 6). Nevertheless, the x-ray data is conclusive for the formation of a supersaturated solid solution up to 26 mole % MoO_3 (sample C). Subsequent heating above 570 °C did result in the expected equilibrium phases.

A previous attempt at forming such a supersaturated solid solution was reported by Hirata et al..[10] They reported that quenching the oxide melt did not increase the molybdenum solubility. The lower temperatures used in the sol-gel route are probably a major factor in allowing for the presence of non-equilibrium phases, which may not be possible using other synthesis techniques.

Surface area analysis did not indicate any trend with increasing molybdenum content. This was somewhat surprising since powder x-ray analysis indicated that the amorphous portion of these gels was stabilized as more molybdenum was added. However, since these gels were dried at ambient conditions (xerogels), the predominant factor affecting surface area was probably the drying process (particularly the mechanism for water loss). Since water has a large surface tension, pores may collapse as water is driven-off during heating. A previous report indicated that solvent exchange for water can produce materials with higher surface areas.[14] In this work, experiments were completed in which the water present after synthesis was replaced with a lower surface tension solvent such as n-pentane. The sample was covered,

allowed to exchange for 10 days, then uncovered and dried at room temperature. The exchange of the solvent resulted in somewhat higher surface areas (~10-20 m^2/g).

6.5 Conclusions

Layered and amorphous mixed phase VMoO gel materials may be formed via the peroxo sol-gel method. The amorphous nature of the gel was stabilized as the molybdenum concentration was increased. The laser Raman and powder x-ray diffraction results obtained after thermal treatment at 350 °C for 4 h in dry air indicated the presence of a supersaturated solid solution for samples containing up to 26 % MoO_3. When heated to 570 °C the expected equilibrium phases were formed.

Acknowledgment. This research was supported at Ames Laboratory by the U.S. Department of Energy, Office of Basic Energy Sciences, Division of Chemical Sciences, under ContractW-7405-Eng-82.

6.6 List of Figures

Figure 1. Laser Raman spectra of as-prepared a) sample A , b) sample B, c) sample C, and d) sample D

Figure 2. Laser Raman spectra of VMoO gels after thermal treatment at 350 °C/ 4 h in air.

Figure 3. Shift of V=O wavenumber as a function of mole % MoO_3

Figure 4. Powder XRD of as-prepared a) sample A, b) sample B, c) sample C, and d) sample D

Figure 5. X-ray diffraction patterns for sample B at: a) 100 °C, b) 300 °C, c) 325 °C, d) 400 °C, e) 550 °C and f) crystalline V_2O_5.

Figure 6. X-ray diffraction patterns for sample D at: a) 100 °C, b) 300 °C, c) 325 °C, d) 400 °C, e) 550 °C f) $V_2MoO_{7.5}$ or V_2MoO_8 [17,18] and g) crystalline V_2O_5.

Figure 7. Powder x-ray diffraction results samples heated in air at 350 °C/4 h for a) crystalline V_2O_5, b) sample A, c) sample B, d) sample C, e) sample D [x 10].

Figure 8. Thermogravimetric analysis of a) sample A, b) sample B, c) sample C, and d) sample D.

Figure 9. Peak location of a) (110) plane and b) (001) plane versus mole % MoO_3 [samples treated at 350 °C/4h in dry air]

6.7 List of Tables

Table 1. Summary of As-Prepared Gel Composition: $H_nV_{12-y}Mo_yO_{30+n/2}(NH_4^+)_{2y}$

6.8 References

[1] Grasselli, R.K., *Applied Catalysis*, **1985**, 15, 127

[2] Brazdil, J.F.; Grasselli, R.K., *Journal of Catalysis*, **1983**, 79, 104

[3] Brazdil, J.F.; *CHEMTECH*, **1999**, January, 23

[4] Schroeder, W.; Fontenot, C.J.; Schrader, G.L. *J. Cat.* **2001**, 203, 382

[5] Schroeder, W.; Schrader, G.L. to be submitted 2001

[6] Bielanski, A.; Inglot, A.; *React. Kinet. Catal. Lett.*, **1977**, 6, 1, 83

[7] Fontenot, C.J.; Wiench, J.W.; Pruski, M.; Schrader, G.L. *J. Phys. Chem B.* **2000**, 104, 11622.

[8] Fontenot, C.J.; Wiench, J.W.; Pruski, M.; Schrader, G.L. *J. Phys. Chem B.* **2001**, 105,10496

[9] Fontenot, C.J.; Wiench, J.W.; Schrader, G.L.; Pruski, M. *J. Am. Chem Soc.*, **2001**, submitted

[10] Hirata, T.; Zhu, H. *J. Phys.: Condens. Matter* **1992**, 4, 7377

[11] Bielański, A.; Dyrek, K.; Poźniczek, J.; Wenda. E. *Bull. de l'acad. Pol. Des Sciences* **1971**, XIX, 8, 507

[12] Bondarenka, V.; Grebinskij, S.; Mickevičius, S.; Volkov, V.L.; Zacharova, G.S. *J. Non-Cryst. Sol.* **1998**, 226, 1
[13] Tong, M.; Dai, G.; Wu, Y.; He, X.; Yan, W.; Gao, D.; Volkov, V.; Zakhaova, G. *Mater. Res. Soc.* **2000**, 15, 12, 2653
[14] Harreld, J.H.; Dong, W.; Dunn, B. *Mater. Res. Bull.* **1998**, 33, 4, 561
[15] Sanchez, C.; Livage, J.; Lucazeau, G. *J. Raman. Spec.* **1982**, 12, 1, 68
[16] Abello, L.; Husson, E.; Repelin, Y.; Lucazeau, G.; *Spectrochemica Acta* **1983**, 39A, 7
[17] Freundlich, P. *Acad. Sci. (Paris)*, **1965**, 261, 153.
[18] Strupler, N.; Morette, A. *C.R. Hebd. Seances Acad. Sci.* **1965**, 260, 7, 1971
[19] Volkov, V.L., *Russian Journal of Physical Chemistry* **1985**, 59, 247
[20] Wiench, J.W.; Fontenot, C.J.; Schrader, G.L.; Pruski, M., **2001**, to be submitted
[21] Morette, A.; Strupler, *N. Fac. Pharm., Paris, Compt. Rend.* **1965**, 261(1(Group 8)), 145
[22] Ono, T.; Numata, H. *Applied Cat. A: General* **1997**, 157, 223

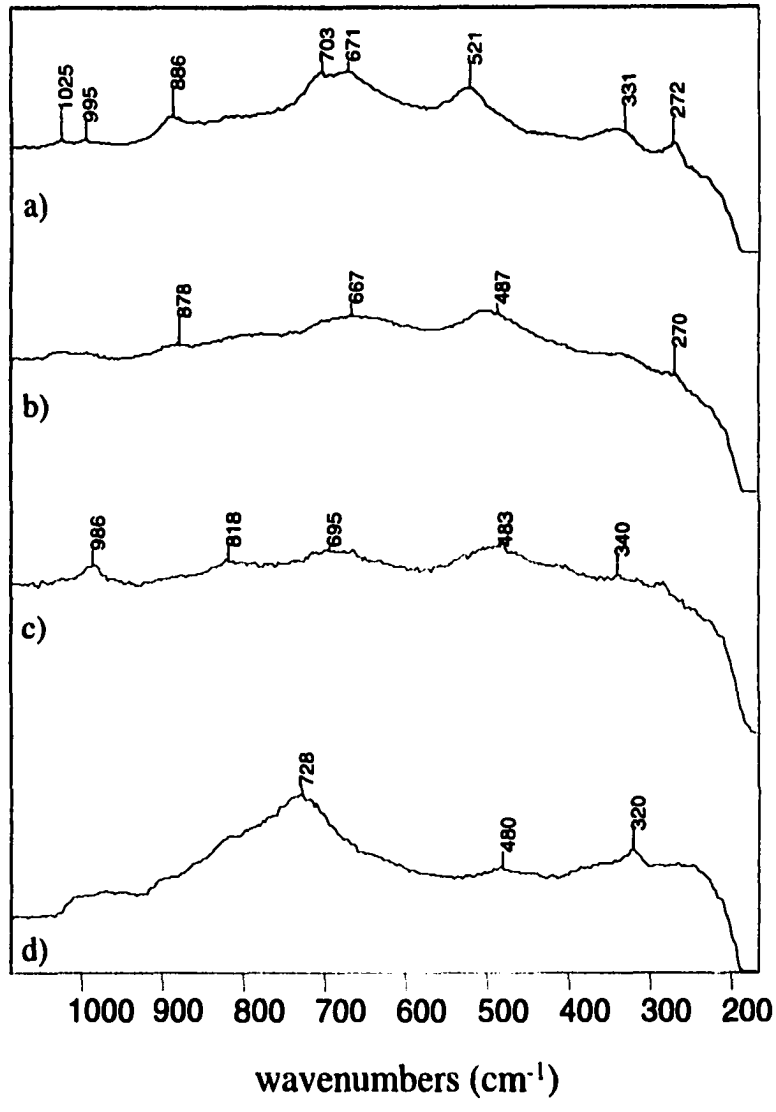

Figure 1. Laser Raman spectra of as-prepared a) sample A , b) sample B, c) sample C and d) sample D

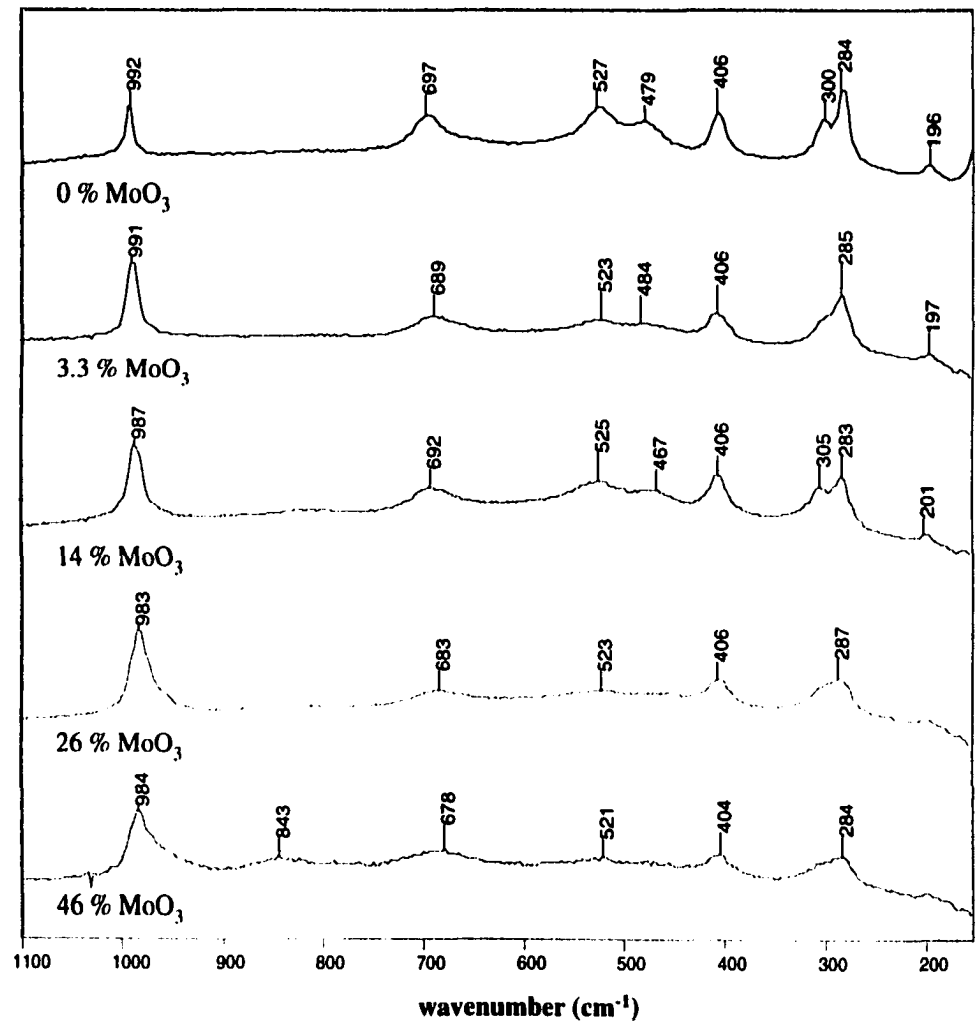

Figure 2. Laser Raman spectra of VMoO gels after thermal treatment at 350 °C/ 4 h in dry air.

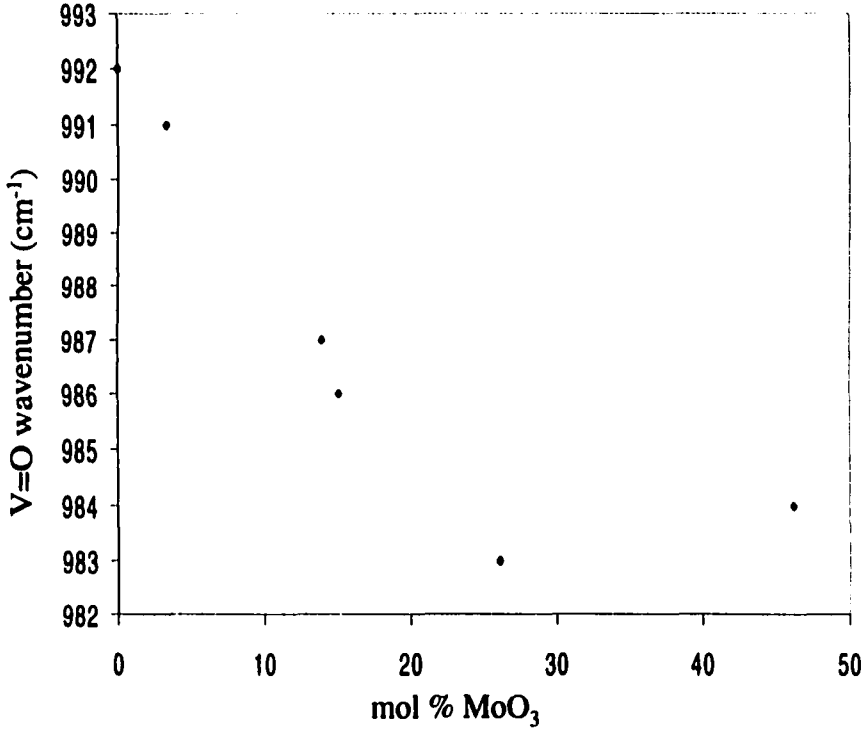

Figure 3. Shift of V=O wavenumber as a function of mole % MoO_3

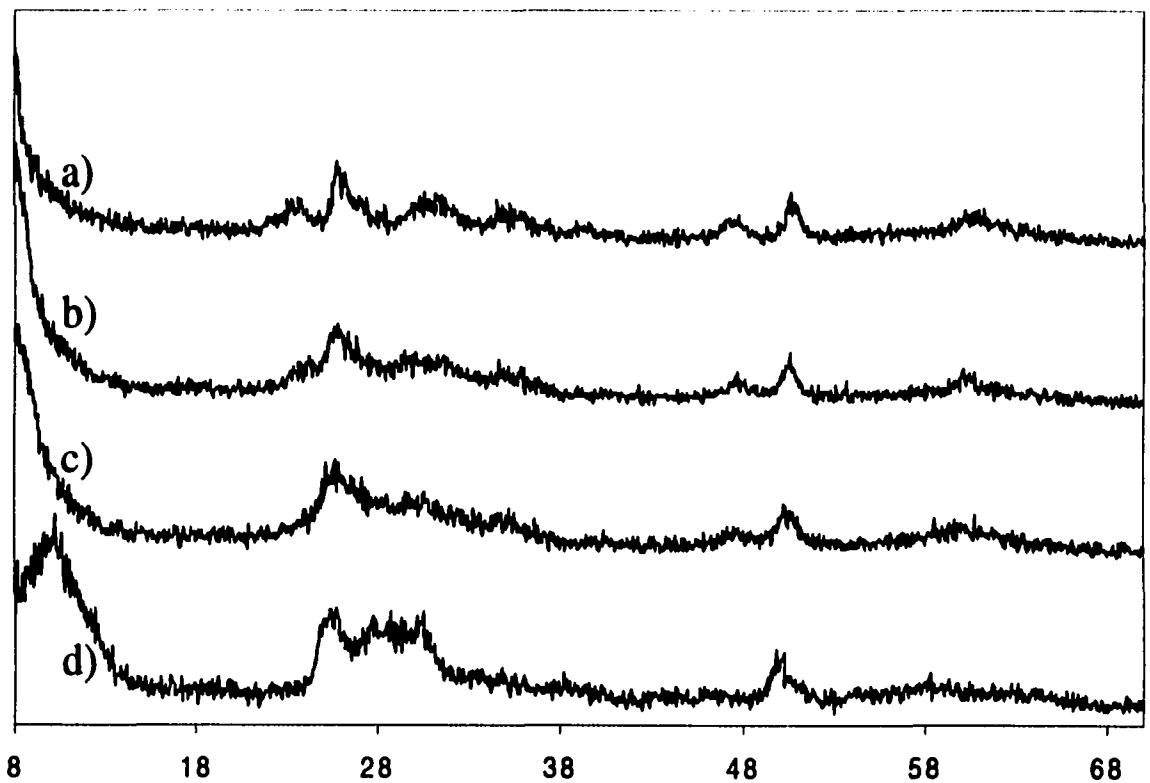

Figure 4. Powder XRD of as-prepared a) sample A, b) sample B, c) sample C and d) sample D

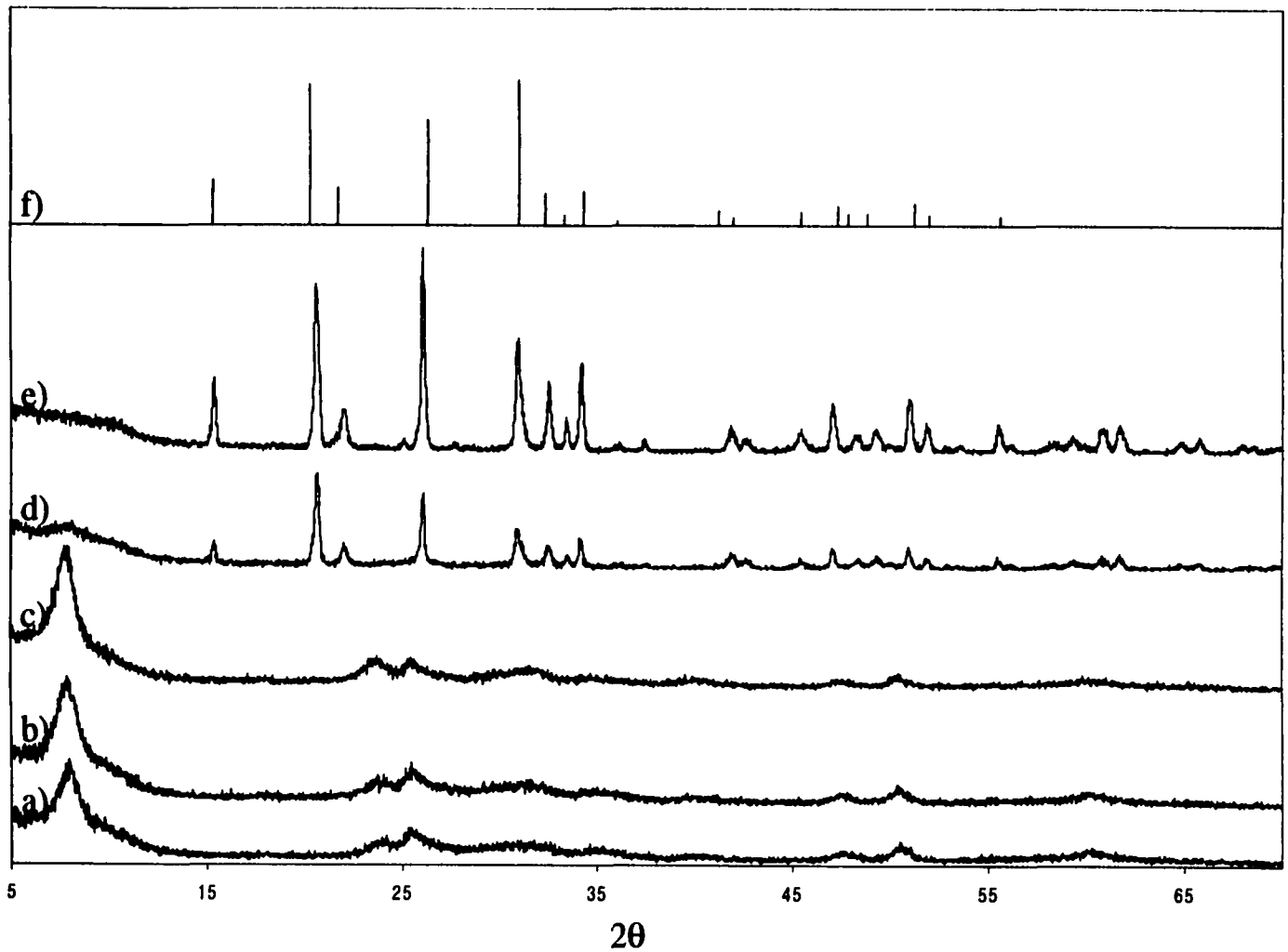

Figure 5. X-ray diffraction patterns for sample B at: a) 100 °C, b) 300 °C,c) 325 °C, d) 400 °C, e) 550 °C and f) crystalline V_2O_5.

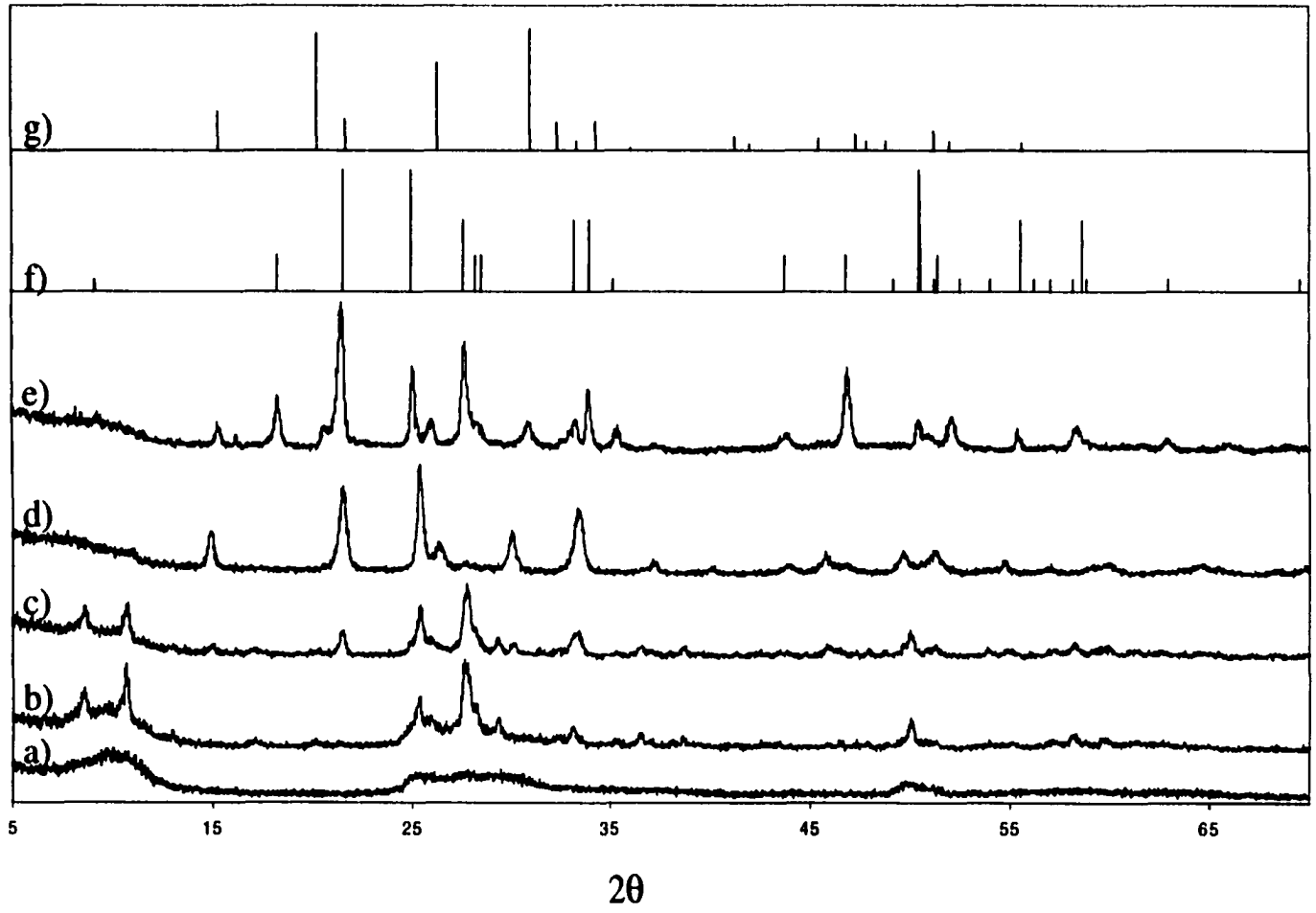

Figure 6. X-ray diffraction patterns for sample D at: a) 100 °C, b) 300 °C,c) 325 °C, d)400 °C, e) 550 °C f) $V_2MoO_{7.5}$ [15] and g) crystalline V_2O_5.

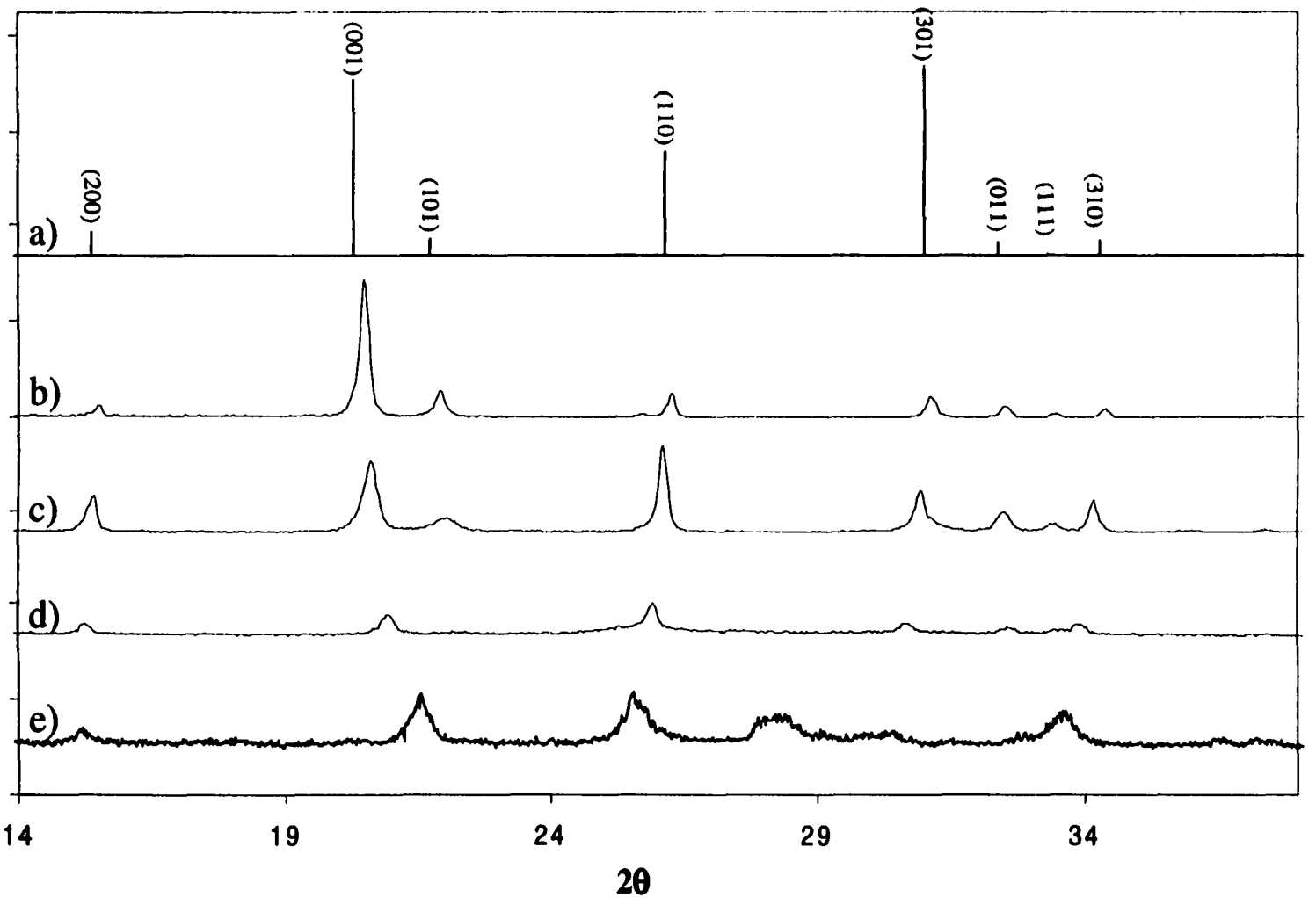

Figure 7. Powder x-ray diffraction results samples heated in air at 350 °C/4 h for a) crystalline V_2O_5, b) sample A, c) sample B, d) sample C, e) sample D [x 10]

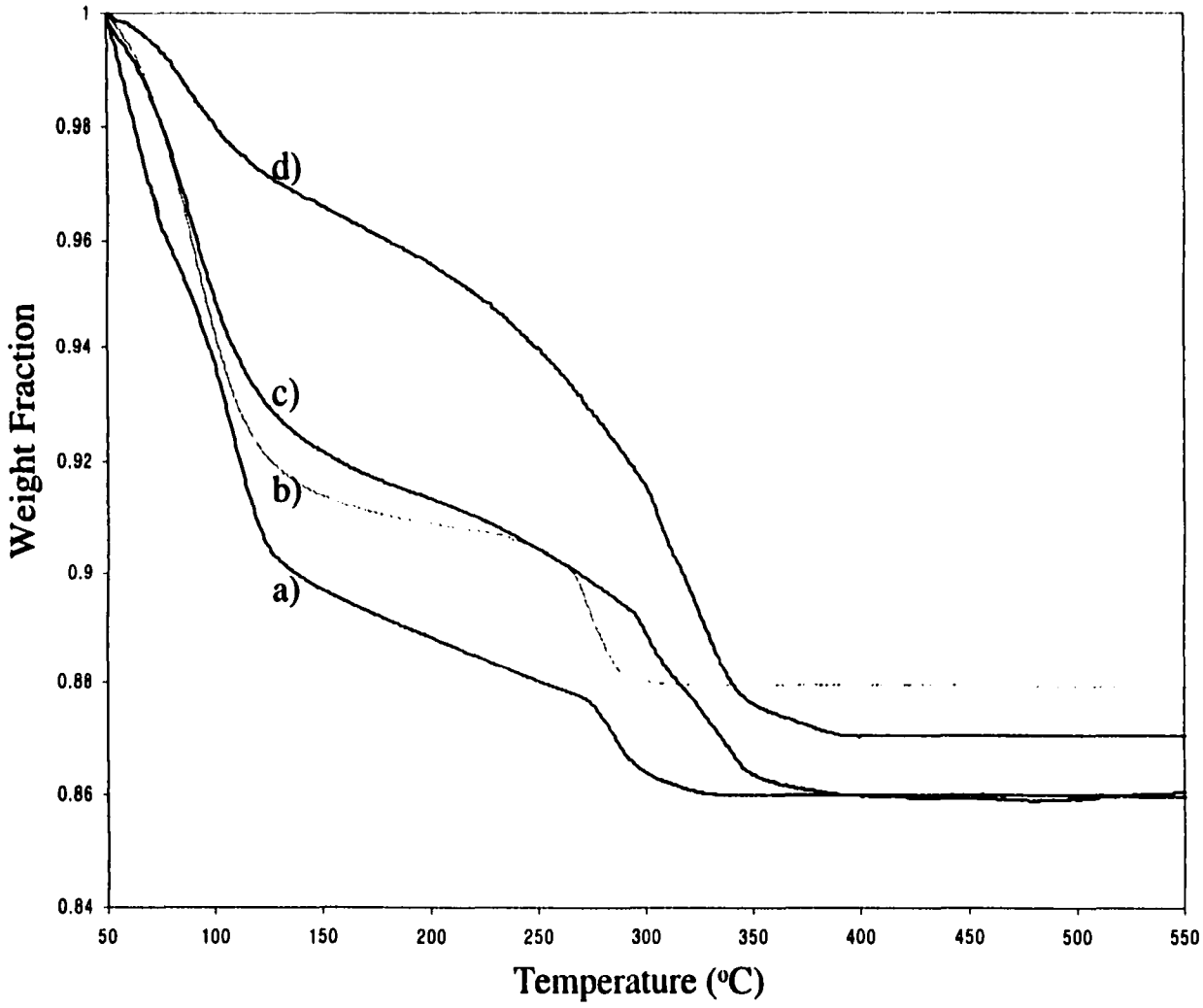

Figure 8. Thermogravimetric analysis of a) sample A, b) sample B, c) sample C, and d) sample D.

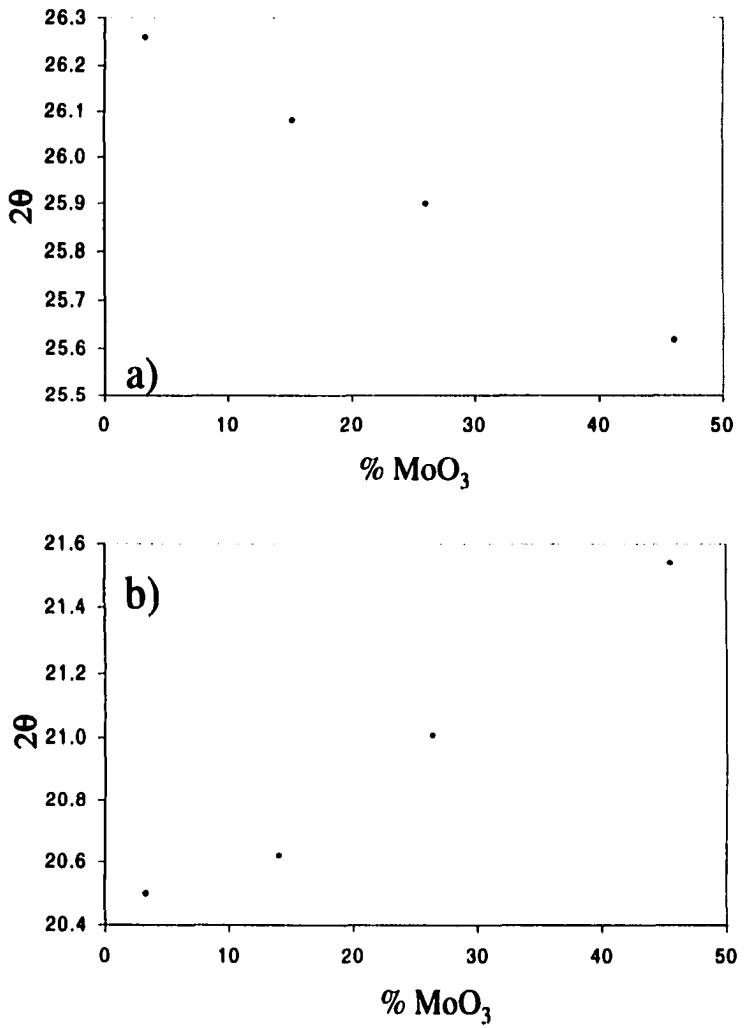

Figure 9. Peak location of a) (110) plane and b) (001) plane versus mole % MoO_3 [samples treated at 350 °C/4h in dry air]

Table 1. Summary of As-Prepared Gel Composition: $H_nV_{12-y}Mo_yO_{30+n/2}(NH_4^+)_{2y}$

Sample	% MoO_3[a]	y
A	3.3	0.20
B	14.0	1.00
C	26.4	2.15
D	45.5	5.0

[a] calculated as mole MoO_3 /(mole MoO_3 + mole V_2O_5)

CHAPTER 7

CONCLUSIONS AND RECOMMENDATIONS

7.1 General Discussion

In general, the peroxovanadate solution sol-gel process can be thought of as consisting of two parts: 1) the decomposition of the peroxo species and 2) cation hydrolysis leading to gelation. By controlling the synthesis conditions, both layered and amorphous compounds can be created. However, the type of water coordination observed in these gels was found to be identical no matter what the long-range order. The current work clarified many of the discrepancies found in the literature and offered much new valuable information. Highlights include the types of vanadium environments present at various stages of hydration, the role of adsorbed water, oxygen exchange from adsorbed water into the gel sites, and the ability to create metastable VMoO solid solution phases. These results could have a variety of impacts on future catalysis research.

7.2 Recommendations for Future Research

Neither the layered vanadia gels, nor the supersaturated solid solutions have been investigated for catalytic activity, and both could prove interesting. Since the sites of water chemisorption are now understood, studies attempting to explain the effect of water in the feedstock could be undertaken. An exploration of the dynamic process involving the oxygen exchange from water to gel sites could provide additional insight or opportunities for use of this material as an oxidation catalyst or possibly an electrocatalyst. Finally, the synthesis procedure is readily adaptable to include other peroxo-metal species. For example, preliminary results indicated that a rhenium-peroxo

species could be formed. Thus, binary or ternary catalysts could be synthesized and evaluated for catalytic activity.

The role of each specific oxygen site is of great interest in selective oxidation catalysis. Since we have been able to synthesize an oxygen site labeled (^{17}O) catalyst, future work could involve microreactor studies with such a labeled catalyst, so that the role of each oxygen site can be understood. Using the same labeled catalyst, further work could be undertaken to determine the sites of oxygen addition in the selectively oxidized products, thereby providing greater insight into the fundamental phenomena occurring on the catalyst surface.

APPENDIX A

PARTIAL CHARGE MODEL (PCM) APPLIED TO THE PEROXOVANADATE SOL-GEL SYSTEM

4.1 General

The following equation relates the electronegativity of the species in solution to the pH of the solution:

$$\chi(H^+) = \chi(H_2O) = \chi(C) = 2.732 - 0.035\ pH$$

A graphical representation of this relationship can be seen below. This relationship gives us the expected electronegativity of the species found in solution as a function of pH.

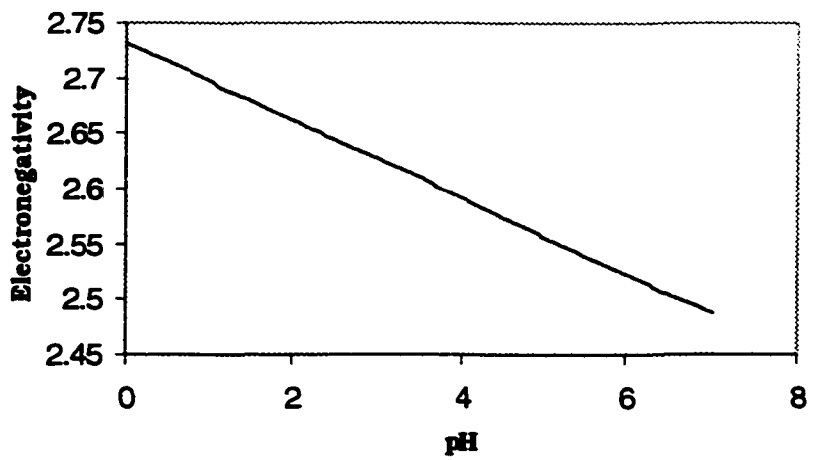

The PCM was applied to the species observed in Samples A and B. The electronegativities were calculated using the equations previously mentioned in Chapter 1. For example, since various hydroxylized forms of the VO_2^+ cation could conceivably exist, we can calculated the predicted electronegativity of each, and compare these to what we expect from the pH model.

The various forms of VO_2^+ can be written in general form as:

$$[VO_x(OH)_y(OH_2)_{N-x-y}]^{(Z-y-2x)+}$$

and now using equation 9,

$$\chi_v = \frac{\sqrt{\chi_V^o} + N\sqrt{\chi_O^o} + (N-x)\sqrt{\chi_H^o} + 1.36(z-y-2x)}{\frac{1}{\sqrt{\chi_M^o}} + \frac{N}{\sqrt{\chi_O^o}} + \frac{N-x}{\sqrt{\chi_H^o}}}$$

χ_v can be calculated for the various forms of VO_2^+.

4.2 Results

Polymerization took place in sample 1 at pH = 1.45 , and in sample 2 at pH = 2.4. Using the PCM we can determine how well the model predicts the experimentally observed species. These results are summarized in the following table:

Hydrolyzed Species of VO_2^+	χ (calculated)	χ (predicted from pH)[1]	χ (predicted from pH)[2]
$[VO_2(H_2O)_4]^+$	2.67	2.69	2.65
$[VO_2(OH)(H_2O)_3]$	2.56	2.69	2.65
$[VO(OH)(H_2O)_4]^{2+}$	2.76	2.69	2.65
$[VO(OH)_2(H_2O)_3]^+$	2.67	2.69	2.65
$[VO(OH)_3(H_2O)_2]^{\circ}$ [§]	2.56	2.69	2.65

[§] Species predicted by Livage[ref]
[1] pH =1.45
[2] pH = 2.1

This same procedure yielded values for the species listed in the following table:

Species	χ (calculated)	χ (predicted from pH)[1]	χ (predicted from pH)[2]
$VO(O_2)(OH_2)_3^+$	2.71	2.69	2.65
$VO(O_2)_2(OH_2)^-$	2.56	2.69	2.65
$[V(O_2)_2]_2O(OH_2)^{\circ}$	2.73	2.69	2.65
$[V_{10}O_{28}]^{6-}$	2.47	2.69	2.65
$[HV_{10}O_{28}]^{5-}$ [§]	2.52	2.69	2.65
$[H_2V_{10}O_{28}]^{4-}$	2.56	2.69	2.65
$[H_3V_{10}O_{28}]^{3-}$	2.60	2.69	2.65
$[H_4V_{10}O_{28}]^{2-}$ [§]	2.64	2.69	2.65

[§] Not observed experimentally
[1] pH =1.45
[2] pH = 2.1

Interestingly, the model seems to predict that both VO_2^+ and $[VO(OH)_2(H_2O)_3]^+$ would be observed in both samples 1 and 2 as polymerization occurred. VO_2^+ was observed using ^{51}V NMR, while $[VO(OH)_2(H_2O)_3]^+$ was not. If $[VO(OH)_2(H_2O)_3]^+$ was present, it had a short life-time and was not observable on the NMR time scale. If it did exist in solution, and if we were to presume that it was the short-lived precursor to polymerization (instead of $[VO(OH)_3(H_2O)_2]^{\circ}$ which was theorized by Livage, we wouldn't expect to necessarily see linear chain formation, which is what was observed experimentally. Therefore, it is unlikely that this species existed in solution.

ACKNOWLEDGEMENTS

I would like to thank my major professor, Dr. Glenn Schrader, for allowing me the freedom to make my own mistakes, to learn my own lessons, and for knowing when guidance was needed. In addition, I would also like to thank Dr. Marek Pruski and Dr. Jurek Wiench, whom with I spent many pleasurable hours. As I look back, I can not imagine working with better group of scientists; it was my good fortune to be a part of such a wonderful collaborative effort. I would also like to thank my wife Mirrya, whom was subjected to many, many hours of technical discussion, whether she liked it or not. I would also like to thank my colleagues, The Nitrocream Guys, Dr. William Schroeder and soon to be Dr. T.J. Paskach for the insights and thoughts they offered during our many discussions.

This work was performed at Ames Laboratory under Contract No. W-7405-Eng-82 with the U.S. Department of Energy. The United States government has assigned the DOE Report number IS-T-2047 to this dissertation.